DISSERTATION

OXIDANT-DEPENDENT REGULATION OF L-TYPE CALCIUM CHANNEL ACTIVITY BY ANGIOTENSIN IN VASCULAR SMOOTH MUSCLE

Submitted by

Nathan L. Chaplin

Department of Biomedical Sciences

In partial fulfillment of the requirements

For the Degree of Doctor of Philosophy

Colorado State University

Fort Collins, Colorado

Fall 2015

Doctoral Committee:

Advisor: Gregory Amberg

Jennifer DeLuca
Michael Tamkun
Susan Tsunoda

ABSTRACT

OXIDANT-DEPENDENT REGULATION OF L-TYPE CALCIUM CHANNEL ACTIVITY

BY ANGIOTENSIN IN VASCULAR SMOOTH MUSCLE

Resistance arteries are a major point of physiological regulation of blood flow. Increases in vessel wall stress or sympathetic activity stimulate vascular wall angiotensin signaling, resulting in smooth muscle contraction which directly increases peripheral resistance. Calcium influx through voltage-gated L-type calcium channels underlies vascular smooth muscle contraction. Roughly half of calcium influx in these cells occurs through a small number of persistently active channels, whose activity increases with membrane depolarization. The number of channels gating in this manner is increased by activation of angiotensin receptors on the cell membrane, and basal L-type channel activity is increased during hypertension. Reactive oxygen species are also generated by vascular smooth muscle in response to vessel stretch and by several paracrine signaling pathways including angiotensin signaling. Oxidative stress and augmented calcium handling resulting from chronic angiotensin signaling in the vasculature each contribute to enhanced vessel reactivity, pathological inflammation and vessel remodeling associated with hypertension.

This study uses a multidisciplinary approach to investigate the role of hydrogen peroxide in angiotensin signaling in vascular smooth muscle. Using calcium- and redox-sensitive fluorescent indicators, local generation of hydrogen peroxide by NAD(P)H oxidase and mitochondria are shown to synergistically promote PKC-dependent persistent gating of plasma membrane L- type calcium channels in response to angiotensin II. We show that broad inhibition of hydrogen peroxide signaling by catalase and targeted inhibition of mitochondrial reactive oxygen species production attenuates cerebral resistance artery constriction to angiotensin. We further demonstrate the role of endothelium-

independent mitochondrial reactive oxygen species in development of enhanced vessel tone and smooth muscle calcium in a murine model of hypertension. Together, these findings contribute to the understanding of intracellular calcium and oxidative signaling in vascular physiology and disease and may provide insight into local signaling dynamics involving these second messengers in various other systems.

TABLE OF CONTENTS

ABSTRACT ii

Chapter 1. Introduction and Background 1

1.1 Introduction 1

1.2 Pial Artery Anatomy 3

1.3 General Physiological of Pial Arterties 5

1.3.1 Sympathetic Innervation 5

1.3.2 Autoregulation of Cerebral Blood Flow 6

1.3.3 Electrophysiology of Vascular Smooth Muscle 9

1.3.4 Smooth Muscle Contraction 18

1.3.5 Circulating Factors 18

1.3.6 Paracrine and Autocrine Factors 20

1.4 L-type Calcium Channel Sparklets 28

1.4.1 Early Characterization of Sparklets 28

1.4.2 Sparklets in Vascular Smooth Muscle 29

1.4.3 High Activity Sparklets 31

1.5 Central Hypothesis and Key Observations 36

Chapter 2. Hydrogen peroxide mediates oxidant-dependent stimulation of arterial smooth muscle L-type calcium channels 37

2.1 Summary 37

2.2 Introduction 38

2.3 Materials and Methods 39

2.4 Results 45

2.5 Discussion 55

Chapter 3. Stimulation of arterial smooth muscle L-type calcium channels by hydrogen peroxide requires protein kinase C 62

3.1 Summary 62

3.2 Introduction 62

3.3 Materials and Methods 64

3.4 Results 67

3.5 Discussion 69

Chapter 4. Arterial smooth muscle mitochondria amplify hydrogen peroxide microdomains functionally coupled to L-type calcium channels 71

4.1 Summary 71

4.2 Introduction 72

4.3 Methods 74

4.4 Results 82

4.5 Discussion 92

Chapter 5. Conclusion 99

5.1 Localization and concerted activation of NAD(P)H oxidase and mitochondria are required for Ang II-derived high activity sparklets 100

5.2 H_2O_2 serves as an oxidant second messenger in Ang II-mediated LTCC sparklet signaling 103

5.3 Oxidative activation of PKC mediates LTCC sparklet stimulation by Ang II 104

5.4 Final Remarks 106

References 109

Appendix: Permissions to Reproduce Copyright Protected Works 132

Chapter 1. Introduction and Background

1.1 Introduction

Arterial tone is a variable factor in regulation of blood flow. In healthy individuals, coordination of cardiac output, neuronal signaling, and local regulation of arterial diameter allows appropriate delivery of oxygen and glucose to and removal of waste from tissues according to metabolic need. Pathologically, each of these controlling factors may become dysregulated and contribute to insufficient vascular bed perfusion or enhanced peripheral artery resistance. The clinical diagnosis of hypertension, when intervention is recommended in otherwise healthy individuals, is defined as systolic or diastolic pressure exceeding 140/ 90mm Hg respectively (Chobanian et al., 2003). The prevalence of hypertension is projected to increase from the current incidence of 25% to include 29% of the global adult population by the year 2025 (Kearney et al., 2005). The comorbidity among hypertension, insulin-resistant diabetes, and obesity is high and has been collectively been labeled the metabolic syndrome (Alberti et al., 2005). While chronically elevated blood pressure arises from various genetic, behavioral, and environmental factors, the resultant enhanced vascular wall stress progressively leads to vascular maladaptation. This, in turn, compounds the risk of myocardial infarction, systemic organ damage, and stroke.

Enhanced vascular resistance is common among hypertension, type II diabetes, and obesity. Mechanical stress on the heart, kidneys, and vasculature arising from chronically elevated vascular resistance contributes to the pathology of these conditions. Central to vascular resistance is the level of contractility to physiological stimuli in the smooth muscle layer which sheaths the arterial tree. Small changes in the contractile state of vascular smooth muscle have a large impact on blood flow and resistance in medium-sized and small arteries. Calcium homeostasis in the smooth muscle layer determines the level of vasoconstriction in resistance arteries and additionally affects gene expression

through calcium-sensitive transcription pathways. Bulk calcium entry into vascular smooth muscle is predominantly through voltage-gated L-type calcium channels (**LTCC**'s), and this event is required for arterial smooth muscle contraction (Knot and Nelson 1998). Modulation of smooth muscle LTCC activity occurs primarily through changes in membrane potential and G-protein coupled receptor signaling cascades. Pathologically, resting membrane potential and response to metabotropic agonists become skewed toward enhanced contractility.

Angiotensin (**Ang II**) is a classical mediator of vasoconstriction and transcription modification, acting primarily through a $G\alpha_{q/11}$ coupled receptor in vascular smooth muscle. Stretch- induced activation of the vascular smooth muscle angiotensin receptor additionally mediates autoregulation of arterial blood flow in resistance arteries (Gonzales et al., 2014; Schleifenbaum et al., 2014). Chronic activation of this pathway in the vasculature is directly involved in hypertensive pathology. In addition to calcium, reactive oxygen species (**ROS**) are a major mediator of physiological Ang II signaling. Intracellular buffering of ROS may become depleted pathologically, leading to nontargeted effects of ROS signaling referred to as oxidative stress. Recent advances in cellular imaging have revealed Ang II enhances LTCC activity partially through a spatially localized redox-sensitive pathway (Amberg et al., 2010), however the details of this signal transduction had not been elucidated. This study aims to clarify the role of local sources of oxidative species in angiotensin receptor signaling in native cerebral vascular smooth muscle. To better appreciate the merit of the present study, the following sections review 1) cerebral artery and smooth muscle physiology and the vascular pathophysiology of hypertension with special attention paid to vascular Ang II and ROS signaling (**Sections 1.2 and 1.3**) and 2) local regulation of LTCC's by Ang II (**Section 1.4**).

1.2 Pial Artery Anatomy

Murine pial arteries are used exclusively in the present investigation. These arteries arise from an anastomotic ring roughly encircling the hypothalamus on the ventral surface of the brain. This structure, known as the Circle of Willis, is supplied chiefly by the left and right internal carotid arteries and the paired vertebral arteries which fuse caudally to form the basilar artery prior to joining the Circle. The basilar artery itself supplies several pairs of small pontine arteries and the larger left and right anterior and posterior cerebellar arteries. The Circle of Willis supplies the paired anterior, middle and posterior cerebral arteries which travel along the pial surface and bifurcate multiple times before diving into the underlying tissue where they give rise to the penetrating arterioles. These arterioles differ markedly from the pial arteries with respect to their physiological regulation and together with intrinsic neurons and astrocytes, form the neurovascular unit (reviewed in Idaecola, 2004).

Pial arteries consist of a relatively thin outer adventitial layer composed primarily of collagen fibers, serving primarily a structural role. The luminal surface of these vessels is composed of a single layer of endothelial cells. These cells are separated from the medial smooth muscle layer by a relatively thick internal elastic lamina, which along with endothelial tight junctions form a fluid barrier to allow isolation of cerebrospinal fluid from the plasma. Fenestrations exist in this layer which allow communication between the endothelium and underlying smooth muscle layers. The medial layer itself consists of circumferentially- oriented smooth muscle cells, the thickness of which ranges from a single layer in small, distal branches to multiple layers in larger vessels such as the basilar and middle cerebral arteries (reviewed in Lee, 1995). Smooth muscle cells in the tunica media are mechanically coupled through adherens junctions between focal adhesions on adjacent cells. Additionally, electrical coupling between adjacent smooth muscle and, likewise, between the smooth muscle and endothelial layer provide coordinated contraction and relaxation to cause vasoconstriction or vasodilation respectively.

Chronic elevation in blood pressure induces significant remodeling in arteries. This has been linked to direct effects of endothelial shear stress and vessel wall stretch, contributing to chronically elevated vessel wall [Ca^{2+}], oxidative stress, and inflammation, mediated in part by vessel wall angiotensin signaling. The changes seen in early stages of hypertension can be seen as protective, in that they attempt to bolster the integrity of the vessel wall. Increased production of collagen and smooth muscle α_1 integrin, responsible for collagen anchoring, occurs in the aorta of rats which have been chronically infused with Ang II (Brassard et al., 2005). This reduces vessel compliance and contributes to enhanced systemic resistance. Additionally, remodeling of the smooth muscle layer occurs, involving both cellular proliferation and migration. This effects a narrowing of the lumen either through smooth muscle hypertrophy in larger arteries or inward, eutrophic remodeling in smaller vessels. Luminal restriction contributes to sustained elevation of arterial resistance (reviewed in Schiffrin and Touyz 2004; Schiffrin, 2010). Remodeling is observed in systemic and cerebral arteries in postmortem studies from hypertensive patients (Rizzoni et al., 2007; reviewed in Schiffrin and Touyz, 2004), cerebral and small mesenteric arteries from rats chronically infused with 100ng/kg Ang II after four weeks (Simon et al., 1998) as well as in mature, selectively bred spontaneous hypertensive rats (**SHR**) (Rizzoni et al., 1994). While these types of remodeling strengthen the vascular wall, consequent narrowing of the lumen results in chronically enhanced resistance to flow and exacerbates elevation of blood pressure. Additionally, enhanced oxidative stress and cytokine synthesis in the vessel wall during hypertension promotes inflammation and subsequent invasion of the tunica media by monocytes, leading to the formation of scleroses which further occlude the vascular lumen and compromise the integrity of the vascular wall (reviewed in Schiffrin and Touyz, 2004).

1.3 General Physiological of Pial Arterties

1.3.1 Sympathetic Innervation

Similar to systemic resistance arteries, pial vessels are extrinsically innervated by the autonomic nervous system. Typically in systemic vasculature, sympathetic efferents tonically release the neurotransmitters norepinephrine and adenosine triphosphate (**ATP**) in the tunica media to stimulate smooth muscle contraction by binding to metabotropic α1 adrenergic receptors (**A1AR**'s) and ionotropic purinergic receptors (**P2XR**'s) respectively on the apposed sarcolemma, resulting in membrane depolarization and smooth muscle contraction. During sympathetic activation via systemic baroreceptors or central pathways, vascular tone is generally increased. Along with sympathetic enhancement of cardiac output, renin release, and norepinephrine release, this results in short-term elevation of blood pressure. During human cases of hypertension and in rat models, the sympathetic nervous system is chronically activated, contributing to augmented peripheral resistance (reviewed in Oparil, 1986).

P2XR's are ionotropic and conduct sodium and calcium currents, directly causing membrane depolarization and subsequent activation of LTCC's (see **Section 1.3.3**). A1AR's are associated with $G_{\alpha q/11}$ G-proteins. A1AR's, like all G-protein coupled receptors, are integral cell membrane proteins with seven transmembrane domains. The intracellular C-terminus binds a heterotrimeric guanine binding regulatory protein (G- protein) composed of α and βγ subunits, the specific identity of which determines the downstream target(s) of receptor activation. Ligand binding to the A1AR induces a conformational change which allows exchange of bound guanosine diphosphate (**GDP**) for guanosine triphosphate (**GTP**). Activation by ligand binding causes dissociation of the heterotrimeric G- protein complex. Canonically, the dissociated α subunit from $G_{\alpha q/11}$ binds to membrane- associated phospholipase C β (**PLCβ**) which then cleaves the phosphodiester bond in plasma membrane constituent

phosphatidylinositol (4,5) bisphosphate (**PIP_2**). PIP_2 cleavage releases the inositol group (1, 4, 5 phosphoinositol**: IP_3**) from the membrane, where it diffuses through the cytosol to activate stromal calcium release through the sarcoplasmic reticulum IP_3 receptor (**IP_3R**). Diacylglycerol (**DAG**), the second product of PIP_2 cleavage, remains at the cell membrane, contributing to activation of membrane-depolarizing currents and additionally increases cytosolic calcium through activation of voltage-dependent LTCC's by directly activating protein kinase C (**PKC**).

Cerebral arteries differ from systemic arteries in their sensitivity to norepinephrine due to relatively low expression of A1AR's in cerebral vessels and loose association between prejunctional sympathetic synaptic varicosities and smooth muscle membranes. Cerebral artery smooth muscle therefore respond only to strong sympathetic input via α2 adrenergic receptor (**A2AR**) (Fujiwata et al., 1982; Ferron et al., 1984). This receptor is coupled to a $G_{\alpha i}$ family heterotrimeric G-protein. Upon GTP/GDP exchange, the active α subunit of A2AR associates with plasma membrane- bound adenylyl cyclase and inhibits its activity. This lowers cytosolic cyclic adenosine monophosphate (**cAMP**) regulated protein kinase (**PKA**) activity, promoting vasoconstriction through decreasing PKA-mediated stimulation of hyperpolarizing plasma membrane potassium channels (reviewed in Liebmann and Bohmer, 2000).

1.3.2 Autoregulation of Cerebral Blood Flow

The brain requires constant perfusion according to its high metabolic demand. In cases of decreased blood supply or poor oxygenation, small arteries in the cerebral vasculature dilate, thus locally increasing blood flow and restoring adequate downstream perfusion. The capacity to increase blood flow to the brain is limited, however. The spatial constraint arising from the rigidity of the skull requires limiting elevation of flow, else this would result in increased intracranial pressure. This would consequentially lead to decreased capillary exchange and tissue damage. Increased flow is therefore met with rapid vasoconstriction to mitigate these effects. Due to the critical nature of maintaining

cerebral blood flow between these two extremes, autoregulation of luminal diameter is a major physiological feature of pial arteries.

Endothelial regulation

The endothelium tempers the reactivity of the smooth muscle layer in response to increased flow. The vascular endothelium communicates with the underlying smooth muscle through releasing diffusible factors which influence its contractility. Furchgott and Zawadski (1980) first discovered its essential role in producing an "endothelium- derived relaxing factor" by comparing the response of arteries with an intact versus mechanically- denuded endothelium to acetylcholine. This factor was subsequently identified as nitric oxide (**NO**) (Palmer et al, 1987) and is produced by the endothelial NO synthase (**eNOS**) in response to calcium and G-protein-coupled receptor signaling. NO diffuses freely across the endothelial cell membrane to adjacent smooth muscle cells. The primary target of NO in smooth muscle is soluble guanylyl cyclase, which catalyzes the conversion of guanosine monophosphate to cyclic guanosine monophosphate (**cGMP**). cGMP binds to the regulatory domain of the serine/ threonine kinase, protein kinase G (**PKG**), resulting in disinhibition of its catalytic activity. PKG targets various effectors, collectively resulting in hyperpolarization of the smooth muscle cell membrane and a decrease in contractility. NO production by the vascular endothelium is tonic and Increases in response to elevated sheer stress in the event of increased blood flow (Corson et al., 1994).

Circulating oxygen and pH also play roles in autoregulation of cerebral blood flow. Dilation of arteries to hypoxia and increased fluid metabolites transiently increase local blood flow during functional hyperemia. Local hypoxia causes vasodilation of cerebral arteries which may be directly mediated by the smooth muscle layer. This effect is inhibited by application of glibenclimide, an inhibitor of ATP- sensitive potassium (**K_{ATP}**) channels (Taguchi et al., 1994), independent of endothelial vasodilatory factors. Efflux of potassium through activated of K_{ATP} channels hyperpolarizes the smooth muscle cell, leading to vasodilation. The endothelium plays a major role in arterial diameter regulation in

response to changes in luminal pH (Kontos et al., 1977). This is in part mediated through stimulation of eicosanoid metabolism in the endothelium to produce prostacyclin (**PGI_2**), evidenced by sensitivity of this response to indomethacin (Fan et al., 2011). PGI_2 targets the smooth muscle IP_1 $G_{\alpha s}$- coupled receptor. The IP_1 receptor GTP- bound α subunit subsequently activates adenylyl cyclase and promotes vasodilation.

In addition to NO and PGI_2- mediated vasorelaxation, gap junctions between smooth muscle and endothelial projections play an important role in myoendothelial feedback. These cellular junctions, formed by apposing hexamers of connexins expressed on both smooth muscle and endothelial membranes via fenestrations in the inner elastic lamina. These conduits provide a two-way communication of electrical potential (deWit, 2003), evidenced by disruption in vascular electrical coordination in $Cx40^{-/-}$ mice. Additionally, small chemical messengers such as calcium and metabolites pass through these channels and are capable of mediating smooth muscle relaxation. This is evidenced by endothelium- dependent relaxation of cerebral arteries in the presence of eNOS inhibitors by a smooth muscle sarcoplasmic reticulum- dependent mechanism (Tran et al., 2012)

During the pathogenesis of hypertension, autoregulation of resistance arteries becomes skewed, favoring chronic restriction of luminal flow. Endothelial damage and oxidative stress promotes cell senescence, disruption of NO production, and formation of peroxynitrite (**$ONOO^-$**). $ONOO^-$ itself is a highly reactive oxidant, leading to downstream nitrosylation of various targets. As a result of these factors, the endothelial vasodilatory response is diminished. Clinically, this has been shown as a decrease in flow-mediated dilation measured by Doppler imaging of the brachial artery in response to pressure cuff-induced transient flow disruption in hypertensive patients (reviewed in Deanfield et al., 2007). Administering the methyl ester of L-N^G-nitro arginine (**LNAME**) in the drinking water of healthy Sprague-Dawley rats induces hypertension by inducing endothelial dysfunction (Dananberg et al., 1993). LNAME competes with the eNOS substrate L-arginine, decreasing NO production. This directly leads to a

rapid rise in blood pressure, which is augmented by secondary activation of the sympathetic nervous system and the renin angiotensin aldosterone system. Chronically elevated blood pressure subsequentlyleads to alterations in vascular signaling and vascular remodeling (Duarte et al, 2002). This model is used to induce hypertension in **Chapter 4** of this document to investigate the role of smooth muscle-derived mitochondrial ROS in the pathogenesis of hypertension.

Myogenic tone

Bayliss (1902) first commented on the constriction and dilation of denervated arteries to an increase or decrease in luminal pressure respectively. Knot and Nelson (1998) demonstrated in isolated cerebral arteries that this arises from endothelium- independent tonic contraction of the smooth muscle layer through smooth muscle depolarization and calcium entry. Recently this has been shown to be dependent on the level of stretch- induced (ligand-independent) activation of type-1 angiotensin receptors (**AT1R**'s) on the cell membrane of smooth muscle from cerebral and mesenteric arteries (Schleifenbaum et al., 2014). This rapid response to fluctuation in systemic blood flow serves to protect downstream arterioles and capillary beds from excessive pressure or insufficient perfusion. The myogenic response is exaggerated in arteries from the SHR model during the development of hypertension compared with Wistar- Kyoto control subjects, but not in older subjects with established hypertension (Rizzoni et al., 1994; Izzard et al., 1996). As the pathology progresses this response is likely diminished due to vessel remodeling. Inward remodeling allows sustained reduction of luminal flow while lessening energy expenditure from chronic smooth muscle contraction.

1.3.3 Electrophysiology of Vascular Smooth Muscle

Ionic gradients and resting membrane potential

Smooth muscle membrane potential is determined by the balance of ionic concentrations across the cell membrane. The plasma membrane Na^+/K^+- ATPase uses active transport to maintain

concentration gradients with relatively high extracellular sodium (**Na^+**) ($[Na^+]_i/[Na^+]_e \approx 0.1$), relatively high $[K^+]_i$ ($[K^+]_i/[K^+]_e \approx 35$) and an electrical gradient, as it moves three sodium ions to the extracellular space in exchange for two potassium (**K^+**) ions. The $[K^+]$ gradient is used by the K^+/Cl^- cotransporter to maintain a chloride (**Cl^-**) gradient ($[Cl^-]_e/[Cl^-]_i \approx 14$). Additionally, a steep cytosolic calcium (**Ca^{2+}**) gradient ($[Ca^{2+}]_i/[Ca^{2+}]_e \approx .0001$) is maintained by the concerted activity of rapid cytosolic calcium buffers (chiefly calbindin and calretinin) and slower extrusion systems including sequestration via the mitochondrial uniporter, the sarco(endo)plasmic reticulum calcium ATPase (**SERCA**), and export through the plasma membrane calcium ATPase (**PMCA**) and the plasmalemmal Na^+/ Ca^{2+}exchanger (reviewed in Clapham, 2007). Low resting $[Ca^{2+}]_i$ and rapid sequestration of transient calcium fluxes provide the framework necessary for activation of contractile machinery in depolarization- induced global $[Ca^{2+}]_i$ elevation, while simultaneously allowing spatially restricted calcium microdomain signaling for other cellular functions.

The resting membrane potential in the smooth muscle layer in relaxed arteries absent myogenic tone is around -70mV (Harder, 1984). Membrane potential is a function of the log of the ratio of the transmembrane ionic concentration gradient and the relative permeability of the membrane to each ion. The hyperpolarized state of vascular smooth muscle under these conditions is due to relatively high permeability to potassium, as it lies near potassium's Nernst equilibrium ($E_K \approx$-90mV) and addition of extracellular potassium spontaneously depolarizes the membrane. The source of resting permeability to potassium has been characterized as an inward- rectifier potassium current (I_{KIR}). The source of this current, the K_{IR} family of ion channels have constituents which consist of tetramers of two-transmembrane segment- containing subunits, lack voltage sensitivity and show voltage- dependent inhibition of outward current by intracellular polyamines. These channels have constitutive activity in isolated vascular smooth muscle, producing barium- sensitive inwardly rectifying currents at voltages negative to E_K and small outward (hyperpolarizing) currents at physiological potentials (Quayle et al.,

1993a). Bath application of barium has similarly been shown to depolarize intact arteries at low intraluminal pressure (reviewed in Nelson and Quayle, 1995). Transient inward (depolarizing) currents have also been identified in isolated cerebral vascular smooth muscle at -70mV. These have been shown to arise from activity of transient receptor potential (**TRP**) channels, namely the calcium-activated TRP melanostatin family member 4 (**TRPM4**) channels (Gonzales et al., 2010a). These channels consist of tetramers of six- transmembrane domain subunits. Spontaneous inward TRPM4 currents can be selectively inhibited pharmacologically by 9-phenanthrol, promoting vasorelaxation in pressurized arteries. TRPM4 activation is dependent on transient calcium release from closely apposed IP_3R's on the sarcoplasmic reticulum (Gonzales et al., 2010)

Mechanotransduction and Stretch- Induced Depolarization

Pressure- induced constriction of medium and small arteries occurs in a variety of vascular beds including pial arteries. This occurs by a graded tonic constriction of arteries across the range of physiological intraluminal pressures, and is an inherent property of the smooth muscle layer, leading to the descriptive title "myogenic tone". Two recent studies have independently demonstrated the smooth muscle AT1R acts as a mechanosensor in cerebral, mesenteric, and renal arteries. In the first study, isolated mesenteric and renal arteries from mice lacking AT1R (*Atr1a*$^{-/-}$) failed to develop pressure-induced tone. This was shown to be ligand-independent, as arteries isolated from mice deficient in the gene for angiotensinogen (*Agt*$^{-/-}$) showed normal vasoconstriction to intraluminal pressure elevation (Schliefenbaum et al., 2014). The second study used the AT1R antagonist losartan to inhibit inward currents evoked in isolated cerebral smooth muscle to osmotic stress or negative pressure delivered through the recording micropipette (Gonzales et al., 2014).

AT1R activation initiates transient calcium signaling which in turn evokes larger calcium-sensitive depolarizing currents. The TRP family of ion channels plays a major role in both initial transient calcium signaling and membrane depolarization. The canonical group of TRP channels (**TRPC**) conduct

nonselective cation currents and are activated downstream of G-protein and receptor tyrosine kinase activation. TRPC6 was shown to be mediate sarcolemmal calcium influx subsequent to stretch- induced AT1R activation via PLC cleavage of PIP_2 in cerebral arteries (Gonzales et al., 2014), leading presumably to direct activation by DAG as demonstrated by Hoffman et al. (1999). This localized Ca^{2+} influxl is amplified by stromal calcium- induced calcium release through IP_3R's, requiring concomitant sensitization by IP_3 (Gonzales et al., 2014). This leads to enhancement of TRPM4 current, also shown to be required for stretch-induced depolarization (Earley et al., 2004). Interestingly, mesenteric arteries from *Trpc6*$^{-/-}$ mice were shown to develop tone normally (Schliefenbaum et al., 2014), perhaps due to vascular bed specificity or compensatory mechanisms. TRPC3 channels have been shown to be activated by agonist- induced activation of cotransfected AT1R's (Gonzales et al., 2010a) and are also dependent on direct activtation by DAG (Hoffman et al;., 1999). TRPC3 activation may therefore contribute to the myogenic response to luminal pressure in mesenteric or other arteries, however this has not been directly investigated. Local calcium transients have additionally been shown to elicit stretch activated inward currents through the calcium-activated chloride channel transmembrane 16A (**TMEM16A**) in vascular smooth muscle (Bulley et al., 2012), implicating chloride currents in smooth muscle membrane depolarization as well.

Pathological changes in AT1R expression promote enhanced pressure-induced constriction of arteries. Vascular AT1R protein expression is enhanced in human and animal hypercholesteremia and hyperinsulinemia, and rat models of high salt diet (reviewed in Nickenig and Harrison, 2002). In arteries from young SHR, enhanced binding of radiolabeled Ang II was observed relative to Wistar- Kyoto control rats (Schiffrin, 1984). Interestingly, in this study radioligand binding levels returned to those of controls in 20wk. specimens, coinciding with the time frame observed for vascular remodeling.

L-type Calcium Channels

Sufficient membrane depolarization leads to the activation of voltage-gated calcium channels **(VGCC**'s), specifically the cardiac isoform of LTCC's, $Ca_V1.2$., translating local calcium signaling into a significant rise in $[Ca^{2+}]_i$. Cardiac LTCC's are expressed in many cell types including neurons, pancreatic β cells, andcardiac and smooth muscle These channels are responsible for coupling membrane depolarization to a wide variety of physiological responses (reviewed in Catterall, 2011). LTCC's feature a large (≈190kd) pore forming α_1 subunit consisting of four tandem domains (**DI- DIV**), each containing six transmembrane segments (**S1-S6**). Similar to TRP channels, the pore is formed by interaction among the fifth and sixth membrane-spanning segment (S5 and S6) in each domain. Unlike TRP channels, the S1- S4 segments act as an intrinsic voltage sensor, similar to the role of the homologous segments of voltage- gated sodium channels suggested by Guy and Seetharamulu (1986). The S4 segment contains a number of basic residues which defelct outward as a result of membrane depolarization, causing a conformational change in the pore to allow selective calcium permeability at more positive membrane potentials. These channels demonstrate increasing voltage-dependent activation with depolarization throughout the physiological range of membrane potential for smooth muscle cells (V_m≈-55 to -35mV).

Depolarization across the entire range of physiological potentials in arterial smooth muscle results in a related biphasic increase in Ca^{2+} influx due to the opposing effects of voltage- dependent activation and voltage- and calcium- dependent inactivation (reviewed in Catterall, 2011). Under physiological conditions, the luminal pressure of cerebral arteries is between 60-140mm Hg. At 60mm Hg, the smooth muscle in pial arteries is partially contracted, the membrane partly depolarized (V_m ≈-45mV (Knot and Nelson, 1998) to -58 mV (Harder, 1984)), and intracellular calcium levels are elevated ($[Ca^{2+}]_i$ ≈190nM) relative to unpressurized arteries (110nM) (Knot and Nelson, 1998). Increasing the intraluminal pressure in pial arteries to 100mm Hg causes vasoconstriction, depolarizes the cell membrane (V_m≈ -35mV), and raises intracellular calcium (($[Ca^{2+}]_i$ ≈315nM). Selectively blocking voltage-gated L-type calcium channels (LTCC's) with diltiazem or nisoldipine prevents pressure-induced elevation

of $[Ca^{2+}]_i$ without preventing membrane depolarization. Global increases in $[Ca^{2+}]_i$ by LTCC activation causes the release of stromal calcium through ryanodine receptors to further elevate $[Ca^{2+}]_i$ through calcium-induced calcium release (Collier et al., 2000). Both IP_3R's and ryanodine receptors open with elevated local $[Ca^{2+}]_i$. The direct contribution of stromal calcium release in facilitating smooth muscle contraction is unclear, however a putative role for propagation of calcium release or "calcium waves" by IP_3R's may exist for activation of contractile machinery deep in the cell (reviewed in Wray and Noble, 2005).

Steady-state inactivation of LTCC's in vascular smooth muscle is marked. General inhibition of channel gating is possibly important to avoid excitotoxicity given the physiological slow depolarization and repolarization typical of myogenic tone. A significant portion of the channels expressed on the membrane are inactive due to inhibition through interaction with the cleaved C-terminal tail fragment of the channel (Hulme et al., 2006; Bannister et al., 2013), additional mechanisms maintain relatively small steady-state calcium currents in these cells at physiological membrane potentials. Steady- state calcium currents in isolated smooth muscle from pial arteries at -40mV are approximately -0.2pA, corresponding to one open channel at any given time in the entire cell. At -20mV, this increases to only -0.8pA (Rubart et al., 1996). LTCC's undergo rapid calcium- dependent inactivation, requiring concentration- dependent binding of 2 calcium ions each to the N- and C- terminal lobes of calmodulin associated with the IQ domain on the $Ca_V1.2$ α_1 C-terminus. Additionally, a slower voltage-dependent inhibition occurs which is evident using barium in place of calcium as a charge carrier. Calcium- and voltage-dependent inhibition activate a common autoinhibitory interaction between the cytosolic DI/DII linker and the channel pore (Kim et al., 2004). The α_1 subunit also interacts with the peripheral α_2ó and intracellular β subunits, involved in membrane trafficking of the α_1 subunit. The β subunit is additionally involved in regulating autoinhibition and interacts with the DI/DII linker of the $\alpha_1$subunit directly.

LTCC activity is highly regulated by kinase activity. PKG has an inhibitory effect on the activity of LTCC's in voltage-clamp studies in cardiomyocytes, however the mechanism for current inhibition is not well characterized. In voltage-clamped cardiomyocytes, PKA was shown to increase whole -cell LTCC current and can potentially phosphorylate several residues on the α_1 subunit and one site on the β subunit (reviewed in Hoffman et al., 2014). Protein kinase C (**PKC**) is capable of phosphorylating the same sites as PKA and also increases channel activity. A major function of PKA phosphorylation appears to be modulation of the interaction between the channel and the post- translationally cleaved inhibitory C-terminal fragment (Hulme et al., 2006).Localization of PKC and PKA with LTCC's is dependent on coordination by a group of proteins known as A- kinase anchoring proteins (**AKAP'**s) which function to localize PKC, PKA, and protein phosphatases with effectors, in large part determining the specificity of kinase-mediated cellular signaling. AKAP 5/79/150 (referred to hereafter as **AKAP150**) directly associates with the c-terminus of $Ca_v1.2$ (Hulme et al., 2003) and additionally regulates calcium-dependent inhibition by docking of the CaM-dependent serine/threonine phosphatase calcineurin in hippocampal neurons (Dittmer et al., 2014). Calcineurin activity also critically mediates transcriptional regulation through the nuclear factor of activated T-cells (**nFAT**) family by dephosphorylating a critical residue, allowing translocation of nFAT to the nucleus. This reveals a mechanism by which local LTCC activation plays a role in transcription regulation.

Smooth muscle LTCC activity and expression are upregulated in models of hypertension, contributing to enhanced myogenic tone and altered gene transcription. SHR rats were shown to have enhanced whole-cell calcium currents in isolated vascular smooth muscle cells from young, pre-hypertensive animals (Ohya et al., 1993, Nieves-Cintrón et al., 2008). The difference in current density is insignificant compared with control animals at later stages in the progression of hypertension. (Ohya et al., 1993). Enhanced α_2ó expression has been implicated in increased α_1 surface trafficking in these animals (Bannister, 2012). Other studies have shown an important role for the β_3 subunit in membrane

recruitment of the α_1 subunit during Ang II infusion, as knockout mice for this gene do not demonstrate functional channel upregulation and display significantly lower elevation in blood pressure (Kharade et al., 2013). Endothelin was also shown to upregulate LTCC protein by redox-sensitive activation of the transcription factor NF-κB. This may be a shared pathway between endothelin and Ang II, as preventing synthesis of Ang II through angiotensin converting enzyme (**ACE**) inhibition was found to decrease elevated channel expression in SHR rats (Cox et al., 2002). In addition, local activity of LTCC's in vascular smooth muscle is heterogeneous and channel activity is generally increased in pathological states. This aspect of LTCC physiology is discussed in **Section 1.4**.

Repolarization of Smooth Muscle Membrane

As with other excitable tissues, vascular smooth muscle membrane depolarization is opposed by activation of repolarizing currents through potassium channels. The two major groups of ion channels promoting membrane repolarization in vascular smooth muscle are voltage- gated and calcium-activated potassium channels. Membrane depolarization is directly opposed by activation of voltage-gated potassium ($\mathbf{K_V}$) channels in cerebral arteries. These channels consist of homo- or heterotetramers of six transmembrane- segment α subunits proteins containing a basic S4 segment similar to LTCC's. Voltage-dependent whole-cell potassium currents originate primarily from $K_V1.2$, $K_V1.5$, and $K_V2.1$ channels (Knot and Nelson, 1995; Albarwani et al., 2003; Amberg and Santana, 2006). Pharmacologically isolated steady- state currents from K_V channels in vascular smooth muscle, similar to LTCC's, are small however due to a majority of expressed channels existing in the inactivated state at physiological membrane potentials. Also similar to LTCC currents, depolarization of the membrane across the physiological range of membrane potential increases potassium conductance through K_V channels. These channels play an important role in regulating basal tone (Robertson and Nelson, 1994; Amberg and Santana, 2006), as application of 4- aminopyridine and stromatoxin independently cause vasoconstriction of pressurized cerebral arteries.

Calcium- activated potassium (**K_{Ca}**) channels, including large (**BK**), intermediate (**IK**) and small (**SK**) single-channel conductance species also oppose membrane depolarization in smooth muscle. These may be activated by local calcium signaling through stromal release by RyR's or IP_3R's, conferring basal activity and coupling their activity to metabotropic receptor activation. Spontaneous activity of BK channels, caused by transient release of stromal calcium through closely apposed RyR's (Nelson et al., 1995) is important for regulating basal tone in pressurized cerebral arteries, evidenced by the vasoconstrictor effect of the selective inhibitor iberotoxin (Brayden and Nelson, 1992). BK channels, unlike other K_{Ca} channels contains a S4 voltage sensor, therefore its activity increases with both depolarization and $[Ca^{2+}]_i$. BK channel activity is also regulated by kinases. Specifically, PKA and PKG phosphorylation stimulate channel opening, whereas PKC inhibits its activity (Zhou et al., 2010).

Regulation of potassium channels in hypertension generally promotes a more depolarized resting membrane potential and diminishes opposing hyperpolarizing currents in response to pressure and agonist-induced depolarization, contributing to hyper-reactivity of vascular smooth muscle. Expression assays from SHR rats show decreased $K_v2.1$ mRNA content in various vascular beds compared with controls (Cox et al., 2001). Functional potassium channel downregulation is due in part to Ang II-mediated stimulation of LTCC's. Ang II- induced hypertension decreases expression of $K_v2.1$ channels in cerebral arteries. This is mediated specifically by LTCC- dependent activation of nFATc3 transcriptional regulation (Amberg et al., 2004). This pathway also downregulates $K_V2.1$ expression in a diet-induced diabetes model (Nieves-Cintrón et al., 2015). BK channel activity in the SHR hypertension model and in Ang II- infused rats is also decreased in hypertension. The β_1 subunit of BK channels, which confers sufficient calcium sensitivity for physiological activation, is downregulated in SHR (Amberg and Santana, 2003). Similar to $K_v2.1$, downregulation of this subunit is mediated through AT1R and LTCC- dependent activation of nFATc3 transcriptional inhibition (Nieves-Cintrón et al., 2007). The local regulation of LTCC's by Ang II in physiology and hypertension is discussed in **Section 1.4**.

1.3.4 Smooth Muscle Contraction

In skeletal and cardiac muscle, calcium activates the contractile machinery by binding to troponin C, causing a conformational change in the thin filament architecture allowing interaction between actin bundles (thin filaments) and myosin bundles (thick filaments) in a cycle dependent on ADP/ ATP exchange and ATP hydrolysis. This calcium-dependent cycle causes a ratchet-like shortening of the thin/thick filament complex (sliding filament theory) resulting in cell contraction. Smooth muscle lacks troponin, and calcium sensitivity focuses on thick filament activation instead. In smooth muscle, this process initiated by activation of cytosolic calmodulin by eevation of global $[Ca^{2+}]_I$. This protein in turn associates with an autoinhibitory domain on the smooth muscle-specific myosin light chain kinase (**MLCK**). Phosphorylation of smooth muscle myosin by MLCK greatly increases its affinity for actin and is the major calcium-dependent step in smooth muscle excitation-contraction coupling. Shortening of the contractile apparatus beyond this step is similar to what occurs in skeletal and cardiac muscle. Myosin light chain phosphatase (**MLCP**) directly opposes the myosin phosphorylation by MLCK and is constitutively active, therefore promoting relaxation of smooth muscle in the absence of elevated $[Ca^{2+}]_i$. The balance of activity between MLCK and MLCP directly determines the contractile state of smooth muscle and is a point of physiological regulation. Endothelial NO release causes PKG-mediated phosphorylation of MLCK, inhibiting its kinase activity (Lincoln et al., 2001). Sensitization of the contractile apparatus occurs chiefly through inhibition of MLCP activity by myosin phosphatase targeting proteins. These are linked to activity of AT1R's by upstream activation of Rho- kinase (reviewed in Nguyen Det Cat and Touyz, 2013).

1.3.5 Circulating Factors

Direct humoral regulation of pial artery diameter is generally limited and occurs primarily through receptor- mediated activity in the endothelial layer due to exclusion of non-diffusible circulating

factors from the *tunica media*. The typical response of the cerebral vasculature to circulating factors is vasodilatory, which in some cases is opposite of their effect in other vascular beds and underscores the importance of endothelial function in regulating cerebral blood flow. An example of this vascular bed-specific response is vasodilation in cerebral arteries to the systemic vasoconstrictor arginine vasopressin (Vanhoutte et al., 1984). The inflammatory mediators bradykinin (Bae et al., 2003), histamine (Toda, 1990), ATP, and uridine triphosphate (**UTP**) likewise bind $G_{aq/11}$- coupled receptors in the pial artery endothelium to cause vasodilation. In many cases of endothelium-derived relaxation, PGI_2 production is supplementary to NO production. The role of gap junction-mediated vasorelaxation is plausible but has not been adequately studied with respect to these vasodilatory factors.

Angiotensin

Circulating Ang II is a major active component of the renin-angiotensin- aldosterone system (**RAAS**), and has been extensively studied (reviewed in Phillips, 1987; Sparks et al., 2014). Circulating Ang II is produced through a series of cleavage reactions of the globular protein angiotensinogen which is primarily produced by the liver and released tonically into the blood. Circulating angiotensinogen is cleaved by renin, a protease released by granular cells in the juxtaglomerular apparatus of the kidney in response to either decreased kidney perfusion or sympathetic stimulation. Renin cleaves angiotensinogen into the decapeptide angiotensin I. Angiotensin I is further hydrolyzed to form the active octapeptide Ang II by angiotensin converting enzyme (**ACE**), which exists as an integral membrane protein in pulmonary epithelia and on vascular endothelial cells.

The primary function of circulating Ang II is to restore or enhance renal filtration. Ang II binds to $G_{\alpha q/11}$- coupled AT1R receptors in various organs in a multipronged approach to accomplish this. Restoration of kidney function by circulating Ang II is accomplished by enhancement of renal Na^+ and water uptake in the proximal and distal convoluted tubules directly and by stimulating aldosterone release by the adrenal cortex (reviewed in Sparks et al., 2014). Lesion- based studies demonstrate

circulating Ang II stimulates outputs from the circumventricular organs, namely the subfornical organ (**SFO**)(Meehan and Collister, 2011) and organ of the vascular lamina terminalis (**OVLT**)(Vieira et al., 2010). Stimulation of these nuclei in turn increases systemic blood pressure through stimulating the release of vasopressin by the posterior pituitary. Vasopressin subsequently increases blood volume by enhancing water resorption by the distal collecting tubules in the kidney. Additionally, neurons in the SFO and OVLT project to the cardiovascular control center in the medulla to increase sympathetic outflow and inhibit baroreflex-mediated inhibition of sympathetic flow (Phillips, 1987). In the pial arteries, circulating Ang II has been shown by Doppler estimation of flow to have a small vasodilatory effect *in vivo* (Krejcy et al., 1997) mediated through endothelial NO production (Pueyo et al., 1998). Sympathetic activation occurs in cases of secondary hypertension as a result of renal artery stenosis or kidney damage. This is centrally mediated primarily by elevated circulating Ang II levels in these patients (Catt et al., 1971, reviewed in Zocalli et al., 2002).

1.3.6 Paracrine and Autocrine Factors

Prostaglandins and Endothelin

As discussed above, the endothelium plays a major role in mediating smooth muscle relaxation through paracrine signaling. The endothelium and smooth muscle in the arterial wall also produce vasoconstrictive factors. These include prostaglandins such as PGE_2 and thromboxane A_2. These arachidonic acid metabolites are formed in response to endothelial or smooth muscle damage and bind to ligand-specific G_{aq} family receptors, promoting inflammation and vasoconstriction (reviewed in Riccotini and FitzGerald, 2011). Endothelial cells also tonically release the peptide endothelin. Endothelin is a potent vasoconstrictor which binds to ET_A receptors on vascular smooth muscle cells. The effect of ET_A receptor activation in smooth muscle exhibits considerable overlap with the effect of Ang II which is described in more detail in the following section. This is owed in part to activation of

similar second- messenger signaling cascades. NO negatively regulates endothelin synthesis, thus in the event of endothelial dysfunction endothelin signaling becomes enhanced (reviewed in Thorin and Webb, 2010).

Local renin-angiotensin system

In addition to circulating Ang II, many local paracrine and autocrine signaling systems including the heart, brain and vasculature produce endogenous Ang II, (reviewed in Paul et al., 2007). Both the endothelium and smooth muscle cells in arteries have been shown to produce endogenous Ang II. Activity of the vascular renin- angiotensin system is upregulated under conditions such as increased shear stress, (Delli Gatti et al., 2008) and insulin resistance (Shinozaki et al., 2004; Lavrentyev, 2007) where ligand-mediated receptor activation acts synergistically with stretch-induced receptor activation. The major plasma membrane target of Ang II in smooth muscle is the AT1R, although these cells additionally express type-2 angiotensin receptors (**AT2R**'s). AT1R activation leads to pleiotropic downstream effects regulating contraction, secretion, and gene transcription, producing immediate and long-term effects with respect to the physiology of these cells.

A major initial step in signal transduction by AT1R activation is PIP_2 cleavage and formation of DAG and IP_3 by PLCβ and/or PLCγ. While PLCβ activation is directly mediated by receptor stimulation, PLCγ is activated by tyrosine phosphorylation. Src- family tyrosine kinases including cSrc and Pyk2 could potentially mediate this pathway, as both are shown to be activated downstream of AT1R in cultured vascular smooth muscle cells (Eguchi et al., 1999; Touyz et al., 2001). Pyk2 is calcium-sensitive and may be activated by IP_3R or plasmalemmal calcium entry, providing a possible link between G-protein and tyrosine kinase activation in vascular smooth muscle. Alternately, the receptor tyrosine kinase, epidermal growth factor receptor (**EGFR**) has also been shown to be rapidly activated following AT1R activation and both cSrc and Pyk2 are activated downstream of this event (Eguchi et al., 1998). DAG along with calcium possibly liberated by IP_3 is crucial in the canonical activation of PKC, in addition to its

previously described role in mediation of stretch- induced depolarization. PKC plays a role in basal and pressure-induced myogenic tone (Osol et al, 1991; Amberg et al., 2007) and local activation of LTCC's in vascular smooth muscle cells (discussed in **Section 1.4**) Phospholipase A (**PLA**) activation occurs downstream of tyrosine kinases, leading to paracrine release of prostaglandins. Phosphatidylinositol- 3 kinase (**PI3K**) activation likewise occurs subsequent to AT1R stimulation, and may be directly mediated by the receptor (Murga et al., 1998) or subsequent to tyrosine kinase activation (Saward and Zahradka, 1997).

Reactive oxygen species

ROS serves as a subcellular and paracrine mediator of $G_{\alpha q}$ and receptor tyrosine kinase signaling. Ang II is a well characterized mediator of agonist-induced ROS production in many cell types including vascular smooth muscle (Griendling et al., 1994), endothelial cells (Li and Shah, 2003), cardoimyocytes (Xie et al., 2001), and neurons (Wang et al., 2004; Sun et al., 2005; Chan et al., 2009). Perivascular adipose tissue and insulin resistance likewise increase vascular ROS signaling.

A major source of cellular ROS produced by Ang II in each of these systems is plasmalemmal NAD(P)H oxidase. The non-phagocytic NAD(P)H oxidase isoform Nox1 primarily mediates ROS formation in vascular smooth muscle (Lassègue et al., 2001) and exists as an inactive heterodimer of the catalytic (Nox1) and membrane-associated (p22) subunits at the plasma membrane. Catalytic activity may be initiated by tyrosine kinase (Touyz et al., 1999) and/or PKC- mediated (Brown and Griendling, 2009) phosphorylation of the cytosolic organizational subunit Noxo1 to facilitate interaction between Noxo1 and the catalytic domain- activating Noxa1 subunits. These are targeted to the cell membrane by Rac1 GTPase, mediated through activity of PI3K (reviewed in Pick, 2014). The assembled tetramer oxidizes NADPH to $NADP^+$ and a free proton, and reduces extracellular oxygen to form superoxide ($\mathbf{O_2^-}$). O_2^- is highly reactive and is rapidly degraded spontaneously or enzymatically to the uncharged stable ROS, hydrogen peroxide (H_2O_2) by superoxide dismutase. H_2O_2 can then passively re-enter the cell and modify

protein activity through oxidation. O_2^- additionally reacts with NO to form the reactive species peroxynitrite (**$ONOO^-$**), reducing NO bioavailability. $ONOO^-$ directly oxidizes the eNOS cofactor BH_4, preventing NO production (reviewed in Fukai and Ushio-Fukai, 2011). $ONOO^-$ forms covalent bonds with amino acid residues on proteins to modify their activity similar to the effect of H_2O_2 discussed below, although the affinity of specific residues for the two species differs.

Another major cellular source of ROS is the mitochondrial electron transport chain (**ETC**), and mitochondrial ROS have been shown to contribute to Ang II-induced oxidative signaling in neurons, cardiomyocytes, vascular endothelium, and smooth muscle. Ideally, this group of enzymes located on the mitochondrial inner membrane oxidize $NADH_2$ or succinate (at complexes I and II respectively) and bind the free electrons from this oxidation. Energy is released by moving these electrons through successively stronger electron acceptor sites on the inner membrane. The released free energy is subsequently used to move protons across the inner membrane from the matrix to the intermembrane space. This creates an electrical and proton gradient across the inner membrane. Two protons and two electrons combine with O_2, the final oxidizing agent in the electron transport chain to form molecular water. The electrochemical gradient across the inner membrane is utilized by ATP synthase to couple proton re-entry to phosphodiester bond formation, converting ADP to ATP.

Occasional premature release of electrons from the ETC results in formation of mitochondrial O_2^-. Similar to O_2^- formed by NAD(P)H oxidase, mitochondrial O_2^- is rapidly converted to H_2O_2. The rate of O_2^- production can be increased by enhanced fatty acid or glucose metabolism. Additionally, mitochondrial ROS production can be stimulated by increasing the matrix volume. Swelling deforms the inner membrane and decreases the efficiency of the assembled ETC complexes. Subsequent transient increases in superoxide production are linked to potassium currents directed into the mitochondrial matrix through mitochondrial K_{ATP} channels (**mitoK_{ATP}**). This has been demonstrated to be crucial in Ang II-mediated cardioprotection during ischemia using the selective mitoK_{ATP} opener diazoxide and inhibitor

5-hydroxydecanoate (5-HD) (Kimura et al., 2005). 5-HD was also demonstrated to attenuate Ang II-induced endothelial dysfunction (Doughan et al., 2008). Cardiomyocyte mitoK_{ATP} channels are redox-sensitive and opening can be obtained by treatment with exogenous H_2O_2 (Facundo et al., 2007). Ang II signaling in neurons (Chan et al., 2009), cardiomyocytes (Kimura et al., 2005), and endothelial cells (Doughan et al, 2008) shows a dependence of mitochondrial ROS release on NAD(P)H oxidase activation. Through this mechanism termed "ROS-induced ROS release", signaling can be amplified beyond a certain threshold of initial activity.

The reversible oxidation of protein sulfhydryl groups is diagrammed in **Figure 1.1**. H_2O_2 modifies thiols on exposed cysteine and methionine residues by formation of sulfenic acid or methionine sulfoxide groups. This is dependent on the stability of the sulfhydryl bond in these residues, preferentially oxidizing low pK_a sites. Sulfenic acids represent a reversible mechanism by which H_2O_2 can participate in intracellular signaling through reversible modification of proteins, analogous to phosphorylation. Sulfenic acids may be spontaneously converted to disulfide bonds by a dehydration reaction involving other thiol groups. These may be from within the same protein, froming an intramolecular disulfide bond, or from another source. Soluble glutathione (**GSH**) may be involved in these reactions to form a glutathionylated product. Intra- or intermolecular disulfide bonds can be reduced enzymatically reduced by thioredoxin (**Trx**). Trx is regenerated by Trx reductase, which couples Trx reduction to oxidation of NADPH to $NADP^+$.

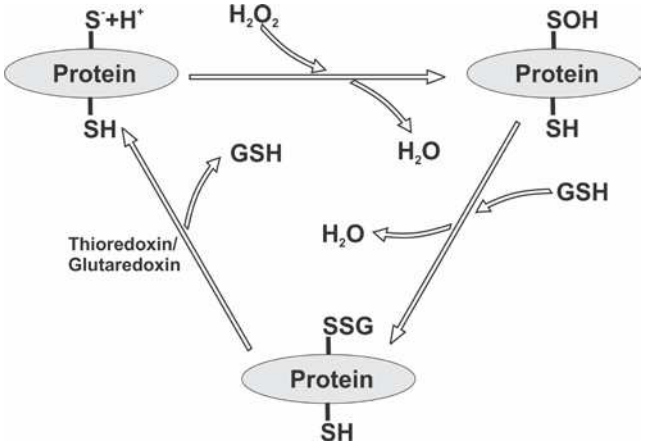

Figure 1.1. Reversible oxidation of low pK_a cysteine thiol residues by H_2O_2. Exposed cysteine residues with weak hydroxyl bonds may be selectively oxidized by H_2O_2 to form sulfenic acid. Sulfenica acid can subsequently form a disulfide bond with another sulfhydryl-containing molecule such as glutathione. Disulfides can be catalytically reduced by thioredoxin or in the case of glutathionylated proteins, glutaredoxin, to regenerate reduced cysteine residues.

Glutationylated cysteines may also be reduced by glutaredoxin (reviewed in Klomsiri et al., 2011).

Tyrosine phosphatase active sites commonly employ acidic cysteine residues at their active site, and these enzymes represent a group of effector proteins for ROS regulation (reviewed by Klomsiri et al., 2011). This illustrates a mechanism through which unchecked ROS activity broadly enhances protein kinase activity, leading to various outcomes. In other proteins, oxidation of sulfhydryl groups causes a conformational change which may up- or down-regulate protein activity. Oxidation of PKCα (Gopalakrishna and Anderson, 1989; Knapp and Klann, 2000) and cSrc (Abe et al., 1997) by low levels of exogenous H_2O_2 has been demonstrated. In both instances, this involves removal of autoinhibition, conferring catalytic activity on these proteins. Because these kinases are involved in inactivation of peroxiredoxins (discussed below) and activation of NAD(P)H oxidase, ROS can be seen as a potential means of feed- forward amplification of Ang II signaling. Physiologically this may be necessary to maintain basal activity of various pathways involved in protein expression and survivability.

Because it is inherently toxic to cells, buffering systems have been developed to neutralize cytosolic and mitochondrial ROS, leading to spatial restriction of its activity under physiological conditions. The rapid conversion of highly reactive O_2^- to H_2O_2 is catalyzed by cytosolic, mitochondrial, or extracellular superoxide dismutase (**SOD1-3**, respectively) (reviewed in Fukai and Ushio-Fukai, 2011). H_2O_2 is neutralized through a series of redox reactions within the cytosol or mitochondrial matrix. This is chiefly accomplished initially through oxidation of the peroxiredoxin (**Prx**) family of enzymes and reduction of H_2O_2. These enzymes exist as homodimers and form disulfide bridges between specific cysteine residues on apposed monomers during H_2O_2 neutralization. These disulfide bonds are reduced by Trx to regenerate Prx dimers, forming an internal disulfide bond in Trx. The reaction rate of Prx with H_2O_2 is several orders of magnitude higher than other oxidative targets, favoring its reaction over other proteins given sufficient activity (reviewed in Rhee et al., 2011). Glutathione peroxidase (**Gpx**), serves as a secondary ROS buffer. Similar to Prx, Gpx can reduce H_2O_2, converting GSH to an oxidized homodimer

containing a disulfide bond (**GSSG**). Gpx activity is limited by the availability of GSH, which typically is abundant in the cytosol. GSSG is reduced by glutathione reductase, which is in turn reduced by oxidation of NADPH (reviewed in Iwasaki et al., 2009). Both Gpx and Prx depend on availability of NADPH for sustained activity. Sustained local ROS production can lead to diminishment of NADPH through regeneration of peroxidase activity and additionally by NAD(P)H) oxidase, forming microdomains which allow oxidation of other targets. Additionally, tyrosine phosphorylation of cytosolic Prx1 inhibits its activity (Rhee et al., 2011), providing another mechanism for local regulation of ROS microdomain signaling.

The spatial restriction of H_2O_2 signaling protects cells from the adverse effects of nonspecific oxidative modification of cellular proteins, while also allowing regulation of divergent signaling processes even within the same cell dependent on the localization of H_2O_2 sources and effectors. This is akin to divergent calcium signaling seen in smooth muscle and other cell types. In support of this concept, exogenous and endogenous H_2O_2 has been shown by different groups to mediate both vasoconstriction (Amberg et al., 2010; Nowicki et al., 2001; Tabet et al., 2004) and vasodilation (Hayabuchi et al., 1998; Iida and Katusic, 2000; Liu et al., 2011; Matoba et al., 2000; Xi et al., 2005) in various arterial beds. The vasoconstrictive response in these studies is derived at least in part from enhancement of LTCC current, while vasodilation was shown to be mediated by increased BK_{Ca}, and K_V channel activity.

Paracrine/ autocrine influence on the pathogenesis of arterial hypertension

Chronic activation of the vascular renin- angiotensin system and enhanced endothelin production contributes largely to the pathogenesis of hypertension. Vascular smooth muscle characteristically undergoes transition between a contractile and proliferative phenotype, dependent on a large number of inputs from its local environment. This is physiologically important for repair of damaged vessel walls and angiogenesis. By activating tyrosine kinase-, calcium-, and redox-sensitive

signaling pathways, paracrine signaling in the vascular wall contributes to maintaining a contractile phenotype and promotes cell survival in smooth muscle.

In general, transcriptional modification in vascular smooth muscle during the pathogenesis of hypertension leads to enhanced tissue inflammation, augmented sensitivity to vasoconstrictor stimuli, remodeling of vascular wall matrix constituents, and increased myogenic tone. As the pathology progresses, this eventually results in sclerotic plaque formation and vessel remodeling as described in **Section 1.2**. Increased calcium signaling specifically through LTCC's in smooth muscle leads to activation of the calcium- sensitive transcription pathways including nFATc3 (Nieves- Cintrón et al, 2008), CREB (Wellman et al, 2001) and contributes to activation of NF-κB (Ortego et al., 1999). Tyrosine kinase-dependent transcriptional pathways activated by Ang II in vascular smooth muscle include extracellular receptor kinase (**ERK**), p38mitogen- activated protein kinase (**p38MAPK**), and c-jun N- terminal kinase (**JNK**) (Eguchi et al., 2001). JNK phosphorylation is additionally involved in calcium sensitization if the contractile apparatus (Guilluy et al., 2010) and plays a direct role in activation of transcription through the AP-1 pathway. Redox- sensitive transcription pathways linked to AT1R activation include NF-κB, p38MAPK, and AP-1. NF-κB and p-38MAPK activation increases expression of pro-inflammatory cytokines in response to AT1R activation (Han et al., 1999) and NF-κB may increase surface trafficking of LTCC's in some hypertensive models (Narayanan et al., 2010). Additionally, NAD(P)H oxidase subunit expression is upregulated by Ang II treatment (Touyz et al., 2002) and in vascular smooth muscle from SHR, and AT1R and ET1 activation enhance its expression in WKY controls (Briones et al., 2011). Upregulation of multiple components of Ang II signaling postulates a feed-forward cycle of vascular reactivity and transcriptional modification pathologically.

1.4 L-type Calcium Channel Sparklets

1.4.1 Early Characterization of Sparklets

The term “sparklets” was first used to describe optical recordings of calcium flux through single L-type calcium channels in isolated ventricular myocytes (Wang et al., 2001). These recordings were performed using a confocal line-scan setup in which cells were stimulated with either membrane depolarization or with a pharmacological L-type channel agonist (FPL64176). Using the cell-permeable ratiometric Ca^{2+} indicator Fura-2, this group was able to simultaneously record unitary Ca^{2} influx events both as increases in fluorescence in a confocal line scan set at the plane of a cell- attached micropipette and complementary inward currents from the electrode. Due to rapid intracellular buffering and diffusion of both calcium and calcium-bound fluorophores away from the channel, temporal resolution of calcium influx was closely comparable between the two data acquisition techniques. Demuro and Parker (2004) successfully added a second dimension to acquisition of sparklet data by developing a total internal reflection fluorescence (**TIRF**) system using a wide-field fluorescence microscope to simultaneously view plasmalemmal calcium transients over a large area of the cell membrane of xenopus oocytes transfected with N-type calcium channels.

Briefly, TIRF utilizes a through-the-lens laser focusing setup and an objective with a large numerical aperture. Thiis allows positioning of the focused light beam at an oblique angle relative to the coverslip such that when the beam encounters the coverslip/imaging solution interface, the change in refractive index causes the beam to be reflected away from the sample rather than penetrate it. While the beam is entirely reflected in this setup, a shallow (<200nm) electromagnetic field is produced within the solution with the same energetic characteristics as the light beam. This wave can therefore excite fluorophores which would be excited by the wavelength of light produced by that beam exclusively within the evanescent field.

1.4.2 Sparklets in Vascular Smooth Muscle

The 2004 study by Demuro and Parker revealed heterogeneity in single- channel gating characteristics among the population of N-type channels within single cells. Subsequent to this discovery, the Santana lab adapted this technique toinvestigate heterogeneous LTCC activity in the cardiovascular system. Smooth muscle sparklets were investigated by Navedo et al., (2005) in isolated myocytes using a TIRF microscope similar to Demuro and Parker (2004). This group used the whole-cell dialyzed configuration of patch- clamp electrophysiology to gain voltage control over the cells. To improve temporal resolution, a high concentration (10mM, compared with 200μM fluorophore) of the calcium chelator ethylene glycol tetraacetic acid (**EGTA**) was included in the intracellular solution , as the incoming calcium binds first to the fluorophore due to preferential binding kinetics, and is subsequently chelated by the nonfluorescent, but more abundant EGTA.

Native LTCC sparklets were characterized pharmacologically by demonstrating their sensitivity to the dihydropyridine agonist Bay-K 8644 and antagonist nifedipine (Navedo et al., 2005). Furthermore, vascular smooth muscle cells from transgenic mice expressing dihydropyridine insensitive $Ca_v1.2$ retained basal sparklet activity in the presence of nifedipine (Navedo et al., 2007). To biophysically associate sparklets with LTCC's, simultaneous TIRF imaging and whole-cell current traces were analyzed. Because the calcium indicator fluo-5F is ratiometric, the change in calcium concentration at the mouth of the channel could be calculated, then converted to instantaneous current by plotting the concentration vs. the measured inward current recorded corresponding to the fluorescence recording. The quantal value was then plotted against voltage by performing a series of voltage step protocols to yield the single- channel slope conductance. This was then compared to the slope conductance given by isolated nifedipine-sensitive single- channel current traces using a similar voltage step protocol. These values were statistically identical (10.1pS from sparklet recordings vs 10.9pS from cell-attached recordings in 20mM $[Ca^{2+}]_e$) (Navedo et al., 2005). Additionally, heterologous expression of $Ca_V1.2$

yielded statistically identical quantal calcium influx concentration profiles under identical recording conditions at various membrane voltages (Navedo et al., 2006).

Native LTCC's in vascular smooth muscle were observed to have heterogeneous activity across the membrane under basal conditions (Navedo, 2005). Cells voltage clamped at -70mV featured rare loci which showed persistent gating termed "high activity sparklets", in addition to occasional gating at other sites termed "low activity sparklets". A bimodal distribution of open probability was observed, determined by the number of quantal influx events per active site during the recording ($\boldsymbol{nP_s}$, analogous to nP_o values obtained from cell-attached or excised patch recordings), identifying the two groups as separate populations. The difference in nP_s between these populations arises from the frequency and number of gating events, in addition to the apparent dwell time in the open state when gating occurs, as time constants for high activity sparklets are best modeled by a slow and fast component (Amberg et al, 2007). Within a sparklet site, multiple quantal events may occur simultaneously. Optically, this results in summation of the fluorescence signature. An all-points histogram shows that the change in $[Ca^{2+}]_i$ fits a multiple- component Gaussian curve with peaks centered around multiples of the quantal value (i.e. 35nM, 70nM, 105nM, etc.).The probability of multiple simultaneous events is low compared with unitary events, and shows a progressive trend toward decreased likelihood as quantal level increases. With exception of these sites the majority of the membrane remained optically silent, fitting with the low (around 10^{-8}) voltage-dependent single channel open probability at -70mV (Quayle et al., 1993b). Although sparklet sites nP_s is higher than predicted, sparklet activity retains voltage dependence. Increasing the membrane voltage from -70mV to -40 increases the mean nP_s of both high and low activity sparklets (Amberg et al., 2007).

1.4.3 High Activity Sparklets

Low and high activity LTCC sparklets differ in both their physiological regulation and the downstream consequences of their activity. While each of these phenomena contribute nearly equally to steady-state global calcium levels under physiological conditions (Amberg et al., 2007), high activity sparklets are upregulated by metabotropic receptor activation and in disease models, where their influence critically affects both smooth muscle contraction and transcription.

Importance in Regulation of Tone

In addition to regulation of transcription, PKC-dependant regulation of sparklet activity is physiologically relevant in smooth muscle contraction. This was demonstrated by Amberg et al. (2007) in dialyzed, voltage clamped (at -70mV) cerebral myocytes by excluding EGTA from the intracellular pipette solution and decreasing extracellular calcium to physiological concentrations. To image both sarcolemmal sparklet events and global calcium levels, the laser angle was adjusted to slightly exceed the critical TIRF angle, allowing visualization of sparklets as spatiotemporally discreet spikes in fluorescence and global cytosolic calcium as a more uniform and stable background signal. In control myocytes, after one or two initial events, individual sparklets resulted in a direct increase in global calcium. The inclusion of a PKC inhibitory peptide prevented sparklet activity and resulted in a slow, diminished increase in global fluorescence. Treatment of cells with the PKC inhibitor of Gö6976 reduces the amplitude of whole-cell calcium currents induced by membrane depolarization by roughly half (Navedo et al., 2008). This also translates to a role in vessel diameter regulation. Bath application of Gö6976 decreases vessel wall [Ca^{2+}] in pressurized resistance arteries to a similar degree and caused vasodilation (Amberg et al., 2007). Additionally, PKC$\alpha^{-/-}$ and AKAP$^{-/-}$ arteries have lower basal arterial wall [Ca^{2+}], and exhibited diminished myogenic tone compared with wild-type controls (Navedo et al., 2008; Nieves-Cintrón et al., 2008). These experiments lead to the conclusion that under physiological

conditions, high activity sparklets under the control of PKCα contribute significantly to the maintenance of smooth muscle calcium to regulate arterial tone.

Regulation by intracellular kinase activity

The heterogeneity of LTCC activity in vascular smooth muscle is mediated not by distribution of the channel across the membrane, but of key regulatory elements which modulate channel gating. A major role for PKC was observed by Navedo et al. (2005) by observing the enhancement of sparklet activity by the DAG analog phorbol 12, 13-dibutyrate (**PDBU**) and abolition of high activity sparklets activity by inclusion of a PKC inhibitory peptide in the intracellular solution, even in the presence of PDBU. A key finding from these experiments was that addition of PDBU increased the number of high activity sparklet sites by upregulating activity at low activity or previously silent sites. PDBU did not increase activity at already established high activity sites. In addition, heterologously expressed functional $Ca_V1.2$ in voltage-clamped tSA201 cells requires coexpression of PKC for basal sparklet activity, and transgenic mice lacking PKCα (*PKCα*$^{-/-}$) do not exhibit high activity sparklets (Navedo et al., 2006). Additionally, pharmacological inhibition of the serine/ threonine phosphatases calcineurin (**CaN**) and protein phosphatase 2A (**PP2A**) each increased the occurrence of high activity sparklets in a PKC-dependent manner in voltage clamped cells (Navedo et al., 2006). Taken together, these studies suggest that basal high activity sparklet sites are under the local control of a kinase/ phosphatase system favoring kinase activity, and that increasing PKC activity can tip the balance in favor of kinase activity at additional sites. Exposure of vascular smooth muscle cells to forskolin, an activator of adenylyl cyclase, similarly results in enhanced LTCC sparklet activity, implicating PKA as an alternate kinase involved in native regulation of sparklets (Navedo et al., 2010).

Regulation by AKAP150

Interestingly, high activity sparklets, even in the presence of agonists such as PDBU and forskolin, and additionally in cells treated with protein phosphatase inhibitors, are confined to a very

small portion of the cell membrane. Conversely, inclusion of the PKC catalytic domain in the intracellular pipette solution causes homogeneous activation of calcium influx across the smooth muscle membrane (Navedo et al., 2005). This suggests functional coupling of active kinases to LTCC's determines local sparklet activity. AKAP150 was shown to mediate this interaction in vascular smooth muscle, as vascular myocytes from transgenic mice lacking the gene for AKAP 150 (*AKAP150*$^{-/-}$) were found to lack basal sparklet activity and are insensitive to PDBU stimulation of sparklet activity (Navedo et al., 2008).

The association with AKAP 150 identifies a potential role for high activity sparklets in transcriptional regulation by nFAT (**see Section 1.3).** This was confirmed in cultured arterial myocytes by transfection with a green fluorescent protein-fused nFATc3 (**nFATc3-EGFP**). Confocal imaging showed nuclear translocation nFATc3-EGFP upon stimulation by PDBU. Translocation was blocked by inhibition of LTCC activity by nifedipine. This was shown to be dependent on a local rather than global increase in $[Ca^{2+}]_i$ by chelating global $[Ca^{2+}]_i$ with the acetomethoxy ester of 1,2-bis(o-aminophenoxy)ethane-N,N,N',N'-tetraacetic acid (**BAPTA-AM**) (Nieves-Cintrón et al., 2008). AKAP150 anchored calcineurin specifically is likely to mediate nFATc3 activation in this setup, where it can interact with calmodulin activated at the mouth of the LTCC prior to BAPTA chelation of $[Ca]_i$.

Regulation by AT1R activation

The known interactions among the signaling components within the Ang II- LTCC sparklet microdomain described in this section are summarized in **Figure 1.2**. Ang II, acting through PKC recruited to the cell membrane by AKAP150, stimulates sparklet activity in smooth muscle in much the same manner as PDBU. Voltage-clamped arterial myocytes exposed to Ang II in the bath solution show an increase in both high and low activity sparklets in a spatially limited manner across the cell membrane (Nieves-Cintrón et al., 2008). Ang II- induced activation of sparklets does not occur in myocytes isolated from *PKCα*$^{-/-}$ or *AKAP150*$^{-/-}$ mice, indicating this pathway was important for Ang II mediated sparklet

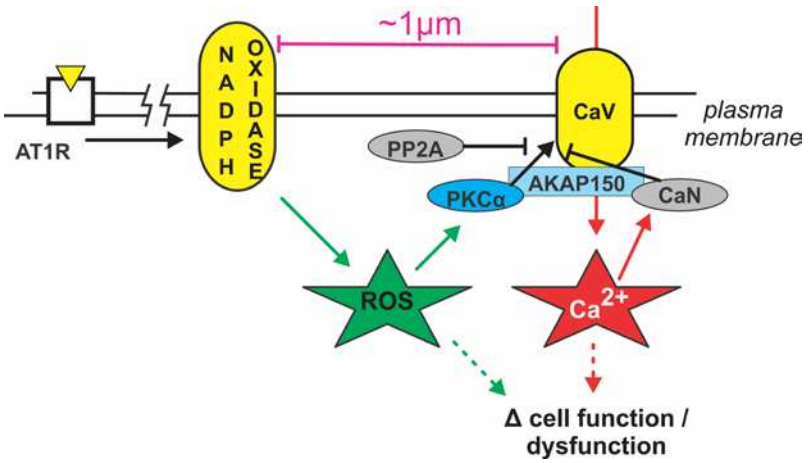

Figure 1.2. Previous model for Ang II-induced activation of LTCC sparklets. Activation of AT1R on the plasma membrane stimulates ROS production by NAD(P)H oxidase. This ROS is released into a plasmalemmal microdomain within 1µm of a target L-type calcium channel. PKC targeted to this microdomain by the scaffolding protein AKAP150 mediates channel activation. This activity is opposed by competing phosphatases present in the cytosol (PP2A) and localized by AKAP150 (CaN).

activity. Mutation of the PKA binding site on AKAP150 does not confer the same insensitivity to Ang II (Navedo et al., 2008). Similarly, pressurized arteries from each of these knockout models groups respond minimally to the vasoconstrictive effect of extraluminal Ang II compared with arteries from wild-type controls. Increased blood pressure resulting from in-vivo chronic Ang II infusion was also diminished in these groups compared to wild-type controls (Nieves-Cintrón et al., 2008; Navedo et al., 2008). Taken together these studies show a direct link between local regulation of smooth muscle LTCC's by Ang II and physiological regulation of myogenic tone.

Ang II- and PKC-dependent sparklet activity is also important in the development of hypertension. This pathway is linked to activation of nFATc3-mediated gene expression, and sparklet activity becomes upregulatied during the pathogenesis of hypertension. Cultured human arterial smooth muscle cells exposed to Ang II for 48h show a decrease in $K_v2.1$ expression, and this action is mediated through an nFAT-sensitive pathway. Fittingly, *PKC*$^{-/-}$ and *AKAP150*$^{-/-}$ mice infused with Ang II do not develop as steep an increase in blood pressure as wild-type mice. Investigation of voltage-controlled isolated arterial myocytes from these three groups shows an increase in basal sparklet activity only in in wild type mice receiving Ang II infusion. Isolated myocytes from SHR rats also exhibit increased basal sparklet activity (Nieves-Cintrón et al., 2008; Navedo et al., 2008), suggesting this signaling pathway is upregulated pathologically.

Role of Reactive Oxygen Species

High activity LTCC sparklets persist over relatively long time-courses. This suggests a mechanism to maintain local kinase/phosphatase activity to favor phosphorylation should occur in the area around high activity sparklet sites. ROS, as a known mediator of Ang II signaling fulfills this role in a spatially discreet manner. As mentioned in **Section 1.3,** PKC and competing phosphatases are targets for modulation by ROS. Cysteine oxidation in either of these targets should encourage temporal stability of high activity sparklets. Fitting with this, Ang II- induced sparklets are demonstrated by Amberg et al. (2010) to be sensitive to the NAD(P)H oxidase inhibitor apocynin. In agreement with previous reports on basal oxidative activity of vascular smooth muscle by NAD(P)H oxidase (Bassett et al, 2009), treatment of vascular smooth cells with the redox-sensitive lipophilic fluorescent indicator 2',7'-dichlorodihydrofluorescein diacetate (**DCF**) reveals rare, punctate (<1µm wide) areas of enhanced fluorescence using TIRF. Exposing these cells to Ang II promotes a significant increase in surface density of these puncta. In cells treated with DCF, exposed to Ang II, and subsequently dialyzed with a calcium fluorophore and voltage clamped, high activity sparklets specifically localize within 1µm of an accompanying plasmalemmal DCF puncta (Amberg et al., 2010).

The role of local kinase/phosphatase balance in this interaction is also demonstrated by Amberg et al. (2010). Bath application of the ROS-generation system xanthine and xanthine oxidase produces high and low activity sparklets in voltage-clamped arterial myocytes with a spatial distribution similar to that of other systems used to promote sparklet activity. The lack of widespread LTCC activation with this treatment suggests channel oxidation is not the mechanism by which local ROS interacts with LTCC's. Furthermore, pretreatment of cells with a PKC inhibitor (Gö6976) attenuated ROS- induced sparklet activity, and immunocytochemistry revealed an increase in surface expression of PKCα in cells exposed to xanthine and xanthine oxidase. In conclusion, this study expands the scope of previous investigations of vascular smooth muscle sparklets by linking observed calcium influx to activation of ROS microdomain

signaling. This association provides a plausible point of convergence for Ang II and other mediators of oxidative stress in chronic elevation of vessel wall calcium contributing to the pathogenesis of hypertension. This study further investigates mechanisms coordinating this signaling pathway and may provide insight into unique therapeutic target for maintaining vascular health in populations at-risk for vascular disease.

1.5 Central Hypothesis and Key Observations

The current study detailed in the following sections expands this investigation of Ang II- and ROS mediated sparklet regulation. The central hypothesis of this dissertation is that the subplasmalemmal hydrogen peroxide sources NAD(P)H oxidase and mitochondria coordinate an oxidative response to extracellular angiotensin signaling which modifies local PKCα activity to promote high activity gating of discreet populations of L-type calcium channels under physiological and pathophysiological conditions. Key observations from the following chapters in support of this hypothesis are:

1. Hydrogen peroxide is required for angiotensin- induced high activity L-type calcium channel sparklets.
2. Cofactor- independent activation of PKCα is required for high activity sparklet activity.
3. NAD(P)H oxidase and mitochondria concertedly produce punctate plasmalemmal hydrogen peroxide domains which directly colocalize with and critically regulate high activity sparklet sites.
4. Both NAD(P)H oxidase and mitochondrial hydrogen peroxide production are required for angiotensin- induced high activity sparklets

Chapter 2. Hydrogen peroxide mediates oxidant-dependent stimulation of arterial smooth muscle L-type calcium channels[1]

2.1 Summary

Changes in calcium and redox homeostasis influence multiple cellular processes. Dysregulation of these signaling modalities is associated with pathology in cardiovascular, neuronal, endocrine, and other physiological systems. Calcium and oxidant signaling mechanisms are frequently inferred to be functionally related. To address and clarify this clinically relevant issue in the vasculature we tested the hypothesis that the ubiquitous reactive oxygen molecule hydrogen peroxide mediates oxidant-dependent stimulation of cerebral arterial smooth muscle L-type calcium channels. Using a combinatorial approach including intact arterial manipulations, electrophysiology, and total internal reflection fluorescence imaging, we found that application of physiological levels of hydrogen peroxide to isolated arterial smooth muscle cells increased localized calcium influx through L-type calcium channels. Similarly, oxidant-dependent stimulation of L-type calcium channels by the vasoconstrictor angiotensin II was abolished by intracellular application of catalase. Catalase also prevented angiotensin II from increasing localized subplasmalemmal sites of increased oxidation previously associated with colocalized calcium influx through L-type channels. Furthermore, catalase largely attenuated the contractile response of intact cerebral arterial segments to angiotensin II. In contrast, enhanced dismutation of superoxide to hydrogen peroxide with superoxide dismutase had no effect on angiotensin-dependent stimulation of L-type calcium channels. From these data we conclude that hydrogen peroxide is important for oxidant-dependent regulation of smooth muscle L-type calcium channels and arterial function. These data also support the emerging concept of hydrogen peroxide as a

[1] Chaplin NL, Amberg GC (2012) Hydrogen peroxide mediates oxidant-dependent stimulation of arterial smooth muscle L-type calcium channels. Am J Physiol Cell Physiol; 302(9):C1382-1393. doi: 10.1152/ajpcell.00222.2011

biologically relevant oxidant second messenger in multiple cell types with a diverse array of physiological functions.

2.2 Introduction

Calcium (Ca^{2+}) and redox signaling cascades are important modulators of cellular function. In many cell types, including arterial smooth muscle, direct and indirect evidence suggests that crosstalk occurs between Ca^{2+} and redox signaling cascades under physiological and pathophysiological conditions (Ermak and Davies, 2002; Hidalgo and Donoso, 2008; Trebek et al., 2010). Consistent with this, concomitant increases in Ca^{2+} influx and oxidative stress are associated with vascular diseases including hypertension, stroke, and atherosclerosis (Nieves-Cintrón, 2008; Touyz, 2000; Touyz and Schiffrin, 2000; Wellman et al., 2001). Thus, examination of mechanisms involved with the crosstalk between Ca^{2+} and redox signaling is of fundamental importance in understanding arterial function and dysfunction in health and disease.

Previously we used total internal reflection fluorescence (TIRF) imaging to investigate oxidant-dependent stimulation of L-type Ca^{2+} channels in arterial smooth muscle cells (Amberg et al., 2010). This approach revealed that exogenous reactive oxygen species (ROS) generated by xanthine oxidase stimulated localized Ca^{2+} influx through L-type Ca^{2+} channels (i.e., "Ca^{2+} sparklets"). Furthermore, the vasoconstrictor angiotensin II (Ang II) induced punctate generation of subplasmalemmal ROS that preceded and colocalized with subsequent L-type Ca^{2+} channel activity. While these observations demonstrate that ROS promote L-type Ca^{2+} channel function and that the spatial distribution of local ROS generation mirrors that of local Ca^{2+} influx through L-type Ca^{2+} channels, the identity of the participating ROS linking these Ca^{2+} and redox signaling events is unclear.

Hydrogen peroxide (H_2O_2) is an important ROS signaling molecule (Forman et al., 2010; Mishina et al., 2011; Veal and Day, 2011). H_2O_2-dependent modulation of protein function is thought to occur by

oxidation of key amino acids (e.g., cysteine) that operate as allosteric redox-dependent switches. As with most cell types, major sources of H_2O_2 in arterial smooth muscle cells include NADPH oxidase (Nox) enzyme complexes and the mitochondrial electron transport chain. Previous work demonstrated that H_2O_2 regulates macroscopic recombinant L-type Ca^{2+} currents (Hudasek et al., 2004). However, the role of H_2O_2 in oxidative stimulation of localized arterial smooth muscle L-type Ca^{2+} channels has not been investigated.

In this study we tested the hypothesis that H_2O_2 mediates oxidant-dependent stimulation of L-type Ca^{2+} channels in rat cerebral arterial smooth muscle cells. We found that exogenous H_2O_2 increased not only macroscopic L-type Ca^{2+} channel currents but, more importantly, that H_2O_2-dependent increases in L-type Ca^{2+} channel function was localized. Conversely, removal of endogenous H_2O_2 with catalase abolished Ang II-dependent stimulation of L-type Ca^{2+} channels. Consistent with these observations, catalase also prevented increases in punctate subplasmalemmal ROS generation following Ang II exposure and attenuated Ang II-dependent constriction of pressurized cerebral arterial segments. In contrast to removal of H_2O_2 with catalase, enhanced dismutation of superoxide (to H_2O_2) had no effect on ROS puncta formation or Ang II-dependent stimulation of L-type Ca^{2+} channels. Taken together, these data provide compelling evidence that in rat cerebral arterial smooth muscle cells, physiologically-relevant oxidant-dependent stimulation of L-type Ca^{2+} channels is mediated by locally produced H_2O_2.

2.3 Materials and Methods

Isolation of rat cerebral arterial myocytes

Adult male Sprague-Dawley rats (Harlan, Indianapolis, IN) were euthanized with sodium pentobarbital (200 mg/kg intraperitoneally; Fort Dodge Animal Health, Fort Dodge, IA) in accordance with institutional guidelines and approved by the Institutional Animal Care and Use Committee of

Colorado State University. Isolated smooth muscle cells were prepared from basilar and cerebral arteries. Arteries were removed, cleaned, and placed in ice-cold Ca^{2+}-free buffer containing (in mM): 140 NaCl, 5 KCl, 2 $MgCl_2$, 10 glucose, and 10 HEPES (adjusted to pH 7.4 with NaOH). Arteries were incubated for 15 min at 37°C in Ca^{2+}-free buffer supplemented with papain (10 U/mL; Worthington Biochemical, Lakewood, NJ) and dithiothreitol (1 mg/mL) followed by a second incubation (15 min at 37°C) in Ca^{2+}-free buffer supplemented with collagenase (300 U/mL, Type II, Worthington Biochemical). Arteries were then washed with and placed in Ca^{2+}-free buffer and kept on ice for 30 min after which trituration with a fire-polished Pasteur pipette was used to create a cell suspension; cells were used within 6 h of dispersion.

Electrophysiology

Freshly prepared smooth muscle cell suspensions were pipetted into a glass bottomed recording chamber and the cells were allowed to adhere for 20 min. Membrane potential was controlled with an Axopatch 200B amplifier (Molecular Devices, Sunnyvale, CA). The perforated whole-cell patch-clamp technique was used to record macroscopic L-type Ca^{2+} channel currents with barium (Ba^{2+}) as the charge carrier. For these experiments the amphotericin B (250 μg/ml) supplemented pipette solution contained (in mM): 120 CsCl, 20 TEA-Cl, 1 EGTA, and 20 HEPES (adjusted to pH 7.2 with CsOH) and cells were superfused with an external solution composed of (in mM): 115 NaCl, 10 TEA-Cl, 0.5 $MgCl_2$, 5.5 glucose, 5 CsCl, 20 $BaCl_2$, and 20 HEPES (adjusted to pH 7.4 with CsOH). The mean capacitance of the cells used for macroscopic L-type Ca^{2+} channel current experiments was 18.2±0.9 pF (n=12 cells). For our Ca^{2+} imaging experiments, we used the conventional dialyzed whole-cell patch-clamp technique. During these experiments cells were superfused with a solution containing (in mM): 120 $NMDG^+$, 5 CsCl, 1 $MgCl_2$, 10, glucose, 10 HEPES, and 20 $CaCl_2$ (adjusted to pH 7.4 with HCl). Pipettes were filled with a solution composed of (in mM): 87 Cs-aspartate, 20 CsCl, 1 $MgCl_2$, 5 MgATP, 0.1 Na_2GTP, 1 NADPH, 10 HEPES, 10 EGTA, and 0.2 fluo-5F (adjusted to pH 7.2 with CsOH). All electrophysiological experiments

were performed at room temperature (22-25°C) and were allowed to progress between 5 and 10 minutes. Only recordings with stable GΩ seals were analyzed.

Total internal reflection fluorescence (TIRF) microscopy

Ca^{2+} influx through L-type channels was visualized with a TILL Photonics (Victor, NY) through-the-lens TIRF system built around an inverted Olympus IX-71 (Center Valley, PA) microscope using a 100X (numerical aperture = 1.45) TIRF oil-immersion objective and an Andor iXON EMCCD camera (Andor Technology, South Windsor, CT). To monitor Ca^{2+} influx, myocytes were loaded with the Ca^{2+} indicator fluo-5F (200 μM; pentapotassium salt; Invitrogen, Carlsbad, CA) and an excess of EGTA (10 mM) via the patch pipette. To preclude potential contaminating Ca^{2+} release events from the sacroplasmic reticulum, the Ca^{2+}-ATPase inhibitor thapsigargin (1 μM) was present during all experiments. Excitation of fluo-5F was achieved with a 491 nm laser and excitation and emission light was separated with appropriate filters. Ca^{2+} influx was recorded at 50 Hz at a holding potential of -70 mV and elevated external [Ca^{2+}] (20 mM) to facilitate the detection of events and provide fluorescent signals of sufficient amplitude (Navedo et al., 2006) to permit quantal analysis.

L-type Ca^{2+} channel sparklet analysis

Background-subtracted fluo-5F fluorescence signals were converted to [Ca^{2+}] (Amberg et al., 2010; Maravall et al., 2000; Navedo et al., 2006) using the equation

$$\left[Ca^{2+}\right] = K_d \frac{F/F_{\max} - 1/R_f}{1 - F/F_{\max}}$$

where F is fluorescence, F_{max} is the fluorescence intensity of fluo-5F in the presence of saturating free Ca^{2+}, F_{min} is the fluorescence intensity of fluo-5F in a solution where [Ca^{2+}] is 0, K_d is the dissociation constant of fluo-5F, and R_f is the F_{max}/F_{min} of fluo-5F. K_d and R_f values for fluo-5F were determined in

vitro and F_{max} was determined at the conclusion of each experiment with ionomycin (10 μM). Fluo-5F fluorescence images were analyzed with custom software (kindly supplied by Dr. L. Fernando Santana) (25). For an elevation in $[Ca^{2+}]_i$ to be considered an L-type Ca^{2+} channel sparklet event, a grid of 3 x 3 contiguous pixels had to have a $[Ca^{2+}]_i$ amplitude equal to or larger than the mean basal $[Ca^{2+}]_i$ plus three times its standard deviation.

Quantal analysis of L-type Ca^{2+} channel sparklet activity (Navedo et al., 2005; Navedo et al., 2006; Amberg et al., 2010) was performed on histograms generated from individual event amplitudes. The resulting histograms were fitted with the multicomponent Gaussian function

$$N = \sum_{j=1}^{n} a_j * \exp\left[-\frac{([Ca^{2+}]_i - jq)^2}{2jb} \right]$$

where a and b are constants, $[Ca^{2+}]_i$ is intracellular Ca^{2+}, and q is the quantal unit of Ca^{2+} influx. L-type Ca^{2+} channel sparklet activity was determined (Amberg et al., 2010; Navedo et al., 2005; Navedo et al., 2006) by calculating the nP_s of each site, where n is the number of quantal levels detected, and P_s is the probability that the site is active. nP_s values were obtained using pCLAMP 10.0 (Molecular Devices, Sunnyvale, CA) on imported $[Ca^{2+}]_i$ time course records. L-type Ca^{2+} channel sparklet activity was quantified using an initial unitary $[Ca^{2+}]_i$ elevation of 38 nM as determined experimentally (Navedo et al., 2005). Consistent with previous reports (Amberg et al., 2007; Amberg et al., 2010; Navedo et al., 2005; Navedo et al., 2006). L-type Ca^{2+} channel sparklet activity was bimodally distributed with sites of low activity (nP_s between 0 and 0.2) and high activity (nP_s greater than 0.2). Active L-type Ca^{2+} channel densities (Ca^{2+} sparklet sites per μm^2) were calculated by dividing the number of active sites by the area of cell membrane visible in the TIRF images.

Detection of reactive oxygen species generation

TIRF microscopy was also used to visualize subplasmalemmal ROS generation as described previously by us (2). Cells were loaded in Ca^{2+}-free buffer supplemented with the cell-permeant ROS indicator 5-(and-6)-chloromethyl-2'7'-dichlorodihydrofluorescein diacetate acetyl ester (DCF; 10 μM; Invitrogen, Carlsbad, CA) for 20 min at room temperature. Following removal of excess DCF with unsupplemented Ca^{2+}-free buffer, excitation of subplasmalemmal DCF was achieved with a 491 nm laser and excitation and emission light was separated with appropriate filters. Analogous to L-type Ca^{2+} channel influx, for an area of elevated DCF fluorescence to be considered a localized site of increased ROS generation (a ROS "puncta"), a grid of 3 x 3 contiguous pixels had to have a fluorescence amplitude equal to or larger than the mean basal DCF fluorescence plus three times its standard deviation (Amberg et al., 2010; Navedo et al., 2005) ROS puncta densities (ROS puncta per μm^2) were calculated by dividing the number of sites detected by the area of cell membrane visible in the TIRF images. Changes in DCF fluorescence (Δ DCF) were calculated from the mean pixel intensities of the total intracellular submembranous slice visible in the TIRF images (average Δ DCF) and the areas confined to nascent ROS puncta (puncta Δ DCF).

Intact arterial diameter measurements

Middle cerebral arteries for intact tissue experiments were isolated and stored in ice-cold MOPS buffer containing (in mM): 145 NaCl, 5 KCl, 1 $MgSO_4$, 2.5 $CaCl_2$, 1 KH_2PO_4, 0.02 EDTA, 2 pyruvate, 5 glucose, 1% bovine serum albumin, and 3 MOPS (adjusted to pH 7.4 with NaOH). Arteries were cleaned of connective tissue and transferred to a vessel chamber (Living Systems, Burlington, VT). One end of the artery was cannulated onto a glass micropipette and secured with monofilament suture. Luminal contents were rinsed and the other end was cannulated onto an opposing micropipette and secured. Arteries were pressurized to 20 mmHg with a bicarbonate-based physiological saline solution (B-PSS) containing (in mM): 119 NaCl, 4.7 KCl, 1.8 $CaCl_2$, 1.2 $MgSO_4$, 24 $NaHCO_3$, 0.2 KH_2PO_4, 10.6 glucose, and

superfused (3 mL/min) with warmed B-PSS (37°C) aerated with a normoxic gas mixture (21% O_2, 6% CO_2, balance N_2). To block the effects of endothelial-derived nitric oxide, the nitric oxide synthase inhibitor N^G-nitro-L-arginine (300 µM) was included in the B-PSS superfusate.

Following a 15-minute equilibration period, intraluminal pressure was increased to 60 mmHg, arteries were stretched appropriately to remove bends, and the pressure was lowered back to 20 mmHg for a second 15-minute equilibration period. Intravascular pressure was then again increased to 60 mmHg and the inner diameter continuously monitored using video microscopy and edge-detection software (Ionoptix, Milton, MA). To assess viability of the preparation, all arteries were exposed to isotonic B-PSS containing 60 mM KCl. Experiments with Ang II (10 nM) and/or PEG-catalase (500 U/mL) were initiated after a stable level of tone was obtained at 60 mmHg and were terminated by superfusing with Ca^{2+}-free B-PSS supplemented with the L-type Ca^{2+} blocker diltiazem (10 µM) to obtain the passive diameter of the artery. Arterial tone (% constriction) was calculated as the percentage difference in active luminal diameter versus passive luminal diameter.

Passive arterial diameters were not different for experiments with Ang II alone (180.6 ± 11.5 µm, n=5 arteries) and for Ang II plus PEG-catalase (193.3 ± 20.1 µm, n=4 arteries; P >0.05). Similarly, myogenic tone at 60 mmHg under control conditions (i.e., with only N^G-nitro-L-arginine present) was also similar for experiments with Ang II alone (39.2 ±3.0%, n=5 arteries) and for Ang II plus PEG-catalase (32.2±6.8%, n=4 arteries; P >0.05). A small increase in arterial diameter was observed following PEG-catalase exposure, 7.7±0.75 µm which corresponded to a 8.5±3.8% loss of tone, but this did not approach statistical significance (P =0.41, n=4 arteries).

Chemicals and statistics

Manganese tetrakis (4-N-methylpyridyl) porphyrin (MnTMPyP) and tempol were from EMD (Gibbstown, NJ); all other chemicals were from Sigma (St. Louis, MO) unless stated otherwise. Normally distributed data are presented as the mean±standard error of the mean (SEM). Two-sample

comparisons of these data were performed using either a paired or unpaired (as appropriate) two-tailed Student's t test and comparisons between more than two groups were performed using a one way ANOVA with Tukey's multiple comparison post-test. L-type Ca^{2+} channel sparklet activity (i.e. nP_s) datasets were bimodally distributed, thus two-sample comparisons of nP_s data were examined with the non-parametric Wilcoxon matched pairs test (two-tailed) and comparisons between more than two groups were performed using the non-parametric Friedman test with Dunn's multiple comparison post-test. Arithmetic means of nP_s datasets are indicated in the figures (solid grey horizontal lines) for non-statistical visual purposes and dashed grey lines mark the threshold for high-activity Ca^{2+} sparklet sites (n$P_s \geq 0.2$) (Amberg et al., 2010; Navedo et al., 2005; Navedo et al., 2006). *P* values less than 0.05 were considered significant and asterisks (*) used in the figures indicate a significant difference between groups.

2.4 Results

To test our hypothesis that H_2O_2 mediates oxidative stimulation of L-type Ca^{2+} channels we proposed four experimental criteria: 1) Application of exogenous H_2O_2 should increase L-type Ca^{2+} channel activity; 2) lowering endogenous H_2O_2 should reduce L-type Ca^{2+} channel activity; 3) lowering endogenous H_2O_2 should also limit arterial constriction in response to oxidative stimuli; and 4) manipulation of other candidate ROS such as superoxide should minimally effect L-type Ca^{2+} channel function.

Catalase attenuates contraction of intact rat cerebral arteries in response to Ang II

We previously reported that ROS generation by Ang II, a known activator of arterial NADPH oxidase complexes (Lassègue et al., 2001; Touyz, 2005) constricted rat cerebral arteries in an L-type Ca^{2+}-channel dependent manner (Amberg et al., 2010). To continue this line of investigation and establish the importance of H_2O_2 as a participating ROS we tested the effect of catalase on pressurized (60 mmHg)

middle cerebral arterial responses to Ang II. Similar to previous reports (Amberg et al., 2010; Touyz and Schiffrin, 2000; Wackenfors et al., 2006), Ang II (10 nM) produced a moderate constriction (19.3±4.0 µm, n=5 arteries) of rat cerebral arterial segments (**Figure 2.1A**). However, in presence of cell-permeable PEG-catalase (500 U/mL), the contractile response to Ang II (3.5±2.2 µm) was nearly abolished (**Figure 2.1B&C**; *P*<0.05, n=4 arteries). These data are consistent with our hypothesis that H_2O_2 is involved in oxidative-dependent contraction of arterial smooth muscle (e.g., stimulation of L-type Ca^{2+} channels).

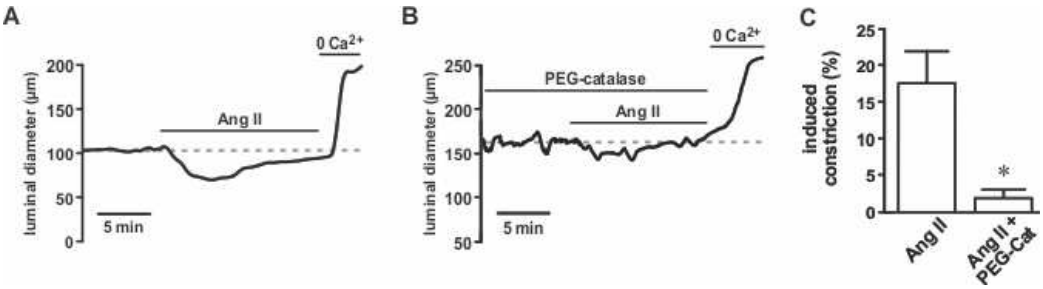

Figure 2.1. PEG-catalase attenuates angiotensin II-dependent constriction of middle cerebral arteries. A & B, Representative time courses showing luminal diameters of pressurized (60 mm Hg) middle cerebral arterial segments exposed to angiotensin II (Ang II; 10 nM) in the absence (panel A) or presence of PEG-catalase (500 U/mL; panel B). C, Plot of the mean±SEM induced constriction (%) by Ang II in the absence (n=5 arteries) or presence of PEG-catalase (n=4 arteries). * P<0.05

Exogenous hydrogen peroxide increases macroscopic L-type Ca^{2+} channel currents in isolated cerebral arterial smooth muscle cells

To investigate if stimulation of L-type Ca^{2+} channels could contribute to the catalase-sensitive component of Ang II-induced arterial constriction we applied a physiologically-relevant concentration of H_2O_2 (100 µM) (Schröder and Eaton, 2008; Stone and Yang, 2006) to isolated arterial myocytes. We found that exogenous H_2O_2 increased macroscopic L-type Ca^{2+} channel currents obtained with the amphotericin B perforated-patch technique using Ba^{2+} as the charge carrier. We arrived at the this conclusion with two voltage-clamp protocols: First we tested the effect of H_2O_2 on macroscopic L-type Ca^{2+} channel currents in response to step depolarizations to 0 mV from a holding potential of -70 mV. As shown **in Figure 2.2A&B**, exogenous H_2O_2 increased diltiazem-sensitive macroscopic L-type Ca^{2+} channel currents (*P*<0.05, n=5 cells). To confirm and illustrate the voltage-dependency of the H_2O_2–induced current, we recorded diltiazem-sensitive macroscopic Ba^{2+} currents during ramp depolarizations from -

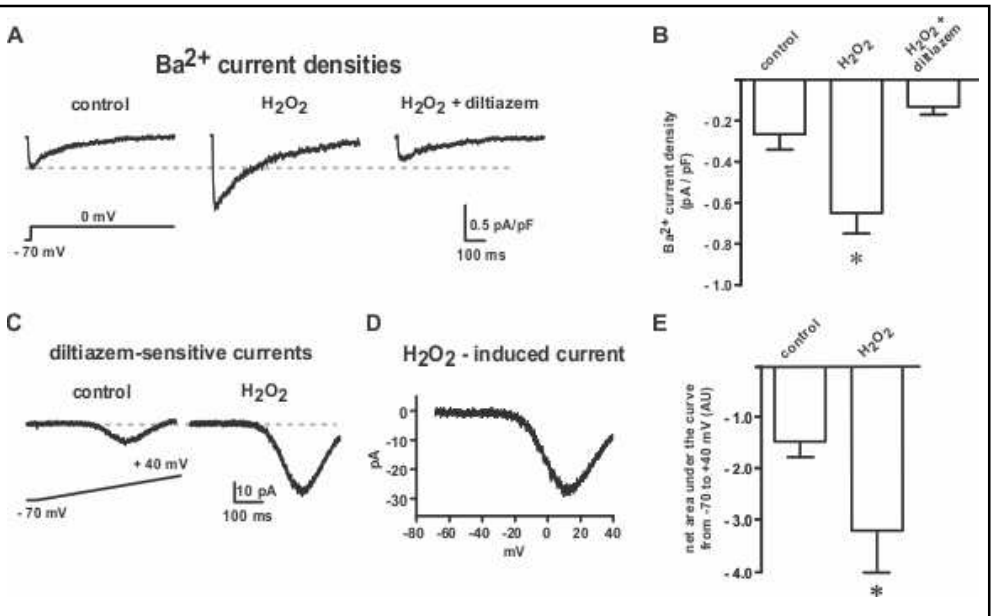

Figure 2.2. Hydrogen peroxide increases macroscopic L-type Ca2+ channel currents in isolated rat cerebral arterial smooth muscle cells. A, Representative Ba2+ current traces during step depolarizations to 0 mV from a holding potential of -70 mV before (left) and after application of H2O2 (100 µM; middle) and H2O2 plus diltiazem (10 µM; right). B, Plot of the mean±SEM peak Ba2+ current densities before and after H2O2 and H2O2 plus diltiazem (n=5 cells). C, Representative diltiazem-sensitive (10 µM) currents evoked during voltage ramps from -70 to +40 mV with a depolarization rate of 220 mV/s before (left) and after application of H2O2 (100 µM; right); the dotted grey line marks the zero current level. D, plot showing the amplitude (pA) of a representative H2O2-induced current as a function of voltage (mV) during a ramp depolarization as described in C. E, Plot of the mean±SEM net area under the curves associated with the diltiazem-sensitive currents recorded during the ramp protocol before and after H2O2 (n=7 cells). * P<0.05

70 to +40 mV before and after application of H_2O_2 (see **Figure 2.2C, D, and E**). As with our recordings obtained during step depolarizations, diltiazem-sensitive currents evoked during continuous ramp depolarizations were increased by H_2O_2 (P<0.05, n=7 cells). The representative difference current in **Figure 2.2D** highlights the voltage-dependency of the diltiazem-sensitive current induced by H_2O_2. Taken together, these observations strongly support our hypothesis that H_2O_2 stimulates voltage-dependent L-type Ca^{2+} channels. However, as evident below, these data also reveal interpretive limitations inherent to conventional macroscopic electrophysiological recordings of L-type Ca^{2+} channel currents.

Exogenous hydrogen peroxide stimulates localized L-type Ca^{2+} channel activity

Our macroscopic current recordings indicate that H_2O_2 stimulates L-type Ca^{2+} channels. However, these data provide no information with regard to the spatial regulation of L-type Ca^{2+} channel function by H_2O_2. To overcome this deficiency we used TIRF microscopy to visualize Ca^{2+} influx through single L-type Ca^{2+} channels with high temporal and spatial resolution. First, however, we used TIRF

microscopy to image subplasmalemmal changes in intracellular oxidation in arterial myocytes exposed to exogenous H_2O_2 with the cell-permeable fluorescent ROS indicator DCF (10 μM; see Materials and Methods). Important for this study, H_2O_2, but not superoxide, is implicated as an experimentally-relevant DCF oxidant (LeBel et al, 1992; Rhee et al., 2010; Zhu et al., 1994). As shown in **Figure 2.3**, exogenous H_2O_2 (100 μM) produced a homogenous (i.e., non-punctate by our criteria) increase in intracellular oxidation as evident in the uniform increase in subplasmalemmal DCF fluorescence (average Δ DCF) throughout the visualized intracellular space (P<0.05, n=5 cells). These observations suggest that increased DCF fluorescence in our TIRF imaging experiments faithfully reports changes in intracellular oxidation throughout the imaged subplasmalemmal space without spatially erroneous confounding biases such as non-uniform intracellular compartmentalization or oxidation of the ROS indicator.

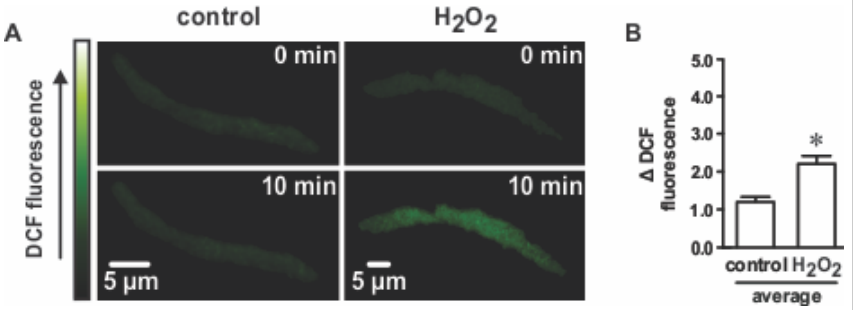

Figure 2.3. Exogenous hydrogen peroxide increases subplasmalemmal DCF fluorescence. A, Representative TIRF images showing DCF fluorescence (indicating intracellular oxidation) in a control arterial myocyte (left) and in a cell incubated with H2O2 (100 uM; right). B, Plot of the mean±SEM changes in spatially averaged DCF fluorescence (average Δ DCF) in control cells and cells incubated with H2O2 (n=5 cells each). * P<0.05

Having demonstrated that H_2O_2 increased intracellular oxidation throughout the imaged subplasmalemmal space, we then used TIRF microscopy to image Ca^{2+} influx through single L-type channels. To do so, we applied H_2O_2 (100 μM) to isolated voltage-clamped (at -70 mV) cerebral arterial myocytes dialyzed with the Ca^{2+} indicator fluo-5F and monitored for changes in Ca^{2+} influx. Consistent with the hypothesis that H_2O_2 stimulates local L-type Ca^{2+} channel activity, punctate sites of Ca^{2+} entry (i.e., "Ca^{2+} sparklets") increased following H_2O_2 application (see **Figure 2.4A**). To link these image stacks to L-type Ca^{2+} channel function we constructed and analyzed event amplitude histograms from fluo-5F fluorescence time courses as shown in **Figure 2.4A**, *right*. Similar to previous reports (Amberg et al., 2010; Navedo et al., 2005; Navedo et al., 2006;

Navedo et al., 2010), the resulting event distributions (see **Figure 2.4B**) revealed that localized Ca^{2+} influx was quantal and that addition of H_2O_2 increased the number of quanta activated (P<0.05, n=5 cells) but not the quantal amplitude (q=35 nM $[Ca^{2+}]_i$ for control and q=34 nM $[Ca^{2+}]_i$ for H_2O_2; P>0.05, n=5 cells). Importantly, the quantal amplitudes before and after H_2O_2 were indistinguishable from each other and approximated those previously reported for arterial smooth muscle L-type Ca^{2+} channels and for Cav1.2 L-type Ca^{2+} channels in heterologous expression systems (Amberg et al., 2010; Navedo et al., 2005; Navedo et al., 2006; Navedo et al., 2007). From these data and consistent with our conventional macroscopic electrophysiological recordings we conclude that H_2O_2 increases Ca^{2+} influx in rat cerebral arterial smooth muscle cells by stimulating local L-type Ca^{2+} channels.

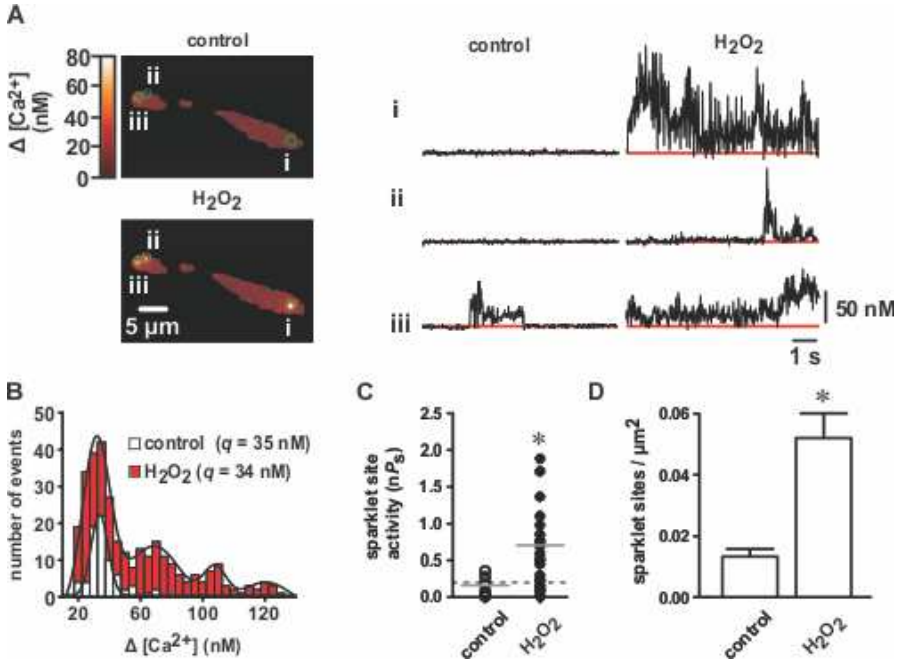

Figure 2.4. Hydrogen peroxide increases L-type Ca2+ channel sparklet activity in isolated rat cerebral arterial smooth muscle cells. A, Representative TIRF images showing Ca2+ influx in an arterial myocyte before and after H2O2 (100 μM). Traces show the time course of Ca2+ influx at the three circled sites before and after H2O2. B, Ca2+ sparklet amplitude histograms before (white) and after H2O2 (red). The solid black lines are best-fits to the control (q=35 nM) and to the H2O2 (q=34 nM) histograms with a multi-component Gaussian function where q is the quantal unit of Ca2+ influx (see Materials and Methods). C, Plot of Ca2+ sparklet site activities (nPs) before and after H2O2 (n=5 cells). The solid grey lines are the arithmetic means of each group and the dashed line marks the threshold for high-activity Ca2+ sparklet sites (nPs≥0.2). D, Plot of the mean±SEM Ca2+ sparklet density (Ca2+ sparklet sites/μm2) before and after H2O2 (n=5 cells). * P<0.05

To further characterize the effect of H_2O_2 on L-type Ca^{2+} channel function we quantified the L-type Ca^{2+} channel activity represented in the fluo-5F fluorescence recordings by calculating nP_s values for each Ca^{2+} influx site where n is the number of quantal levels observed and P_s is the probability that the site is active. As evident in

the event amplitude histograms shown in **Figure 2.4B**, H_2O_2 increased L- type Ca^{2+} channel function (as quantified by nP_s) with the number of high-activity Ca^{2+} influx sites (n$P_s \geq 0.2$) (Navedo et al., 2005) increasing from 2 to 14 (**Figure 2.4C**; $P<0.05$, n=5 cells). Furthermore, the density (sites per μm^2) of L-type Ca^{2+} channel influx increased 3.9-fold (**Figure 2.4D**; $P<0.05$, n=5 cells). These data indicate that H_2O_2 stimulated L-type Ca^{2+} channel function by increasing the number of channels active and by increasing the overall activity of these channels.

Oxidative-dependent stimulation of L-type Ca^{2+} channels is prevented by hydrogen peroxide removal

Next, we examined if endogenous H_2O_2 contributes to oxidative stimulation of L-type Ca^{2+} channels by manipulating H_2O_2 within arterial smooth muscle cells with exogenous catalase. For these experiments we used Ang II to generate ROS in isolated arterial smooth muscle cells. While superoxide is the de novo product of NADPH oxidase, superoxide is rapidly converted to H_2O_2 and oxygen by superoxide dismutase catalysis or spontaneous dismutation (Forman et al., 2010).

We recently demonstrated that Ang II promotes localized ROS generation in isolated arterial smooth muscle cells (Amberg et al., 2010). To further investigate local oxidant signaling in arterial smooth muscle we again used TIRF microscopy to image subplasmalemmal ROS production in myocytes loaded with the ROS indicator DCF. Similar to our previous findings (Amberg et al., 2010), Ang II (100 nM) increased the observed incidence of ROS puncta as illustrated in the DCF fluorescence images shown in **Figure 2.5A&B** ($P<0.05$, n=5 cells). Indicative of a localized ROS signaling mechanism, Ang II failed to induce a significant change in the average Δ DCF fluorescence in submembranous slices visible in the TIRF images of these cells (**Figure 2.5C**; $P>0.05$, n=5 cells). However, in contrast to the average Δ DCF, the increase in DCF fluorescence of nascent ROS puncta was $\approx$ 4 times greater than the average Δ DCF ($P<0.05$, n=5 cells) after Ang II application. Interestingly, the Δ DCF fluorescence of ROS puncta (**Figure 2.5C**) was not statistically different from the average Δ DCF produced by exogenous (100 uM)

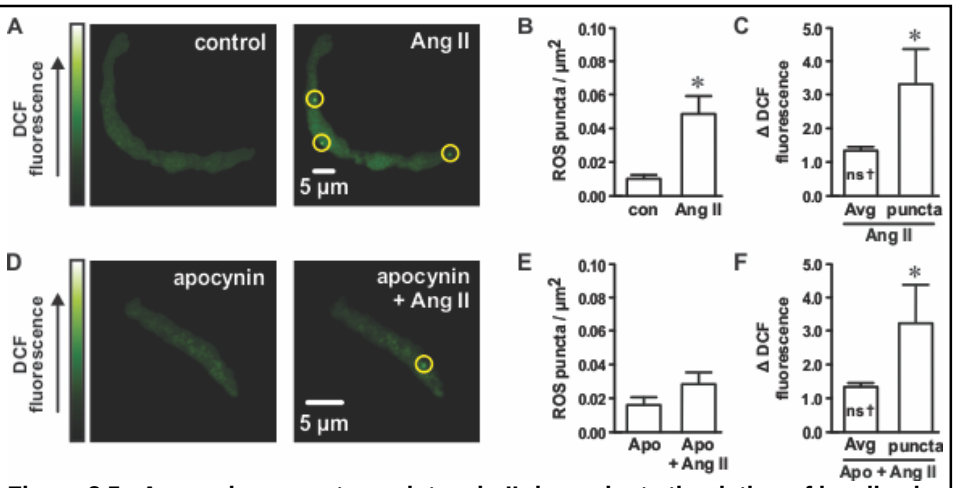

Figure 2.5. Apocynin prevents angiotensin II-dependent stimulation of localized subplasmalemmal ROS generation. A, Representative TIRF images showing punctate DCF fluorescence (indicating ROS generation) in an arterial myocyte before and after Ang II (100 nM). B, Plot of the mean±SEM ROS puncta density before and after Ang II (n=5 cells). C, Plot of the mean±SEM change in the spatially averaged DCF fluorescence (Avg Δ DCF) and that of nascent ROS puncta in cells exposed to Ang II (n=5 cells). D, Representative TIRF images showing punctate DCF fluorescence before and after Ang II in the presence of apocynin (25 µM). E, Plot of the mean±SEM ROS puncta density before and after Ang II plus apocynin (n=5 cells). F, Plot of the mean±SEM change in the spatially averaged DCF fluorescence (Avg Δ DCF) and that of nascent ROS puncta in cells exposed to Ang II plus apocynin (n=5 cells). Note that only sites of DCF fluorescence circled in yellow satisfied the criteria to be considered as a site of increased local ROS generation (see Materials and Methods). * P<0.05; ns† = not significant relative to control cells presented in **Figure 2.3**.

H_2O_2 as shown in **Figure 2.3** above (*P*>0.05, n=5 cells). These data indicate that acute Ang II exposure induces localized changes in intracellular oxidation in isolated arterial myocytes and that application of exogenous H_2O_2 (100 uM) replicates this effect by creating an experimentally equivalent degree (albeit homogenously) of subplasmalemmal oxidation.

To examine if increased ROS puncta density involves NADPH oxidase we tested the effect of the putative NADPH oxidase inhibitor apocynin on Ang II-dependent ROS generation. Suggesting NADPH oxidase involvement, apocynin (10 µM) abolished the effect of Ang II on localized ROS generation (**Figure 2.5D&E**; *P*>0.05, n=5 cells). This finding is consistent with our previous observation (Amberg et al, 2010) that apocynin prevented Ang II stimulation of localized L-type Ca^{2+} channel activity and further supports the general concept of oxidative regulation of Ca^{2+} influx in arterial smooth muscle via L-type Ca^{2+} channels. Ang II in combination with apocynin had no effect on either the average Δ DCF fluorescence or nascent puncta Δ DCF fluorescence (Figure **2.5F**; *P*>0.05, n=5 cells). Note that in the TIRF images presented in **Figure 2.5** (and **Figure 2.8** below), only sites of DCF fluorescence circled in yellow

satisfied the criteria to be defined as a site of increased local ROS generation (see Materials and Methods).

To examine the necessity of H_2O_2 for oxidant-dependent regulation of L-type Ca^{2+} channels we used catalase to convert endogenous H_2O_2 to oxygen and water. The TIRF images in **Figure 2.6A** show the effect of Ang II on arterial L-type Ca^{2+} channel function. As reported previously (Amberg et al., 2010; Navedo et al., 2008; Nieves-Cintrón, 2008), Ang II (100 nM) increased L-type Ca^{2+} channel activity by increasing the number of active channel sites and by increasing the activity of the channels at those sites (**Figure 2.6B**; *P*<0.05, n=5 cells). Dialyzing cells with catalase by including 500 U/mL of the enzyme in the pipette solution abolished stimulation of L-type Ca^{2+} channels by Ang II (Figure **2.6C&D**; *P*<0.05, n=5 cells). Catalase had no effect on basal L-type Ca^{2+} channel activity (*P*>0.05). From these data we conclude that H_2O_2 is necessary for Ang II-dependent stimulation of arterial smooth muscle L-type Ca^{2+} channels.

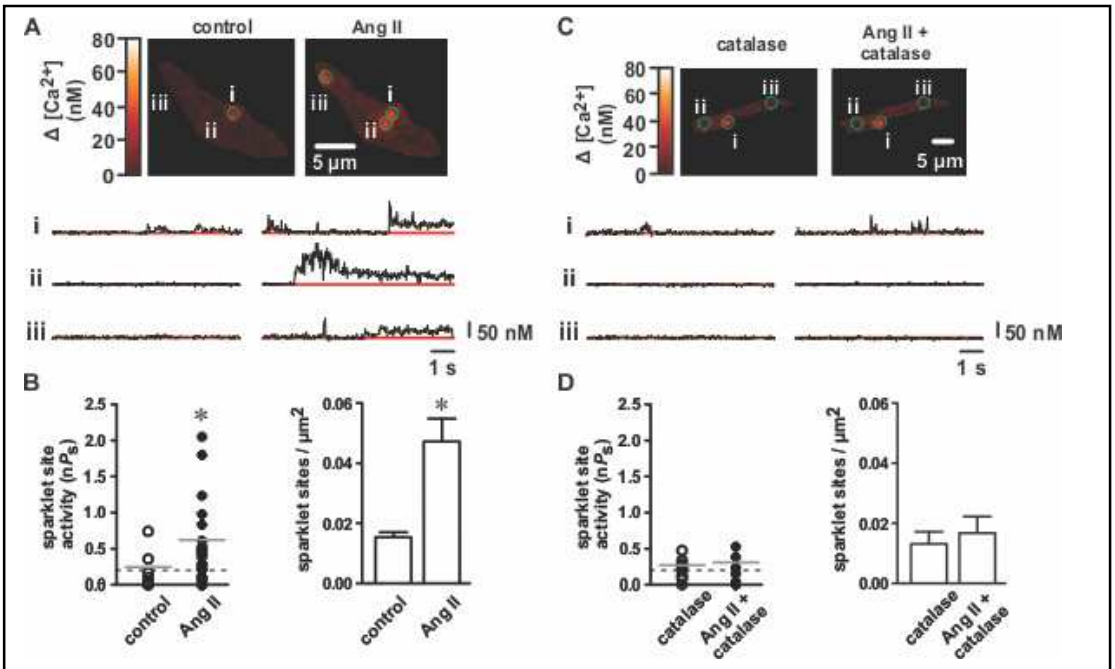

Figure 2.6. Catalase prevents angiotensin II-dependent stimulation of L-type Ca2+ channel sparklet activity. A, Representative TIRF images showing Ca2+ influx in an arterial myocyte before and after application of Ang II (100 nM). Traces show the time course of Ca2+ influx at the three circled sites. B, Plot of Ca2+ sparklet site activities (nPs) and plot of mean±SEM Ca2+ sparklet density (Ca2+ sparklet sites/µm2) before and after Ang II (n=5 cells). C, Representative TIRF images showing Ca2+ influx in an arterial myocyte before and after application of Ang II (100 nM) in the presence of intracellular catalase (500 U/mL). Traces show the time course of Ca2+ influx at the three circled sites. D, Plot of Ca2+ sparklet site activities (nPs) and plot of mean±SEM Ca2+ sparklet density (Ca2+ sparklet sites/µm2) before after Ang II in the presence of intracellular catalase (n=5 cells). * P<0.05

Ang II-dependent stimulation of L-type Ca^{2+} channels is unaffected by enhanced superoxide dismutation

Thus far we have demonstrated that H_2O_2 stimulates L-type Ca^{2+} channels and is necessary for increased channel activity in response to Ang II. As noted above, H_2O_2 produced by NADPH oxidase results from dismutation of catalytically produced superoxide (Forman et al., 2010). However, our data does not necessarily preclude a direct contributory role for superoxide. To address this possibility we examined the effect of enhanced superoxide dismutation on stimulation of L-type Ca^{2+} channels by Ang.

First, we included superoxide dismutase (50 U/mL) in the pipette solution and recorded L-type Ca^{2+} channel activity before and after exposure to Ang II. Unlike catalase, dialysis of arterial smooth muscle cells with superoxide dismutase did not prevent Ang II-dependent stimulation of L-type Ca^{2+} channels (**Figure 2.7A**). Indeed, the density of L-type Ca^{2+} channel sparklet sites and the activity at those sites following application of Ang II was unaffected by the presence of exogenous superoxide dismutase (**Figure**

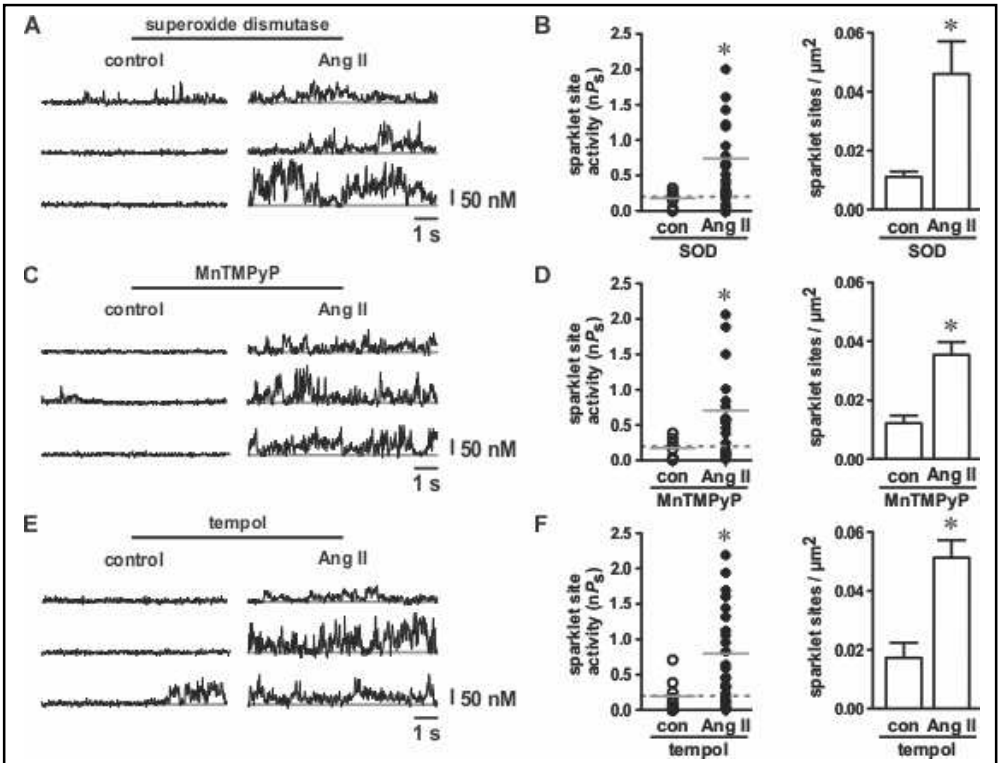

Figure 2.7. Superoxide dismutase does not prevent angiotensin II-dependent stimulation of L-type Ca2+ channel sparklet activity. A, C, & E, Representative traces showing time courses of Ca2+ influx in arterial myocytes before and after application of Ang II (100 nM) in the presence of 50 U/mL intracellular superoxide dismutase (SOD; A), 10 µM MnTMPyP (C), and 5 mM tempol (E). B,D, & F, Plots showing Ca2+ sparklet site activities (nPs) and mean±SEM Ca2+ sparklet densities (Ca2+ sparklet sites/µm2) before after Ang II in the presence of superoxide dismutase (B), MnTMPyP (D), and tempol (F); (n=5 cells each). * P<0.05

2.7B; *P*<0.05, n=5 cells). Similar to catalase, superoxide dismutase had no effect on basal L-type Ca^{2+} channel activity (*P*>0.05).

We also tested the effect two structurally unrelated cell-permeable small molecule superoxide dismutase mimetics on Ang II-dependent stimulation of L-type Ca^{2+} channels: The metalloporphyrin MnTMPyP and the nitroxide tempol. Similar to superoxide dismutase itself, MnTMPyP (10 μM) and tempol (5 mM) had no effect on Ang II-dependent stimulation of L-type Ca^{2+} channels (**Figure 2.7C-F**; *P*<0.05, n=5 cells each); basal L-type Ca^{2+} channel activity was also unaffected by these two compounds (*P*>0.05). These data are consistent with the hypothesis that, in contrast to H_2O_2, superoxide in and of itself does not directly contribute to oxidative stimulation of arterial smooth muscle L-type Ca^{2+} channels.

As noted above, we previously found that localized sites of ROS generation precede and colocalize with subsequence L-type Ca2+ channel activity (Amberg et al., 2010). To relate the effectiveness of catalase and ineffectiveness of superoxide dismutase on preventing Ang II from stimulating L-type Ca2+ channels to ROS, we examined the effect of these two enzymes on subplasmalemmal ROS generation with TIRF microscopy. **Figure 2.8A** shows near-membrane DCF fluorescence in a myocyte exposed to cell-permeant PEG-catalase (500 U/mL) before and after Ang II and Figure 2.8D shows a cell exposed to PEG-superoxide dismutase (PEG-SOD; 100 U/mL) before and after Ang II. While neither enzyme had an effect (P>0.05) on baseline ROS production, which was minimal to begin with, PEG-catalase, but not PEG-SOD, abolished the increase in ROS puncta density in response to Ang II (**Figure 2.8B&E**; *P*<0.05, n=5 cells each).

Similar to Ang II alone or with apocynin (see Figure 5), the average Δ DCF fluorescence was not increased by Ang II in the presence of PEG-catalase (Figure **2.8C**; *P*>0.05, n=5 cells). In contrast, in the presence of PEG-SOD, Ang II increased the average Δ DCF fluorescence (**Figure 2.8F**; *P*<0.05, n=5 cells). This increase was not significantly different (*P*>0.05) than that induced by exogenous H_2O_2 (see **Figure**

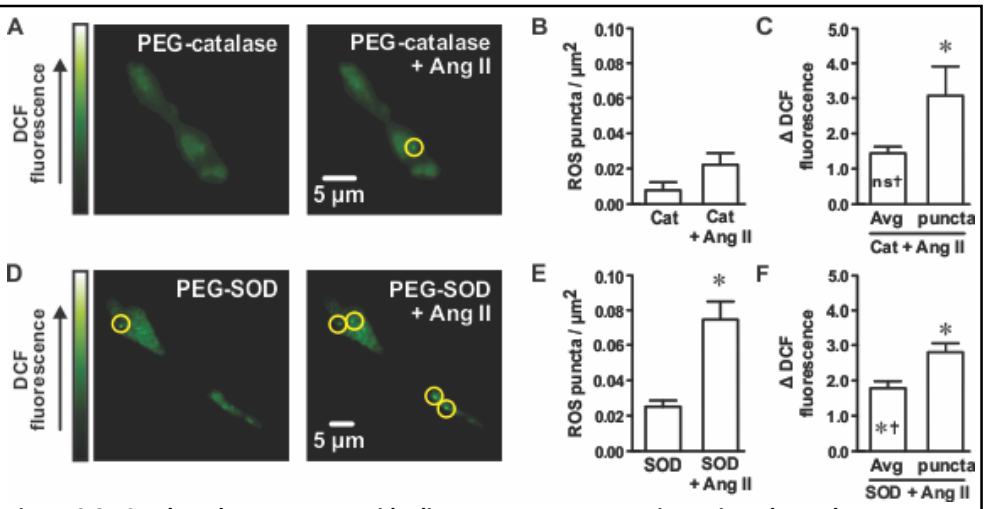

Figure 2.8. Catalase, but not superoxide dismutase, prevents angiotensin II-dependent stimulation of localized subplasmalemmal ROS generation. A, Representative TIRF images showing punctate DCF fluorescence (indicating ROS generation) in an arterial myocyte before and after Ang II (100 nM) in the presence of PEG-catalase (500 U/mL). B, Plot of the mean±SEM ROS puncta density before and after Ang II plus PEG-catalase (n=5 cells). C, Plot of the mean±SEM change in the spatially averaged DCF fluorescence (Avg Δ DCF) and that of nascent ROS puncta in cells exposed to Ang II plus PEG-catalase (n=5 cells). D, Representative TIRF images showing punctate DCF fluorescence before and after Ang II in the presence of PEG-superoxide dismutase (PEG-SOD; 100 U/mL). E, Plot of the mean±SEM ROS puncta density before and after Ang II plus PEG-SOD (n=5 cells). F, Plot of the mean±SEM change in the spatially averaged DCF fluorescence (Avg Δ DCF) and that of nascent ROS puncta in cells exposed to Ang II plus PEG-SOD (n=5 cells). Note that only sites of DCF fluorescence circled in yellow satisfied the criteria to be considered as a site of increased local ROS generation (see Materials and Methods). * P<0.05; ns† and *† = not significant and significant, respectively, relative to control cells presented in **Figure 2.3**.

2.2). Note however, that non-punctal increases in oxidation observed with H_2O_2 and PEG-SOD plus Ang II were not associated with uniform increases in L-type Ca^{2+} channel function (see **Figures 2.4& 2.7**). Indeed, L-type Ca^{2+} channel activity was independent of the average Δ DCF as Ca^{2+} sparklet site densities in cells exposed to either H_2O_2 or Ang II plus SOD (where average Δ DCF fluorescence increased) were not different from cells exposed to Ang II alone (where average Δ DCF fluorescence was unchanged; *P*>0.05; n=5 cells each). Ang II in combination with PEG-catalase and PEG-SOD had no effect on puncta Δ DCF fluorescence (**Figure 2.8C&F**; *P*>0.05, n=5 cells each). In context with our other experiments, these data support our hypothesis that localized generation of H_2O_2 stimulates L-type Ca^{2+} channels in arterial smooth muscle cells.

2.5 Discussion

In this study experiments were performed to test the hypothesis that H_2O_2 mediates oxidant-dependent stimulation of rat cerebral arterial smooth muscle L-type Ca^{2+} channels. Using a combination

of arterial diameter measurements, conventional electrophysiology, and TIRF microscopy, in agreement with this hypothesis, we found that: 1) depletion of H_2O_2 with catalase all but abolished oxidative-dependent contraction of cerebral arterial segments by Ang II; 2) application of exogenous H_2O_2 increased L-type Ca^{2+} channel activity in isolated arterial smooth muscle cells; 3) catalase reduced oxidant-dependent stimulation of L-type Ca^{2+} channels; 4) catalase also attenuated sites of localized ROS production associated with L-type Ca^{2+} channel activity; and 5) enhanced superoxide dismutation with superoxide dismutase or small molecule superoxide dismutase mimetic compounds were without effect. From these data we conclude that H_2O_2 is an important local mediator of oxidant signaling in arterial smooth muscle by stimulating L-type Ca^{2+} channels.

We reported previously (Amberg et al., 2010) that exogenous ROS generated by xanthine oxidase stimulated L-type Ca^{2+} channels in arterial smooth muscle cells. Similar to NADPH oxidase, xanthine oxidase produces superoxide and H_2O_2 (Knapp and Klann, 2000) with H_2O_2 representing the majority of the detectable ROS (Kelley et al., 2010). From a biochemical perspective, H_2O_2 is well-suited to function as a classical second messenger while superoxide is not (Forman et al., 2010). Here we observed that the effect of exogenous H_2O_2 on L-type Ca^{2+} channels recapitulated our previous results with xanthine oxidase where superoxide and H_2O_2 were produced (Amberg et al., 2010). Consistent with this, removal of endogenous H_2O_2 with catalase abolished L-type channel stimulation by Ang II while enhanced superoxide dismutation was without effect. These data suggest that H_2O_2 is sufficient in mediating oxidant-dependent stimulation of arterial smooth muscle L-type Ca^{2+} channels and that any role of superoxide is likely to be indirect (i.e., as a biochemical precursor to H_2O_2 via dismutation).

H_2O_2 has been shown to stimulate native macroscopic L-type Ca^{2+} channel currents in cultured neurons (Akaishi et al.,2004) and L-type Ca^{2+} currents produced by recombinant channel subunits expressed in HEK 293 cells (Hudasek et al., 2004). Similarly, we found that exogenous ROS generated by xanthine oxidase (where H_2O_2 and superoxide are produced) increased whole-cell L-type Ca^{2+} channel

currents in rat cerebral arterial myocytes (Amberg et al., 2010). Consistent with these published reports, here we found that exogenous H_2O_2 stimulated arterial smooth muscle L-type Ca^{2+} channel currents. In these experiments, H_2O_2 increased diltiazem-sensitive L-type Ca^{2+} channels (with Ba^{2+} as the charge carrier) using the amphotericin-perforated patch technique to preserve intracellular constituents such as endogenous antioxidants. H_2O_2 increased L-type Ca^{2+} channel currents in step and continuous ramp depolarizations. These currents displayed kinetic and voltage-dependent properties consistent with L-type Ca^{2+} channels (Catterall, 2000). From these observations we conclude that exogenous H_2O_2 stimulates L-type Ca^{2+} channels in cerebral arterial smooth muscle cells. Although of significant interest in and of themselves, these data provide no information regarding the spatial regulation of arterial smooth muscle L-type Ca^{2+} channels by H_2O_2.

We previously reported (Amberg et al., 2010) that oxidative stimulation of L-type Ca^{2+} channels in arterial smooth muscle cells is highly localized, not homogenously distributed throughout the plasma membrane. As with ROS generated by xanthine oxidase, here we found that application of exogenous H_2O_2 increased L-type Ca^{2+} channel activity that was limited to approximately 6 sites of Ca^{2+} influx per 100 μm^2 of membrane imaged. Importantly, the majority of oxidant-induced Ca^{2+} influx events at these sites were produced by the opening of single L-type Ca^{2+} channels (see **Figure 2.4B** and Amberg et al., 2010). This observation provides empirical evidence in direct opposition to the alternative hypothesis that intracellular oxidation with H_2O_2 produces non-uniform Ca^{2+} influx by stimulating spatially heterogeneous clusters of L-type Ca^{2+} channels. To highlight the spatial sequestration of this Ca^{2+} influx, rat cerebral arterial smooth muscle cells are reported to have approximately 5 L-type Ca^{2+} channels per μm^2 (Rubart et al., 1996). Thus, the number of channels activated by exogenous H_2O_2 is much less than expected based on conventional electrophysiological recordings. This does not preclude a contribution from direct channel stimulation by H_2O_2. However, prior evidence (Amberg et al., 2010; Navedo et al., 2006; Navedo et al., 2008) indicates that additional proteins with limited plasmalemmal distributions

such as AKAP150 and protein kinase C α (PKCα) are necessary for oxidant-dependent stimulation of L-type Ca^{2+} channels in arterial smooth muscle cells. Indeed, in our previous report we found that exogenous ROS generated by xanthine oxidase (which includes H_2O_2) induced irregular punctate translocation of PKCα to the plasma membrane and that PKCα activity was necessary for ROS-dependent stimulation of L-type Ca^{2+} channels (Amberg et al., 2010).

In arterial smooth muscle cells NADPH oxidase signaling complexes and the mitochondrial electron transport chain are two potential sources of H_2O_2 generation (Lee and Griendling, 2008; Manea, 2010). In each case, H_2O_2 is generally produced indirectly by the dismutation of superoxide. NADPH oxidase-derived H_2O_2 is postulated to remain within a submembranous compartment a few μm from its site of generation (Mishina et al., 2011; Woo et al., 2010). Our visualization of discrete subplasmalemmal catalase-sensitive punctate ROS generation following Ang II exposure with TIRF microscopy is in agreement with these findings (this chapter and Amberg et al., 2010). Furthermore, while Ang II increased the density of ROS puncta approximately 4-fold, we found no change in the average Δ DCF fluorescence in these cells. We did, however, find that exogenous H_2O_2 and Ang II plus PEG-SOD resulted in an increase in average Δ DCF fluorescence. Importantly, these diffuse increases in intracellular oxidation were not associated with concomitant spatially-dispersed increases in L-type Ca^{2+} channel activity. Thus, in agreement with prior work (Amberg et al., 2010; Navedo et al., 2005; Navedo et al., 2006; Navedo et al., 2008; Navedo et al., 2010), these data strongly suggest that oxidative stimulation of L-type Ca^{2+} channels in arterial smooth muscle requires additional molecular participants (e.g., AKAP150 and/or PKCα as noted above) thus giving rise to its local nature.

Our TIRF imaging also suggests that NADPH oxidase is involved in ROS-dependent stimulation of L-type Ca^{2+} channels in arterial smooth muscle: Inhibition of NADPH oxidase with apocynin prevented Ang II-dependent stimulation of punctate ROS generation (**Figure 2.5**) as well as localized L-type Ca^{2+} channel function (Amberg et al., 2010). However, apocynin is reported to have intrinsic antioxidant

properties that are independent of NADPH oxidase inhibition (Heumuller et al., 2008). Although these effects were shown at concentrations greater than that used in this study (25 μM), it is possible that a portion of the observed inhibitory effect of apocynin on ROS puncta generation and L-type Ca^{2+} channel function could result from antioxidant activity rather than NADPH oxidase inhibition. This implies that other sources of H_2O_2 (e.g., mitochondria) could participate in oxidant-dependent regulation of arterial smooth muscle L-type Ca^{2+} channels. Future studies should address this hypothesis.

Catalase was effective in preventing increased localized ROS production and stimulation of L-type Ca^{2+} channels by Ang II. In contrast to H_2O_2 removal with catalase, superoxide dismutase did not prevent Ang II from increasing localized ROS generation and stimulating L-type Ca^{2+} channels. The small molecule superoxide dismutase mimetics MnTMPyP and tempol were also ineffective in preventing L-type Ca^{2+} channel stimulation. The outcome of the superoxide dismutase experiments are consistent with our hypothesis that H_2O_2 is the ROS involved in oxidant-dependent stimulation of L-type Ca^{2+} channels. However, the ineffectiveness of MnTMPyP and tempol is somewhat unexpected as these two compounds are reported to have catalase-like activity in addition to their effects on superoxide (Day et al., 2008; Wilcox and Pearlman, 2008). The reason for this apparent discrepancy is not entirely clear. However, evidence suggests that nitroxides including tempol can cause transient increases in vascular H_2O_2 and that catalase-like activity of these compounds require other intracellular molecular constituents (e.g., heme proteins or peroxidases) (Krishna et al., 1996; Mehlhorn and Swanson, 1992) that could be sufficiently diluted by cell dialysis with the pipette solution. Alternatively, it is possible that the catalase-like activity of these agents is temporally insufficient to remove H_2O_2 before stimulation L-type Ca^{2+} channels.

As superoxide dismutase increases the formation of H_2O_2 it is reasonable to predict that pharmacologically enhanced dismutation of superoxide to H_2O_2 would result in increased oxidant-dependent L-type Ca^{2+} channel activity and ROS puncta formation. Although there was a trend for

increased channel activity and ROS puncta formation with enhanced superoxide dismutation these differences did not reach statistical significance. This was the case for basal and Ang II-induced L-type Ca^{2+} channel activity and ROS puncta formation. These observations suggest, at least under our experimental conditions, that superoxide production in response to Ang II is sufficiently dismutated to H_2O_2 to an extent that additional dismutation has little or no effect on L-type Ca^{2+} channel function. Importantly, this appears to be the case in intact cells (i.e., ROS puncta experiments) and in cells following intracellular dialysis with an exogenous solution (i.e., L-type Ca^{2+} channel sparklet experiments). Note, however, that SOD did increase the average Δ DCF although this was not associated with an increase in L-type Ca^{2+} channel activity.

Our data obtained from isolated arterial smooth muscle cells showing H_2O_2-dependent Ca^{2+} influx through L-type Ca^{2+} channels is in agreement with prior work examining the effect of H_2O_2 on intact arterial preparations. In our previous publication (Amberg et al., 2010) we found that ROS generated by xanthine oxidase (which includes H_2O_2) induced arterial contraction. Others have shown that application of H_2O_2 also resulted in arterial contraction (Tabet et al., 2004), an effect which was enhanced in tissues collected from hypertensive animals and dependent on Ca^{2+} influx through L-type Ca^{2+} channels. H_2O_2 may also participate in the generation of the arterial myogenic contractile response (Nowicki et al., 2001). Consistent with these reports, here we found that cell permeable PEG-catalase largely attenuated the contractile response of pressurized middle cerebral arterial segments to Ang II.

In contrast to the reports referenced above and data presented in this paper, H_2O_2 has also been shown to be an endothelium-derived relaxation factor that acts at least in part by hyperpolarization of arterial smooth muscle via activation of large-conductance Ca^{2+}-activated potassium (BK) channels (Hayabuchi et al., 1998; Iida and Katusic, 2000; Liu et al., 2011; Matoba et al., 2000). At a minimum this discrepancy could arise from different experimental conditions and the arterial bed under investigation. However, the highly localized nature of subplasmalemmal H_2O_2 generation and subsequent coupling to

L-type Ca^{2+} channels demonstrated in our work (Amberg et al., 2010 and this chapter) provides a possible mechanistic explanation for these apparently contradictory observations: Local sites of H_2O_2 generation functionally coupled to proteins associated with contraction (e.g., L-type Ca^{2+} channels) lead to vasoconstriction while those coupled to proteins associated with relaxation (e.g., BK channels) lead to vasodilation. Thus, H_2O_2 may function in vivo as either a vasoconstrictor or vasodilator depending on the cellular processes to which it is functionally coupled. Similarly, during in vitro experimentation, H_2O_2 could cause either vasodilation or vasoconstriction depending on the relative balance of vasodilatory and vasoconstrictive processes stimulated under the prevailing experimental circumstances including but not limited to the presence of a functional endothelium, concentration of H_2O_2 used, and method of delivery.

To conclude, in this manuscript we provide strong evidence supporting our hypothesis that H_2O_2 is the ROS responsible for oxidant-dependent stimulation of arterial smooth muscle L-type Ca^{2+} channels. In addition, our data further support the concept of local crosstalk between ROS and Ca^{2+} signaling in arterial smooth muscle. These observations also add to a growing body of evidence indicating that H_2O_2 acts as a local second messenger regulated in time and space with defined functions in multiple biological systems.

Chapter 3. Stimulation of arterial smooth muscle L-type calcium channels by hydrogen peroxide requires protein kinase C[2]

3.1 Summary

Changes in intracellular calcium regulate countless biological processes. In arterial smooth muscle, voltage-dependent L-type calcium channels are major conduits for calcium entry with the primary function being determination of arterial diameter. Similarly, changes in intracellular redox status, either discrete controlled changes or global pathological perturbations, are also critical determinants of cell function. We recently reported that in arterial smooth muscle cells, local generation of hydrogen peroxide leads to colocalized calcium entry through L-type calcium channels. Here we extend our investigation into mechanisms linking hydrogen peroxide to calcium influx through L-type calcium channels by focusing on the role of PKC. Our data indicate that stimulation of L-type calcium channels by hydrogen peroxide requires oxidant-dependent increases in PKC catalytic activity. This effect is independent of classical cofactor-dependent activation of PKC by diacylglycerol. These data provide additional experimental evidence supporting the concept of oxidative stimulation of L-type calcium channels.

3.2 Introduction

Voltage-dependent Cav1.2 L-type Ca^{2+} channels are the primary point of Ca^{2+} entry in mammalian arterial smooth muscle. Therefore, changes in the open probably of L-type Ca^{2+} channels in arterial smooth muscle cells in response to vasoconstrictors or vasodilators correlates with changes arterial diameter. Our group and others have used TIRF microscopy to investigate mechanisms

[2] Chaplin NL, Amberg GC (2012) Stimulation of arterial smooth muscle L-type calcium channels by hydrogen peroxide requires protein kinase C. Channels (Austin). 6(5):385-389. doi: 10.4161/chan.21708

governing L-type Ca^{2+} channel function with high temporal and spatial resolution (Amberg et al., 2007; Amberg et al., 2010; Navedo et al., 2005; Navedo et al., 2006; Navedo et al., 2007; **Section 2**). These studies revealed that L-type Ca^{2+} channel functionality is heterogeneously dispersed throughout the smooth muscle cell sarcolemma as a consequence of spatially limited distributions of key regulatory molecules and subcellular processes.

Recently, our group reported that the vasoconstrictor Ang II leads to punctate generation of ROS by NADPH oxidase (Amberg et al., 2010; **Chapter 2**). This increase in local ROS production, H_2O_2 to be more precise, in turn promotes discrete colocalized Ca^{2+} influx events via PKC-dependent activation of L-type Ca^{2+} channels. Our observations suggest that oxidative activation of PKC is involved with ROS-dependent stimulation of L-type Ca^{2+} channels in arterial smooth muscle cells (Amberg et al., 2010; **Chapter 2**). Indeed, the PKC inhibitor Gö6976 prevented oxidant-dependent stimulation of L-type Ca^{2+} channels by exogenous ROS produced by xanthine oxidase (Amberg et al., 2010).

Here we expand on this topic by furthering our investigation into the mechanisms underlying oxidative activation of L-type Ca^{2+} channels by PKC. Our data indicate that H_2O_2, as with ROS generated enzymatically by xanthine oxidase (which includes superoxide and H_2O_2) stimulates L-type Ca^{2+} channels in a PKC-sensitive manner. Consistent with the importance of oxidative activation of PKC, as opposed to classical activation mechanisms such as DAG, we found that inhibition of PKC activation by DAG had no effect on Ang II stimulation of L-type Ca^{2+} channels. In the context of our prior work, (Amberg et al., 2010; **Section 2**) these data indicate that oxidant-dependent activation of arterial smooth muscle L-type Ca^{2+} channels by H_2O_2 following Ang II exposure involves oxidative activation of PKC.

3.3 Materials and Methods

Isolation of rat cerebral arterial myocytes

Adult male Sprague-Dawley rats (Harlan) were euthanized with sodium pentobarbital (200 mg/kg intraperitoneally; Fort Dodge Animal Health) in accordance with institutional guidelines and approved by the Institutional Animal Care and Use Committee of Colorado State University. Isolated smooth muscle cells were prepared from basilar and cerebral arteries. Arteries were removed, cleaned, and placed in ice-cold Ca^{2+}-free buffer containing (in mM): 140 NaCl, 5 KCl, 2 $MgCl_2$, 10 glucose, and 10 HEPES (adjusted to pH 7.4 with NaOH). Arteries were incubated for 15 min at 37°C in Ca^{2+}-free buffer supplemented with papain (10 U/mL; Worthington Biochemical) and dithiothreitol (1 mg/mL) followed by a second incubation (15 min at 37°C) in Ca^{2+}-free buffer supplemented with collagenase (300 U/mL, Type II, Worthington Biochemical). Arteries were then washed with and placed in Ca^{2+}-free buffer and kept on ice for 30 min after which trituration with a fire-polished Pasteur pipette was used to create a cell suspension; cells were used within 6 h of dispersion.

Electrophysiology and total internal reflection fluorescence (TIRF) microscopy

Freshly prepared smooth muscle cell suspensions were pipetted into a glass bottomed recording chamber and the cells were allowed to adhere for 20 min. Membrane potential was controlled with an Axopatch 200B amplifier (Molecular Devices). For our Ca^{2+} imaging experiments, we used the conventional dialyzed whole-cell patch-clamp technique. During these experiments cells were superfused with a solution containing (in mM): 120 $NMDG^{+}$, 5 CsCl, 1 $MgCl_2$, 10, glucose, 10 HEPES, and 20 $CaCl_2$ (adjusted to pH 7.4 with HCl). Pipettes were filled with a solution composed of (in mM): 87 Cs-aspartate, 20 CsCl, 1 $MgCl_2$, 5 MgATP, 0.1 Na_2GTP, 1 NADPH, 10 HEPES, 10 EGTA, and 0.2 fluo-5F (adjusted to pH 7.2 with CsOH). All experiments were performed at room temperature (22-25°C).

Ca^{2+} influx through L-type channels was visualized with a TILL Photonics through-the-lens TIRF system built around an inverted Olympus IX-71 microscope using a 100X (numerical aperture = 1.45)

TIRF oil-immersion objective and an Andor iXON EMCCD camera (Andor Technology). To monitor Ca^{2+} influx, myocytes were loaded with the Ca^{2+} indicator fluo-5F (200 µM; pentapotassium salt; Invitrogen) and an excess of EGTA (10 mM) via the patch pipette. Excitation of fluo-5F was achieved with a 491 nm laser and excitation and emission light was separated with appropriate filters. Ca^{2+} influx was recorded at 50 Hz at a holding potential of -70 mV and elevated external [Ca^{2+}] (20 mM) to facilitate the detection of events and provide fluorescent signals of sufficient amplitude [4] to permit quantal analysis. All experiments were allowed to progress between 5 and 10 minutes and only recordings with stable GΩ seals were analyzed. All experiments were performed at room temperature (22-25°C).

L-type Ca^{2+} channel sparklet analysis

Background-subtracted fluo-5F fluorescence signals were converted to [Ca^{2+}] (Amberg et al., 2010; Maravall et al., 2000; Navedo et al., 2006) using the equation

$$\left[Ca^{2+}\right] = K_d \frac{F/F_{\max} - 1/R_f}{1 - F/F_{\max}}$$

where F is fluorescence, F_{max} is the fluorescence intensity of fluo-5F in the presence of saturating free Ca^{2+}, F_{min} is the fluorescence intensity of fluo-5F in a solution where [Ca^{2+}] is 0, K_d is the dissociation constant of fluo-5F, and R_f is the F_{max}/F_{min} of fluo-5F. K_d and R_f values for fluo-5F were determined in vitro and F_{max} was determined at the conclusion of each experiment with ionomycin (10 µM). Fluo-5F fluorescence images were analyzed with custom software (Navedo et al., 2006). For an elevation in $[Ca^{2+}]_i$ to be considered an L-type Ca^{2+} channel sparklet event, a grid of 3 x 3 contiguous pixels had to have a $[Ca^{2+}]_i$ amplitude equal to or larger than the mean basal $[Ca^{2+}]_i$ plus three times its standard deviation.

L-type Ca^{2+} channel sparklet activity was determined Amberg et al., 2010, Navedo et al., 2005; Navedo et al., 2006) by calculating the nP_s of each site, where n is the number of quantal levels detected, and P_s is the probability that the site is active. nP_s values were obtained using pCLAMP 10.0 (Molecular Devices) on imported $[Ca^{2+}]_i$ time course records. L-type Ca^{2+} channel sparklet activity was quantified using an initial unitary $[Ca^{2+}]_i$ elevation of 38 nM as determined experimentally (Navedo et al., 2005). Consistent with previous reports (Amberg et al,.,2007; Amberg et al., 2010, Navedo et al., 2005; Navedo et al., 2006), L-type Ca^{2+} channel sparklet activity was bimodally distributed with sites of low activity (nP_s between 0 and 0.2) and high activity (nP_s greater than 0.2). Active L-type Ca^{2+} channel densities (Ca^{2+} sparklet sites per μm^2) were calculated by dividing the number of active sites by the area of cell membrane visible in the TIRF images.

Chemicals and statistics

All chemicals were from Sigma unless stated otherwise. Normally distributed data are presented as the mean±standard error of the mean (SEM). Two-sample comparisons of these data were performed using either a paired or unpaired (as appropriate) two-tailed Student's t test and comparisons between more than two groups were performed using a one way ANOVA with Tukey's multiple comparison post-test. L-type Ca^{2+} channel sparklet activity (i.e. nP_s) datasets were bimodally distributed, thus two-sample comparisons of nP_s data were examined with the non-parametric Wilcoxon matched pairs test (two-tailed) and comparisons between more than two groups were performed using the non-parametric Friedman test with Dunn's multiple comparison post-test. Arithmetic means of nP_s datasets are indicated in the figures (solid grey horizontal lines) for non-statistical visual purposes and dashed grey lines mark the threshold for high-activity Ca^{2+} sparklet sites (n$P_s \geq 0.2$) (Amberg et al., 2010, Navedo et al., 2005; Navedo et al., 2006). *P* values less than 0.05 were considered significant and asterisks (*) used in the figures indicate a significant difference between groups.

3.4 Results

For our hypothesis that oxidative activation of PKC is necessary for H_2O_2-dependent stimulation of L-type Ca^{2+} channels to be valid, following oxidant exposure, inhibition of cofactor-dependent activation of PKC (i.e., via DAG) should be without effect while inhibition of PKC catalytic activity should prevent channel stimulation.

To begin, we tested the hypothesis that inhibiting the interaction between DAG and PKC (i.e., cofactor-dependent activation of PKC) would not impede oxidant-dependent stimulation of arterial smooth muscle L-type Ca^{2+} channels. We recorded L-type Ca^{2+} channel activity optically using a combination of voltage-clamp electrophysiology and TIRF microscopy as previously described (Amberg et al., 2010; **Chapter 2**). L-type Ca^{2+} channel activity was quantified in two ways: 1) the number of active L-type channel Ca^{2+} influx sites per μm^2 (Ca^{2+} sparklet site density) and 2) the activity of the L-type Ca^{2+} channels at these sites as determined by their calculated nP_s values (n is the number of quantal levels observed and P_s is the probability that the site is active)(Navedo et al., 2005).

For these experiments we generated endogenous ROS by activating NADPH oxidase with Ang II (Griendling et al., 1994). We demonstrated previously that ROS, specifically H_2O_2, is necessary for oxidant-dependent stimulation of L-type Ca^{2+} channels in arterial smooth muscle cells (**Chapter 2**). In agreement with earlier findings, (Amberg et al., 2010; Navedo et al., 2008; Nieves-Cintrón et al., 2008; **Chapter 2**), Ang II (100 nM) increased L-type Ca^{2+} channel activity in isolated arterial smooth muscle cells (see **Fig. 3.1**) Ang II increased the density of L-type channel Ca^{2+} sparklet sites as well as the activity (nP_s) of those sites ($P<0.05$, n=5 cells). To test if oxidative stimulation of L-type Ca^{2+} channels requires DAG-dependent activation of PKC we repeated our Ang II experiments in the presence of the PKC inhibitor safingol, which inhibits PKC activation by competitively interacting with the regulatory DAG/phorbol binding domain of the kinase (Hannun et al., 1986). Interestingly, we found that safingol (50 μM) had no effect on Ang II-dependent stimulation of L-type Ca^{2+} channels. As noted above, the PKC catalytic site

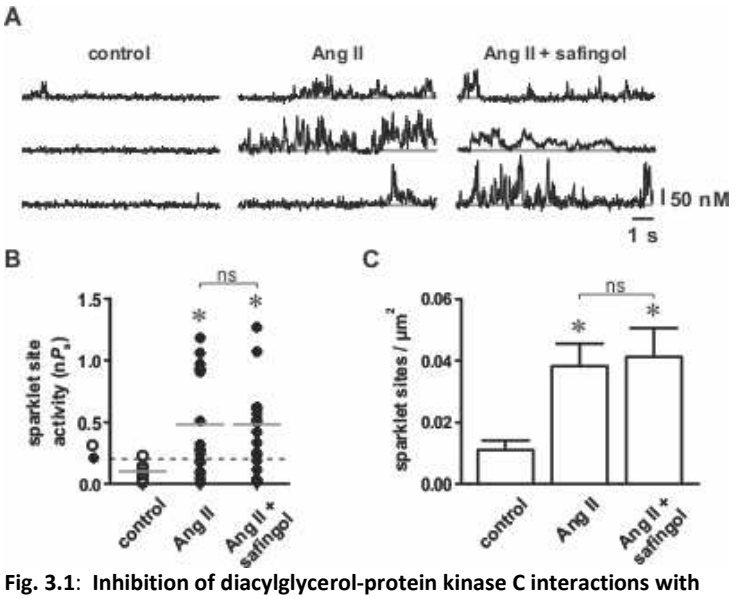

Fig. 3.1: **Inhibition of diacylglycerol-protein kinase C interactions with safingol does not prevent angiotensin II-dependent stimulation of arterial smooth muscle L-type Ca2+ channels**. A, Representative traces showing the time course of Ca2+ influx under control conditions (left), in the presence of Ang II (100 nM; middle), and in the presence of Ang II plus safingol (10 µM; right). B, Plot of L-type Ca2+ channel sparklet site activities (nPs) under control conditions, in the presence of Ang II, and in the presence of Ang II plus safingol (n=5 cells each). The solid grey lines are the arithmetic means of each group and the dashed line marks the threshold for high-activity Ca2+ sparklet sites (nPs≥0.2). C, Plot of the mean±SEM L-type Ca2+ channel sparklet site densities (Ca2+ sparklet sites/µm2) under control conditions, in the presence of Ang II, and in the presence of Ang II plus safingol (n=5 cells each). * P<0.05

inhibitor Gö6976 abolished stimulation of L-type Ca^{2+} channels by exogenous ROS generated by xanthine oxidase (Amberg et al., 2010). From these accumulated data we conclude that oxidative stimulation of L-type Ca^{2+} channels does not require DAG-dependent activation of PKC. Rather, we suggest that during increased oxidative stress, activation of PKC, which is necessary for stimulation of L-type Ca^{2+} channels, could occur via an oxidant-dependent mechanism (Gopalakrishna and Anderson, 1989).

Next, we examined if H_2O_2-dependent stimulation of arterial smooth muscle L-type Ca^{2+} channels requires PKC catalytic activity by testing the effect of the PKC catalytic site inhibitor Gö6976 (100 nM) on H_2O_2-dependent activation of L-type Ca^{2+} channels. Consistent with our previous observations (**Section 2**), in the absence of Gö6976, H_2O_2 (100 µM) produced robust L-type Ca^{2+} channel activity (see **Fig. 3.2**). In contrast, in the presence of Gö6976, H_2O_2 had minimal effect on L-type Ca^{2+} channel function. Specifically, Gö6976 abolished the increase in the number of active L-type Ca^{2+} channel sites observed following H_2O_2 exposure under control conditions (P<0.05, n=5 cells). Surprisingly, the activity of L-type Ca^{2+} channel that were observed (i.e., nP_s) following H_2O_2 were not statistically different in the absence or presence of Gö6976 (P>0.05, n=5 cells). Note, however, that the number of L-type channel Ca^{2+} influx events observed was reduced ≈ 4-fold from 17 events under

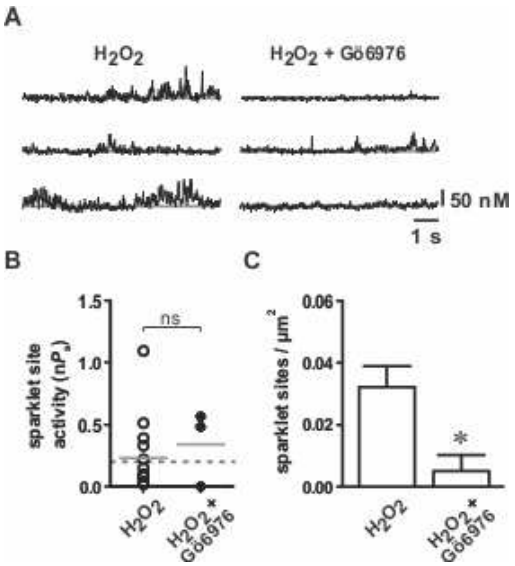

Fig. 3.2. Inhibition of protein kinase C catalytic activity with Gö6976 prevents H2O2-dependent stimulation of arterial smooth muscle L-type Ca2+ channels. A, Representative traces showing the time course of Ca2+ influx in the presence of H2O2 (100 µM; left) and in the presence of H2O2 plus Gö6976 (100 nM; right). B, Plot of L-type Ca2+ channel sparklet site activities (nPs) in the presence of H2O2 and in the presence of H2O2 plus Gö6976. (n=5 cells each). The solid grey lines are the arithmetic means of each group and the dashed line marks the threshold for high-activity Ca2+ sparklet sites (nPs≥0.2). C, Plot of the mean±SEM L-type Ca2+ channel sparklet site densities (Ca2+ sparklet sites/µm2) in the presence of H2O2 and in the presence of H2O2 plus Gö6976. (n=5 cells each). * P<0.05

control conditions to only 4 events in the presence Gö6976 (n=5 cells). Thus, we conclude that stimulation of L-type Ca^{2+} channels by H_2O_2 requires catalytic PKC activity.

3.5 Discussion

Here we continued our characterization of the role of PKC in the oxidative stimulation of arterial smooth muscle L-type Ca^{2+} channels. We observed that: 1) Inhibition of the interaction between DAG and PKC did not prevent Ang II from stimulating L-type Ca^{2+} channels, which we had previously shown to be oxidant-dependent (Amberg et al., 2010; **Section 2**); and 2) stimulation of L-type Ca^{2+} channels by H_2O_2 was abolished by inhibition of PKC catalytic activity. From these data and our published work (Amberg et al., 2010; **Section 2**) we conclude that stimulation of arterial smooth muscle L-type Ca^{2+} channels by H_2O_2 involves oxidative activation of PKC.

Previous studies have shown that ROS increase the activity of PKC isoforms (such as PKCα) by oxidizing reactive of cysteine residues in the kinase regulatory domain leading to constitutive cofactor-independent activity (Gopalakrishna and Anderson, 1989; Knapp and Klann, 2002; Palumbo et al., 1992). Conversely, oxidation of cysteine residues in the catalytic domain leads to enzyme inactivation. Importantly, oxidative modification of the PKC regulatory and enzymatic domains is concentration dependent: Cysteine residues in the regulatory domain are more sensitive to oxidative modification than those in the catalytic domain (Gopalakrishna and Anderson, 1989). As a result, limited exposure to

mild oxidative conditions increases kinase activity while prolonged pathological oxidative insults promote inhibition.

We have shown that Ang II produces punctate elevations in ROS production in isolated arterial myocytes (Amberg et al., 2010**; Section 2**). Our results presented here therefore suggest a potential mechanistic basis for differential activation of discrete functional pools of PKC in arterial smooth muscle ells: PKC molecules in close proximity to sites of localized ROS generation would be subject to oxidative activation while those distal to these sites would not. Thus, targeting of PKC to specific subcellular sites (e.g., through interacting with the scaffolding protein AKAP150) (Navedo et al., 2008) could result in initiation of oxidant-dependent and independent PKC signaling cascades with different physiological outcomes.

To conclude, our data indicate that local oxidative activation of PKC and subsequent stimulation of adjacent L-type Ca^{2+} channels gives rise to coordinated sites of ROS generation and Ca^{2+} entry. We suggest that oxidative regulation of arterial smooth muscle PKC represents a critical intracellular signaling nexus where perturbations in oxidative status translate into changes in arterial smooth muscle function via regulation of L-type Ca^{2+} channel activity. Our data clearly indicate that local ROS production stimulates colocalized Ca^{2+} influx through L-type channels (Amberg et al., 2010; **Section 2**). Interestingly, Ca^{2+} is known to stimulate NADPH oxidase activity via PKC (Brown and Griendling , 2009).Thus, it is reasonable to propose that colocalized ROS and Ca^{2+} microdomains may form a reciprocal coupling mechanism leading to sustained ROS generation and Ca^{2+} influx via NADPH oxidase and L-type Ca^{2+} channels, respectively. Future studies should address this intriguing hypothesis.

Chapter 4. Arterial smooth muscle mitochondria amplify hydrogen peroxide microdomains functionally coupled to L-type calcium channels[3]

4.1 Summary

Mitochondria are key integrators of convergent intracellular signaling pathways. Two important second messengers modulated by mitochondria are calcium and reactive oxygen species. To date, coherent mechanisms describing mitochondrial integration of calcium and oxidative signaling in arterial smooth muscle are incomplete. To address and add clarity to this issue we tested the hypothesis that mitochondria regulate subplasmalemmal calcium and hydrogen peroxide microdomain signaling in cerebral arterial smooth muscle.

Using an image-based approach we investigated the impact of mitochondrial regulation of L-type calcium channels on subcellular calcium and ROS signaling microdomains in isolated arterial smooth muscle cells. Our single cell observations were then related experimentally to intact arterial segments and to living animals. We found that subplasmalemmal mitochondrial amplification of hydrogen peroxide microdomain signaling stimulates L-type calcium channels and that this mechanism strongly impacts the functional capacity of the vasoconstrictor angiotensin II. Importantly, we also found that disrupting this mitochondrial amplification mechanism *in vivo* normalized arterial function and markedly attenuated the hypertensive response to systemic endothelial dysfunction.

From these observations we conclude that mitochondrial amplification of subplasmalemmal calcium and hydrogen peroxide microdomain signaling is a fundamental mechanism regulating arterial smooth muscle function. As the principle components involved are fairly ubiquitous and positioning of

[3] Chaplin NL, Nieves-Cintrón M, Fresquez AM, Navedo MF, Amberg GC (2015) Arterial Smooth Muscle Mitochondria Amplify Hydrogen Peroxide Microdomains Functionally Coupled to L-Type Calcium Channels.Circ Res. pii: CIRCRESAHA.115.306996. [Epub ahead of print]

mitochondria near the plasma membrane is not restricted to arterial smooth muscle, this mechanism could occur in many cell types and contribute to pathological elevations of intracellular calcium and increased oxidative stress associated with many diseases

4.2 Introduction

Mitochondria are central to eukaryotic aerobic metabolism. One consequence arising from the shuttling of electrons onto molecular oxygen during mitochondrial respiration is the formation of reactive oxygen species (ROS). Given the resultant necessity and subsequent ubiquity of ROS formation it is not surprising then that these generally toxic products of metabolism also function as purposeful second messenger molecules (Clempus and Griendling, 2006; Hool, 2006).

Advances in cellular pathophysiology implicate mitochondrial dysfunction in the development and progression of illnesses including cancer (Lynam-Lennon et al., 2014), neurodegeneration (Gonzalez-Lima et al., 2014), diabetes (Peinado et al., 2013), and cardiovascular disease Dikalov and Nazarewicz, 2012; Serpillon et al., 2009). As such, mitochondria are being evaluated as potential therapeutic targets for novel disease prevention and management strategies (Dikalova et al., 2010). If mitochondria are to be viable therapeutic targets then a mechanistic understanding of mitochondrial function in multiple cell types is necessary to rationally predict and account for pharmacological responses to mitochondrial perturbations.

Here we investigated mitochondrial ROS signaling-dependent regulation of Ca^{2+} influx in arterial smooth muscle. These cells are an ideal experimental model for this work due to their large surface area and because their geometry and morphological simplicity minimizes confounding variables possible in cells with more complex structural features. Furthermore, mitochondria, ROS, and Ca^{2+} are each integral to arterial smooth muscle function and are thought to be involved in the development of cardiovascular disease.

Ca^{2+}, as with ROS, is a ubiquitous signaling molecule that influences many processes ranging from contraction to gene expression. Ca^{2+} and ROS as second messenger signaling molecules share at least four key attributes relevant to this study: First, Ca^{2+} and ROS signaling events are known to be functionally coupled (Feissner et al., 2009; Hidalgo and Denoso, 2008); second, Ca^{2+} and ROS signaling cascades attain specificity in part by subcellular compartmentalization Berridge et al., 2000; Terada, 2006), third, Ca^{2+} and ROS signaling events are influenced by mitochondria(Feissner et al., 2009) ; and fourth, Ca^{2+} and ROS signaling cascades are implicated in the development of disease (Hidalgo and Denoso, 2008; Hool, 2008).

In accordance with the first two attributes, our prior work showed that formation of punctate sites of ROS generation involving NADPH oxidase leads to colocalized Ca^{2+} influx through L-type Ca^{2+} channels (Amberg et al., 2010; **Chapters 2 and 3**). We found that oxidative activation of protein kinase C (PKC), which promotes localized Ca^{2+} influx through L-type Ca^{2+} channels (Amberg et al., 2007; Navedo and Amberg, 2013; Navedo et al., 2005), functionally links Ca^{2+} and ROS microdomain signaling in this context. Here we addressed the second pair of Ca^{2+} and ROS signaling attributes listed above by investigating mitochondrial ROS-dependent regulation of arterial smooth muscle L-type Ca^{2+} channels in relation to the development of hypertension-associated arterial dysfunction.

Experiments were performed on single cells, on excised arterial segments, and in living animals. Using this progressive subcellular *in vitro*-to-organismal *in vivo* approach we conclude that amplification of hydrogen peroxide (H_2O_2) microdomain signaling by subplasmalemmal mitochondria promotes the opening of adjacent L-type Ca^{2+} channels and subsequently the development of hypertension-associated arterial dysfunction.

4.3 Methods

Chemicals

All chemicals were from Sigma unless stated otherwise.

Isolation of rat cerebral arterial myocytes

Adult male Sprague-Dawley rats (Harlan) were euthanized with sodium pentobarbital (200 mg/kg intraperitoneally; MWI Veterinary Supply) in accordance with institutional guidelines and approved by the Institutional Animal Care and Use Committee of Colorado State University and the University of California, Davis. Isolated smooth muscle cells were prepared from basilar and cerebral arteries. Arteries were removed, cleaned, and placed in ice-cold Ca^{2+}-free buffer containing (mmol/L): 140 NaCl, 5 KCl, 2 $MgCl_2$, 10 glucose, and 10 HEPES (adjusted to pH 7.4 with NaOH). Arteries were incubated for 15 min at 37°C in Ca^{2+}-free buffer supplemented with papain (10 U/mL; Worthington Biochemical) and dithiothreitol (1 mg/mL) followed by a second incubation (15 min at 37°C) in Ca^{2+}-free buffer supplemented with collagenase (300 U/mL, Type II, Worthington Biochemical). Arteries were then washed with and placed in Ca^{2+}-free buffer and kept on ice for 30 min after which trituration with a fire-polished Pasteur pipette was used to create a cell suspension; cells were used within 6 h of dispersion.

Confocal microscopy

Laser scanning confocal microscopy was used to image the plasma membrane and mitochondria. Freshly prepared smooth muscle cell suspensions were pipetted into a glass bottomed recording chamber. The extracellular face of the plasma membrane was marked with a wheat germ agglutinin Alexa 555 conjugate (Life Technologies; 5 µg/mL for 15 min) and mitochondria were labelled with MitoTracker Green (Life Technologies; 1 µmol/L for 15 min). Alexa 555 was excited with a 543 nm laser and MitoTracker Green was excited with a 488 nm laser; excitation and emission light was separated with appropriate filters. Data were analyzed with Volocity 3D Image Analysis Software

(PerkinElmer). Mitochondrial-associated fluorescence located ≤0.5µm from the center of the Alex 555-WGA signal was designated as peripheral as this value falls within the predicted functional distance of intracellular signaling H_2O_2 (Winterbourne, 2008; Winterbourne, 2013).

Electrophysiology

Smooth muscle cell suspensions were pipetted into a glass bottomed recording chamber and the cells were allowed to adhere for 20 min. Membrane potential was controlled with an Axopatch 200B amplifier (Molecular Devices). The perforated whole-cell patch-clamp technique was used to record macroscopic L-type Ca^{2+} channel currents with barium (Ba^{2+}) as the charge carrier. For these experiments the amphotericin B (250 µg/ml) supplemented pipette solution contained (mmol/L): 120 CsCl, 20 TEA-Cl, 1 EGTA, and 20 HEPES (adjusted to pH 7.2 with CsOH) and cells were superfused with an external solution composed of (mmol/L): 115 NaCl, 10 TEA-Cl, 0.5 $MgCl_2$, 5.5 glucose, 5 CsCl, 20 $BaCl_2$, and 20 HEPES (adjusted to pH 7.4 with CsOH).

For our Ca^{2+} imaging experiments, we used the conventional dialyzed whole-cell patch-clamp technique. During these experiments cells were superfused with a solution containing (mmol/L): 120 $NMDG^+$, 5 CsCl, 1 $MgCl_2$, 10, glucose, 10 HEPES, and 20 $CaCl_2$ (adjusted to pH 7.4 with HCl). Pipettes were filled with a solution composed of (mM): 87 Cs-aspartate, 20 CsCl, 1 $MgCl_2$, 5 MgATP, 0.1 Na_2GTP, 1 NADPH, 10 glutathione, 10 HEPES, 10 EGTA, and 0.2 fluo-5F (adjusted to pH 7.2 with CsOH). All electrophysiological experiments were performed at room temperature (22-25°C) and were allowed to progress between 5 and 10 minutes. Only recordings with stable GΩ seals were analyzed.

TIRF microscopy

Ca^{2+} influx through L-type channels was visualized with a TILL Photonics through-the-lens TIRF system built around an inverted Olympus IX-71 microscope using a 100X (numerical aperture = 1.45) TIRF oil-immersion objective and an Andor iXON EMCCD camera. To monitor Ca^{2+} influx, myocytes were loaded with the Ca^{2+} indicator fluo-5F (200 µmol/L; pentapotassium salt; Invitrogen) and an excess of

EGTA (10 mmol/L) via the patch pipette. To preclude potential contaminating Ca^{2+} release events from the sacroplasmic reticulum, the Ca^{2+}-ATPase inhibitor thapsigargin (1 µmol/L) was present during all experiments. Excitation of fluo-5F was achieved with a 491 nm laser and excitation and emission light was separated with appropriate filters. Ca^{2+} influx was recorded at 50 Hz at a holding potential of -70 mV and elevated external [Ca^{2+}] (20 mmol/L) to facilitate the detection of events and provide fluorescent signals of sufficient amplitude[3] to permit quantal analysis.

L-type Ca^{2+} channel sparklet analysis.

Background-subtracted fluo-5F fluorescence signals were converted to [Ca^{2+}] (Amberg et al., 2010; Navedo et al., 2006; Maravall et al., 2000) using the equation

$$\left[Ca^{2+}\right] = K_d \frac{F/F_{\max} - 1/R_f}{1 - F/F_{\max}}$$

where F is fluorescence, F_{max} is the fluorescence intensity of fluo-5F in the presence of saturating free Ca^{2+}, F_{min} is the fluorescence intensity of fluo-5F in a solution where [Ca^{2+}] is 0, K_d is the dissociation constant of fluo-5F, and R_f is the F_{max}/F_{min} of fluo-5F. K_d and R_f values for fluo-5F were determined in vitro and F_{max} was determined at the conclusion of each experiment with ionomycin (10 µmol/L). Fluo-5F fluorescence images were analyzed with custom software (Navedo et al., 2006). For an elevation in $[Ca^{2+}]_i$ to be considered an L-type Ca^{2+} channel sparklet event, a grid of 3 x 3 contiguous pixels had to have a $[Ca^{2+}]_i$ amplitude equal to or larger than the mean basal $[Ca^{2+}]_i$ plus three times its standard deviation.

Quantal analysis of L-type Ca^{2+} channel sparklet activity (Amberg et al., 2010; Navedo et al., 2005; Navedo et al., 2006) was performed on histograms generated from individual event amplitudes. The resulting histograms were fitted with the multicomponent Gaussian function

$$N = \sum_{j=1}^{n} a_j * \exp\left[-\frac{([Ca^{2+}]_i - jq)^2}{2jb}\right]$$

where a and b are constants, $[Ca^{2+}]_i$ is intracellular Ca^{2+}, and q is the quantal unit of Ca^{2+} influx. The quantal amplitude of the Ca^{2+} sparklets observed in this study was 36.2±3.2 nmol/L $[Ca^{2+}]$.

L-type Ca^{2+} channel sparklet activity was determined (Amberg et al., 2010; Navedo et al., 2005; Navedo et al., 2006) by calculating the nP_s of each site, where n is the number of quantal levels detected, and P_s is the probability that the site is active. nP_s values were obtained using pCLAMP 10.0 (Molecular Devices) on imported $[Ca^{2+}]_i$ time course records. L-type Ca^{2+} channel sparklet activity was quantified using an initial unitary $[Ca^{2+}]_i$ elevation of 38 nmol/L as determined experimentally (Navedo et al., 2005). Consistent with previous reports (Amberg et al., 2007; Amberg et al., 2010; Navedo et al., 2005; Navedo et al., 2006), L-type Ca^{2+} channel sparklet activity was bimodally distributed with sites of low activity (nP_s between 0 and 0.2) and high activity (nP_s greater than 0.2). Active L-type Ca^{2+} channel densities (Ca^{2+} sparklet sites per μm^2) were calculated by dividing the number of active sites by the area of cell membrane visible in the TIRF images.

Imaging of subplasmalemmal mitochondria

TIRF microscopy was also used to image subplasmalemmal mitochondria in isolated cells. Briefly, dispersed arterial smooth muscle cells were incubated with MitoTracker Green or MitoTracker Red CM-XRos (1 µmol/L) for 15 min. Subplasmalemmal MitoTracker Green was excited with a 491 nm laser and MitoTracker Red was excited with a 561 nm laser and excitation and emission light was separated with appropriate filters. For an area of elevated MitoTracker fluorescence to be considered indicative of subplasmalemmal mitochondria the fluorescence amplitude had to be equal to or larger than the mean basal fluorescence plus three times its standard deviation. Using this criterion we generated thresholded MitoTracker TIRF images to establish clear mitochondrial boundaries. The % of plasma membrane associated with subplasmalemmal mitochondria was calculated by dividing the area of membrane associated with mitochondria by the area of plasma membrane visible. We defined

mitochondrial-associated L-type Ca^{2+} channel sparklet sites as those sites with peaks (pixels of highest intensity) ≤0.5 μm from the edge of the nearest thresholded MitoTracker signal.

Note that the subplasmalemmal MitoTracker fluorescence image shown in **Figure 4.2A** was obtained from a cell where we also recorded Ca^{2+} influx. This required placing a glass pipette onto the top of the cell. With this experimental configuration, MitoTracker fluorescence was associated with 8.52±2.22% of the visible plasma membrane (n=5 cells). We attribute this modest increase in plasma membrane associated with mitochondria (versus 3.29±0.26% in non-patched cells; $P<0.05$) to the downward pressure exerted on the cell from the dorsally placed pipette. Regardless, our TIRF images indicate that subplasmalemmal mitochondria are associated with a relatively small fraction of the plasma membrane (≈5%).

Euclidean distance mapping analysis was used to quantitate the distance of observed Ca^{2+} sparklet site peaks from the nearest thresholded MitoTracker signal and from 100 randomly distributed points located within visible TIRF footprint of the cells analyzed. Each cumulative distribution was fit with a single exponential function $Y=Y_0+(\text{plateau}- Y_0)*[1-\exp(-(\ln 2/X_{0.5})*X)]$ where Y is the cumulative frequency, Y_0 is the Y value when X (distance) is zero, plateau is the Y value at infinite times, and $X_{0.5}$ (half-distance) is X where 50 % of the Y values are distal to X=zero.

Detection of reactive oxygen species generation

TIRF microscopy was also used to visualize subplasmalemmal ROS generation as described previously by us (Amberg et al., 2010). Cells were loaded in Ca^{2+}-free buffer supplemented with the cell-permeant ROS indicator 5-(and-6)-chloromethyl-2'7'-dichlorodihydrofluorescein diacetate acetyl ester (DCF; 10 μmol/L; Invitrogen) for 20 min at room temperature. Following removal of excess DCF with unsupplemented Ca^{2+}-free buffer, excitation of subplasmalemmal DCF was achieved with a 491 nm laser and excitation and emission light was separated with appropriate filters. Analogous to L-type Ca^{2+} channel influx, for an area of elevated DCF fluorescence to be considered a localized site of increased

ROS generation (a ROS "puncta"), a grid of 3 x 3 contiguous pixels had to have a fluorescence amplitude equal to or larger than the mean basal DCF fluorescence plus three times its standard deviation (Amberg et al., 2010; Navedo et al., 2005). ROS puncta densities (ROS puncta per μm^2) were calculated by dividing the number of sites detected by the area of cell membrane visible in the TIRF images. Changes in DCF fluorescence (Δ DCF) were calculated from the mean pixel intensities of the total intracellular submembranous slice visible in the TIRF images (average Δ DCF) and the areas confined to nascent ROS puncta (puncta Δ DCF).

Intact arterial diameter measurements

Intact arterial diameters were recorded from middle cerebral arterial segments as previously described(Amberg et al., 2010; **Chapter 2**). Briefly, isolated arteries were stored in ice-cold MOPS buffer containing (mmol/L): 145 NaCl, 5 KCl, 1 $MgSO_4$, 2.5 $CaCl_2$, 1 KH_2PO_4, 0.02 EDTA, 2 pyruvate, 5 glucose, 1% bovine serum albumin, and 3 MOPS (adjusted to pH 7.4 with NaOH). Arteries were transferred to a vessel chamber (Living Systems), one end of the artery was cannulated onto a glass micropipette and secured with monofilament suture and the other end was cannulated onto an opposing micropipette. Arteries were pressurized to 20 mmHg with a bicarbonate-based physiological saline solution containing (mmol/L): 119 NaCl, 4.7 KCl, 1.8 $CaCl_2$, 1.2 $MgSO_4$, 24 $NaHCO_3$, 0.2 KH_2PO_4, 10.6 glucose, and superfused (3 mL/min) with warmed physiological saline solution (37°C) aerated with a normoxic gas mixture (21% O_2, 6% CO_2, balance N_2). To block the effects of endothelial-derived nitric oxide, the nitric oxide synthase inhibitor N^{ω}-nitro-L-arginine (L-NNA; 300 µmol/L) was included in the superfusate.

Following a 15-minute equilibration period, intraluminal pressure was increased to 60 mmHg, arteries were stretched to remove bends, and the pressure was lowered back to 20 mmHg for a second 15-minute equilibration period. Intraluminal pressure was then increased back to 60 mmHg and the inner diameter continuously monitored using video microscopy and edge-detection software (Ionoptix). To assess viability, all arteries were exposed to isotonic physiological saline solution containing 60

mmol/L KCl. For experiments with mitoTEMPO (Enzo Life Sciences) and TEMPOL (EMD Millipore), these antioxidants were added after a stable level of tone was obtained at 60 mmHg. Following stabilization with mitoTEMPO and TEMPOL, Ang II was added and experiments were terminated by superfusing with a nominally Ca^{2+}-free physiological saline solution to obtain the passive diameter of the artery. Arterial contraction was calculated as the percentage difference in active luminal diameter versus passive luminal diameter. Passive luminal diameters were not different for our all experimental groups (P>0.05) and myogenic tone at 60 mmHg under control conditions (i.e., with only L-NNA present) in arteries from normotensive rats was also not different between all groups (P>0.05).

L-NAME-induced hypertension, mitoTEMPO infusion, and blood pressure monitoring

Hypertension was induced in adult male Sprague Dawley rats by including N^{ω}-nitro-L-arginine methyl ester (L-NAME; 0.75 mg/mL) in their drinking water for ten days (Takemoto et al., 1997; Bartunek et al., 2000; Lu et al., 2008; Marañon et al., 2014). Daily water consumption in these rats was ≈70 mL/kg/day resulting in a dose of ≈50 mg/kg per day. Rats were also implanted with subcutaneous osmotic minipumps (Alzet) eluting mitoTEMPO (150 μg/kg per day) or saline (for control) as previously described (Dikalova et al., 2013).

Arterial blood pressure was monitored continuously in conscious freely moving rats by telemetry (Data Science International). Briefly, rats were anesthetized with isoflurane and a ventral midline incision through the abdominal wall was made. The intestines were manipulated with sterile cotton tip applicators to locate the abdominal aorta. Once located, the intestines were retracted using a sterile 4 x 4 gauze sponge. The overlying tissue was separated from the aorta surface, just caudal to the crossover of the left renal vein and cranial to the iliac bifurcation with sterile cotton tips and the aorta was temporary occluded with suture. A 22-gauge needle with the tip bent to a 90° angle was used to pierce the artery cranial to the iliac bifurcation and the catheter was inserted. The entry site was dried of blood and a small amount of tissue adhesive was applied to prevent leakage and maintain the

catheter in place. Tension was carefully released from the occlusion suture and the catheter entry area monitored for leakage. The catheter was anchored in place using a small sterile fiber patch and secured with tissue adhesive. The transmitter was placed on top of the intestines parallel to the long axis of the body. The abdominal wall was close using non-absorbable sutures of appropriate size. An absorbable suture was used to close the skin. Osmotic minipumps were implanted concurrently to avoid additional pain and distress associated with a second survival surgery; L-NAME administration (when appropriate) was initiated ≈5 days later.

Statistics

Statistical analyses were performed with GraphPad Prism 6 and OriginPro 8.1 software. Normally distributed data are presented as the mean±standard error of the mean (SEM). Two-sample comparisons of these data were performed using either a paired or unpaired (as appropriate) two-tailed Student's t test and comparisons between more than two groups were performed using a one way ANOVA with Tukey's multiple comparison post-test. L-type Ca^{2+} channel sparklet activity (i.e. nP_s) datasets were bimodally distributed (Amberg et al., 2010; Navedo et al, 2006; **Chapter 2**), thus two-sample comparisons of nP_s data were examined with the non-parametric Wilcoxon-Mann-Whitney test (two-tailed) and comparisons between more than two groups were performed using the non-parametric Friedman test with Dunn's multiple comparison post-test. Arithmetic means of nP_s datasets are indicated in the figures (solid grey horizontal lines) for non-statistical visual purposes and dashed grey lines mark the threshold for high-activity Ca^{2+} sparklet sites (nP_s≥0.2) (Amberg et al., 2010; Navedo et al., 2005; Navedo et al., 2006).

To account for potential variability associated with cell isolation, all single myocyte experimental groups were comprised of cells obtained from a minimum of 4 rats. Effect sizes, represented in the figures as bracketed values, are reported as Pearson's *r* (range -1.0 to 1.0; 0 indicates no effect) (Cohen, 1988; Rosenthal et al., 1994; Rosenthal and Rubin, 2003; Rosnow et al., 2003). $P<0.05$ were considered

significant and asterisks (*) used in the figures are included to indicate significance; ns = not significantly different (Rosenthal and Rubin, 2003; Rosnow et al., 2003).

4.4 Results

A subpopulation of mitochondria associates with the arterial smooth muscle cell plasma membrane at sites of elevated L-type Ca^{2+} channel activity

To assess the subcellular distribution of mitochondria in arterial smooth muscle we marked the plasma membrane of cells with a wheat germ agglutinin conjugate (Alexa 555-WGA, red), labelled mitochondria with MitoTracker Green, and visualized the fluorescence with confocal microscopy (**Figure 4.1A**). We found that 8.64±0.42% of the total cell volume was occupied by mitochondria; this volume is consistent with prior reports (Somlyo, 1985). While the majority of the MitoTracker signal was located centrally (>0.5 µm from the center of the Alexa 555-WGA signal), 7.50±0.77% of the mitochondrial volume was peripheral (≤0.5 µm; yellow signal in **Figure 4.1A, panel 3**).

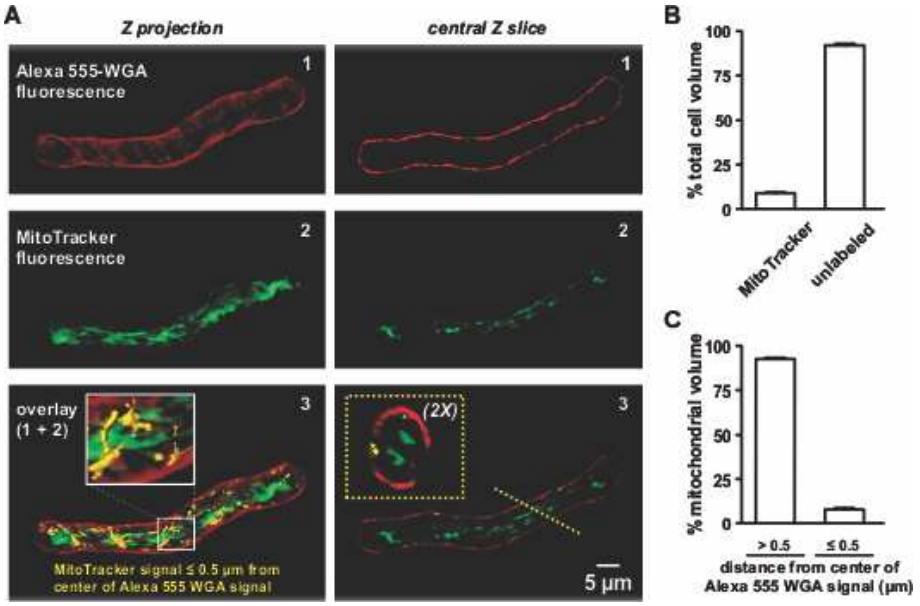

Figure 4.1. Subplasmalemmal mitochondria are present but sparse in rat cerebral arterial smooth muscle cells. A, Representative confocal images showing the plasma membrane (Alexa 555-WGA fluorescence, red) and mitochondria (MitoTracker fluorescence, green) in an isolated rat cerebral arterial smooth muscle cell. In panel 3, subplasmalemmal mitochondria (≤0.5µm from the plasma membrane) are highlighted yellow. The inset in panel 3 shows z projections at the x and y positions indicated by the dashed yellow lines. B, Plot of the mean±SEM mitochondrial and non-mitochondrial volumes (% of total cell volume; n=5 cells). C, Plot of the mean±SEM non-peripheral (>0.5 µm from the plasma membrane) and subplasmalemmal (≤0.5 µm) mitochondrial volumes (% total mitochondrial volume; n=5 cells).

Next we examined MitoTracker-loaded cells with TIRF microscopy. Our images showed regions

of MitoTracker fluorescence indicating the presence of subplasmalemmal mitochondria (**Figure 4.2A**, **panel 1**). Analysis of thresholded MitoTracker images revealed that only 3.29±0.26% (n=7 cells) of the visible plasma membrane was associated with mitochondria (**Figure 4.2A, panel 2**). We imaged Ca^{2+} influx with a combination of TIRF microscopy and voltage-clamp electrophysiology (Amberg et al., 2007; Amberg et al., 2010; Navedo et al., 2005). This approach permits visualization of Ca^{2+} influx through L-type Ca^{2+} channels ("Ca^{2+} sparklets"). To evoke Ca^{2+} sparklets we exposed cells to angiotensin II (Ang II; 100 nM), which is known to promote mitochondrial ROS production (Dikalov and Nazarewicz, 2012). Similar to our previous reports (Amberg et al, 2010; Nieves-Cintrón, 2008; **Chapters 2 and 3**), Ang II induced L-type Ca^{2+} channel sparklet sites as revealed by localized changes in fluorescence of the Ca^{2+} indicator fluo-5F (**Figure 4.2A, panel 3**). The L-type Ca^{2+} channel sparklets induced by Ang II in this study were not different from the L-type Ca^{2+} channel sparklets observed previously in terms of quantal amplitude (36.2±3.2 nmol/L [Ca^{2+}]) and site densities and activities (see below) (Amberg et al, 2010; **Chapters 2 and 3**).

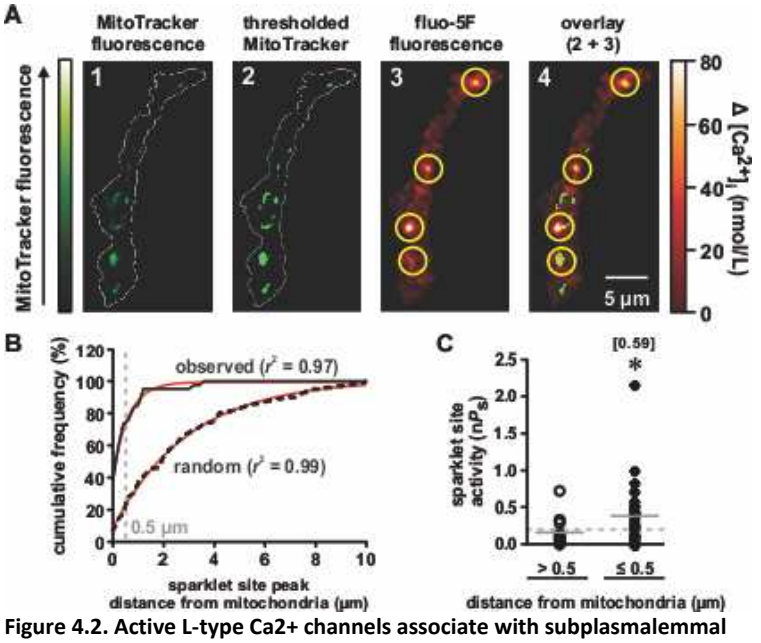

Figure 4.2. Active L-type Ca2+ channels associate with subplasmalemmal mitochondria. A, Representative TIRF images showing subplasmalemmal mitochondria (MitoTracker fluorescence, panel 1; thresholded MitoTracker fluorescence, panel 2), L-type Ca2+ channel-mediated Ca2+ influx (fluo-5F fluorescence; panel 3), and an overlay of panels 2 & 3 (panel 4). Yellow circles in panels 3 and 4 indicate sites of bone fide L-type Ca2+ channel sparklet activity. B, Euclidean distance mapping analysis showing cumulative distribution functions representing the distance of observed Ca2+ sparklet site peaks from mitochondria (solid black line; n=7 cells) and from 100 randomly distributed points within visible TIRF footprint of the cells analyzed (dashed black line). Solid red lines are best fits of the cumulative distributions with a single exponential function. The vertical dashed grey line marks the distance separating mitochondrial associated (≤0.5 µm) and non-associated (>0.5 µm) Ca2+ sparklet sites. C, Plot of Ca2+ sparklet site activities (nPs, where n is the number of quantal levels detected and Ps is the probability that the site is active) at sites >0.5 µm and ≤0.5 µm from the nearest thresholded MitoTracker signal (n=5 cells). The horizontal dashed grey line marks the threshold for high-activity Ca2+ sparklet sites (nPs≥0.2;). Bracketed values indicate effect size (r). * P<0.05

To visualize the spatial relationship between L-type Ca^{2+} channel activity and

subplasmalemmal mitochondria we overlaid our fluo-5F and thresholded MitoTracker images (**Figure 4.2A, panel 4**). We then measured the distance from L-type Ca^{2+} channel sparklet site peaks (pixels of highest intensity) to the edge of the nearest MitoTracker signal and plotted the cumulative values (**Figure 4.2B**). Mitochondrial-associated L-type Ca^{2+} channel sparklet sites were defined *a priori* as those sites with peaks ≤0.5 μm from the edge of the nearest thresholded MitoTracker signal; this is represented by the vertical dashed grey line in **Figure 4.2B**. We found that L-type Ca^{2+} channel function was associated with subplasmalemmal mitochondria (**Figure 4.2B**; n=5 cells). The half-distance of the observed L-type Ca^{2+} channel sparklet sites (n=41 sites) to the nearest mitochondria was 0.43 μm (95% CI [0.39 to 0.47]) whereas the half-distance of 100 random points within the visible plasma membrane to the nearest mitochondria was 2.10 μm (95% CI [1.99 to 2.19]).

Next we compared the activity of mitochondrial-associated (distance ≤0.5 μm) and non-associated L-type Ca^{2+} channel sparklet sites. L-type Ca^{2+} channel sparklet site activity can be expressed by the descriptor nP_s, where n is the number of quanta detected (i.e., number of functional channels) and P_s is the probability that the site is active (Navedo et al., 2005). Ang II-induced L-type Ca^{2+} channel sparklet sites associated with mitochondria were more active than those not associated with mitochondria (**Figure 4.2C**; $P<0.05$, $r=0.59$, n=5 cells). Indeed, mitochondrial-associated L-type Ca^{2+} channel sparklet sites accounted for ≈73% of the total Ca^{2+} sparklet activity observed. From these data we conclude that the spatial distribution of L-type Ca^{2+} channel activity is highly correlated with subplasmalemmal mitochondria.

Mitochondrial-derived H_2O_2 stimulates L-type Ca^{2+} channels

We reported previously that localized H_2O_2 microdomains stimulate L-type Ca^{2+} channels in arterial smooth muscle via a PKC-dependent mechanism (Amberg et al, 2010; Navedo and Amberg, 2013; **Chapters 2 and 3**). As mitochondria are a major source of ROS, we tested the hypothesis that localized H_2O_2 generated by subplasmalemmal mitochondria stimulate nearby L-type Ca^{2+} channels.

To promote mitochondrial ROS generation we exposed cells to the electron transport chain complex III inhibitor antimycin (500 nmol/L) (Murphy, 2009; Zorov et al., 2014). First we investigated the effect of antimycin on subplasmalemmal ROS production by loading cells with the fluorescent ROS indicator 5-(and-6)-chloromethyl-2'7'-dichlorodihydrofluorescein diacetate acetyl ester (DCF; 10 µmol/L) and monitored for changes in subplasmalemmal fluorescence (**Figure 4.3A**). Similar to Ang II (Amberg et al., 2010; **Chapter 2**), antimycin induced localized sites of elevated DCF fluorescence ("ROS puncta";(Amberg et al., 2010) **Figure 4.3A and B**; $P<0.05$, $r = 0.65$, n=5 cells); comparable ROS puncta formation was not apparent in time-matched controls. In contrast to the ≈ 6-fold increase in DCF fluorescence associated with ROS puncta, the spatially averaged DCF fluorescence in cells treated with antimycin did not increase (data not shown; $P>0.05$; n=5 cells). This observation is consistent with the concept of localized ROS generation by subplasmalemmal mitochondria.

Antimycin also induced localized L-type Ca^{2+} channel sparklets (**Figure 4.3C and D**). Ca^{2+} sparklet activity was not observed following antimycin treatment in cells pre-treated with nicardipine (10 µmol/L; $P>0.05$; n=5 cells, data not shown) or the PKC inhibitor Gö6976 (100 nmol/L; **Figure 4.3D**). Similarly, dialyzing cells with catalase (500 U/mL) prevented the stimulatory effect of antimycin on L-type Ca^{2+} channels (**Figure 4.3D**). These data are consistent with the hypothesis that antimycin-dependent promotion of localized mitochondrial H_2O_2 generation stimulates neighboring L-type Ca^{2+} channels via a PKC-dependent mechanism.

Our previous work indicates that NADPH oxidase activity is necessary for local regulation of L-type Ca^{2+} channels by Ang II-induced H_2O_2 microdomain signaling (Amberg et al., 2010; **Chapter 2**). Ang II also induces mitochondrial ROS generation (Dikalov, 2011; Dikalov and Nazarewicz, 2012). Therefore, we tested the effect of inhibiting mitochondrial ROS generation on Ang II-dependent stimulation of L-type Ca^{2+} channels.

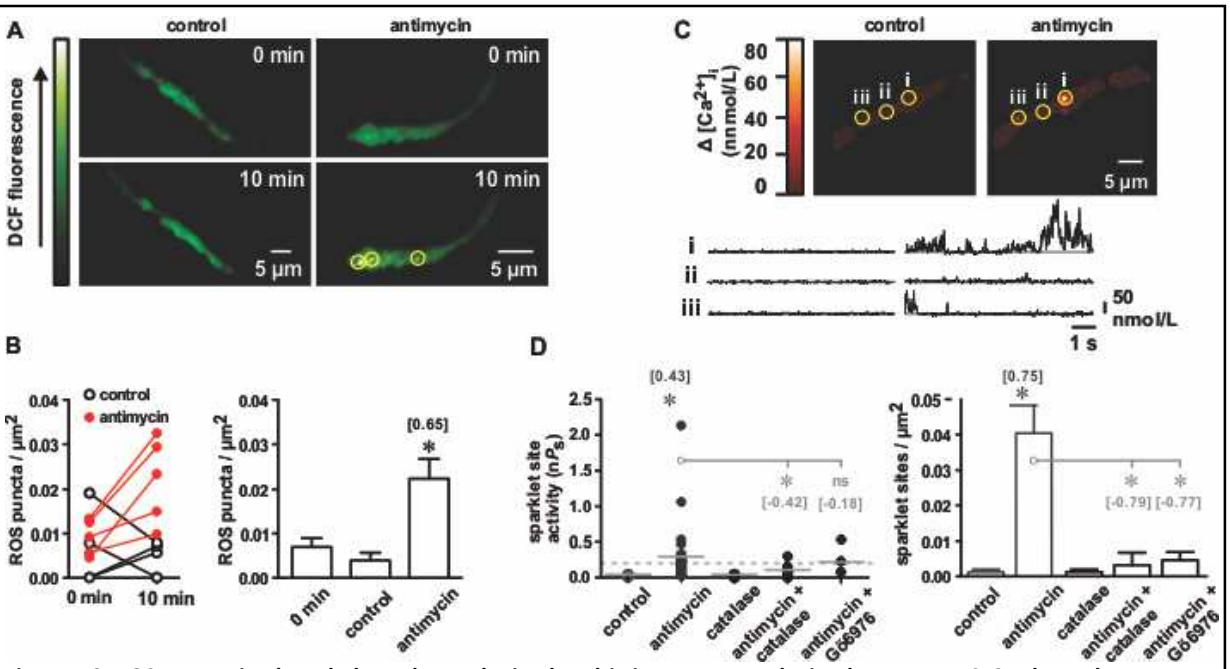

Figure 4.3. ROS generation by subplasmalemmal mitochondria is punctate and stimulates L-type Ca2+ channels. A, Representative TIRF images showing subplasmalemmal DCF fluorescence (indicating intracellular oxidation) in a control cell (left) and in a cell incubated with the mitochondrial electron transport chain complex III inhibitor antimycin (500 nmol/L; right) at the times indicated. Yellow circles indicate sites of bone fide ROS puncta formation. B, Plot of individual ROS puncta densities in control cells (open circles; n=5 cells) and cells treated with antimycin (filled red circles; n=5 cells) at 0 min and at 10 min (left) and plot of mean±SEM ROS puncta densities at 0 min (all values) and at 10 min in control and antimycin-treated cells (right). C, Representative TIRF images showing Ca2+ influx in a cell before and after application of antimycin (500 nmol/L). Traces show the time course of Ca2+ influx at the 3 circled sites. D, Plot of Ca2+ sparklet site activities (nPs) and plot of mean±SEM Ca2+ sparklet densities (Ca2+ sparklet sites/µm2) before and after antimycin in untreated cells (n=5 cells) and in cells pretreated with catalase (n=7 cells) or Gö6976 (n=5 cells). The horizontal dashed grey line marks the threshold for high-activity Ca2+ sparklet sites (nPs≥0.2). Bracketed values indicate effect size (r). * P<0.05

The mitochondrial-targeted antioxidant mitoTEMPO attenuates the production of H_2O_2 by mitochondria in response to Ang II (Dikalov and Nazarewicz, 2012; Dikalova et al., 2010; Dikalov, 2011; Dikalov and Ungvari, 2013). We found that Ang II did not promote ROS puncta formation in cells pre-treated with mitoTEMPO (25 nmol/L for 15 min; **Figure 4.4A and B**; *P*>0.05, *r*=-0.80, n=5 cells). MitoTEMPO also attenuated the stimulatory effect of Ang II on L-type Ca^{2+} channel sparklet site activity (**Figure 4.4C** and D; *P*>0.05, *r*=-0.39, n=5 cells). The L-type Ca^{2+} channel sparklet site activity (nP_s; *r*=0.59) and density (sites/µm^2; *r*=0.93) induced by Ang II was not different from that observed with antimycin (**Figure 4.3D**; *P*>0.05, n=5 cells). Interestingly, and in contrast to NADPH oxidase inhibition or catalase (Amberg et al., 2010; **Chapter 2**), mitoTEMPO did not prevent the increase in L-type Ca^{2+} channel sparklet site density (sites/um^2) induced by Ang II (**Figure 4.4D**; *P*<0.05, *r*=-0.09, n=5 cells). . Similar

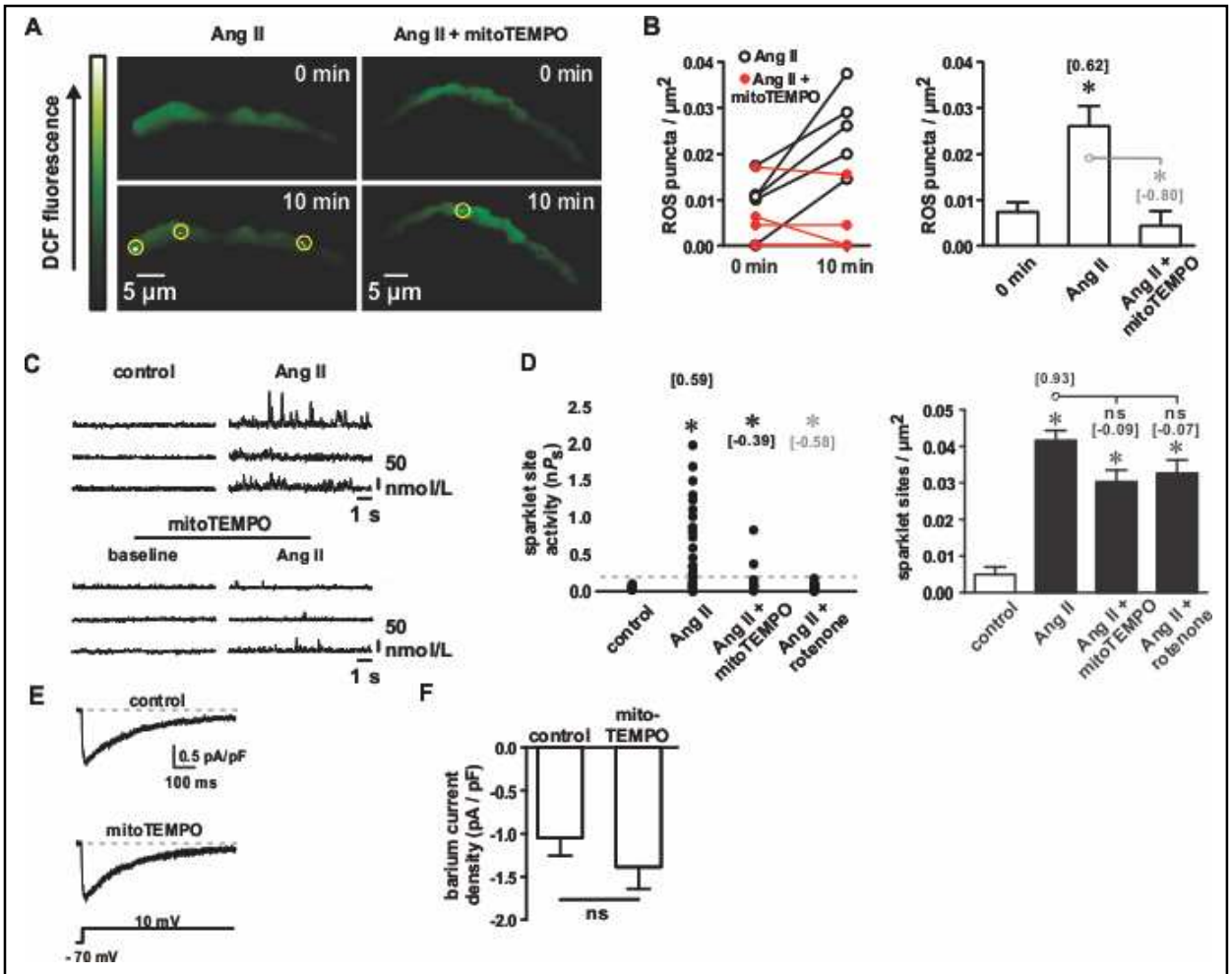

Figure 4.4. Mitochondria contribute to angiotensin II-dependent ROS and Ca2+ microdomain signaling. A, Representative TIRF images showing subplasmalemmal DCF fluorescence in a cell before and after application of Ang II (100 nmol/L; left) and in a cell before and after Ang II in the presence of the mitochondrial targeted antioxidant mitoTEMPO (25 nmol/L; right). Yellow circles indicate sites of ROS puncta formation. B, Plot of individual ROS puncta densities in cells exposed to Ang II (open circles; n=5 cells) and cells exposed to Ang II in the presence of mitoTEMPO (filled red circles; n=5 cells) at 0 min and at 10 min (left) and the plot of mean±SEM ROS puncta densities at 0 min (all values) and at 10 min in Ang II and Ang II in the presence of mitoTEMPO (right). C, Representative traces showing time courses of Ca2+ influx in cells before and after application of Ang II (100 nmol/L) in control cells and in the presence of the mitochondrial targeted antioxidant mitoTEMPO (25 nmol/L). D, Plots showing Ca2+ sparklet site activities (nPs) and mean±SEM Ca2+ sparklet densities (Ca2+ sparklet sites/µm2) before after Ang II in control cells and in the presence of mitoTEMPO or rotenone (n=5 cells each). E, Representative macroscopic L-type Ca2+ channel currents traces using barium (Ba2+) as the charge carrier during step depolarizations to 10 mV from a holding potential of -70 mV before (top) and after mitoTEMPO (25 nmol/L; bottom). F, Plot of the mean±SEM peak barium current densities (pA/pF) before and after mitoTEMPO (n=5 cells). The horizontal dashed grey line marks the threshold for high-activity Ca2+ sparklet sites (nPs ≥0.2). Bracketed values indicate effect size (r). * P<0.05

results were observed when mitochondrial ROS production was limited with rotenone (**Figure 4.4D**; for sparklet activity: P<0.05 vs. Ang II, P>0.05 vs. mitoTEMPO, for density P>0.05). MitoTEMPO did not have apparent nonspecific effects on macroscopic L-type Ca^{2+} channel currents (**Figure 4.4E-F**; P>0.05, n=5

cells). These data suggest that in the presence of mitoTEMPO, Ang II-induced Ca^{2+} influx is minimal despite increasing the number of observed L-type Ca^{2+} channel sparklet sites

Mitochondrial ROS production contributes to angiotensin II-mediated arterial contraction

L-type Ca^{2+} channels are the primary conduit for contractile Ca^{2+} in arterial smooth muscle (Knot and Nelson, 1998). As mitoTEMPO reduced Ang II-dependent stimulation of L-type Ca^{2+} channels we reasoned that inhibiting mitochondrial H_2O_2 production with mitoTEMPO should decrease contractile responses to Ang II. To test this we applied Ang II to excised arterial segments pressurized to 60 mmHg. These experiments were performed in the presence of the nitric oxide synthase inhibitor N^{ω}-nitro-L-arginine (L-NNA, 300 µmol/L) to prevent vasodilatory influences of endothelial-derived nitric oxide.

In control experiments Ang II constricted arteries to 14.86±0.99% below their baseline diameter (**Figure 4.5A**). In arteries incubated with mitoTEMPO (1 µmol/L for 15 min) Ang II induced a smaller contraction to only 3.98±0.99% below baseline (**Figure 4.5B**; $P<0.05$, $r=-0.93$, n=5 arteries). MitoTEMPO by itself had no apparent effect on baseline arterial constriction or the contractile response to 140 mmol/L KCl ($P>0.05$, n=3 arteries, data not shown). We reported previously that the non-targeted antioxidant TEMPOL does not suppress Ang II-dependent stimulation of L-type Ca^{2+} channels (**Chapter 2**). Therefore, we replicated our contractile experiments with Ang II on arteries incubated with TEMPOL (10 µmol/L for 15 min). In contrast

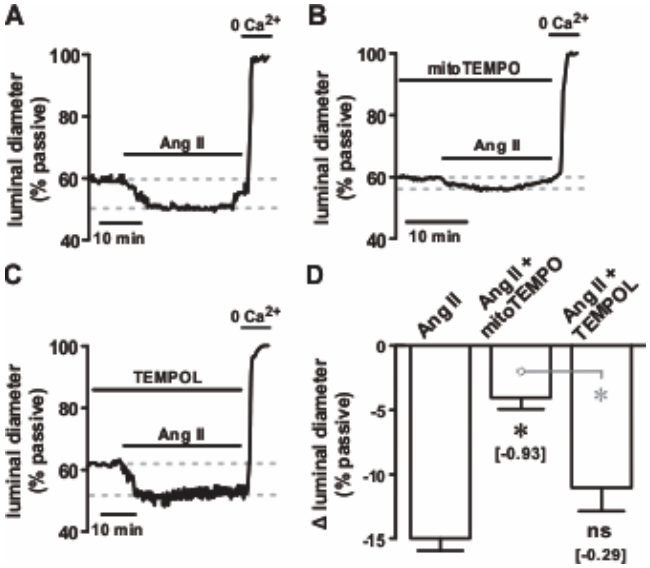

Figure 4.5. Smooth muscle mitochondrial ROS contribute to angiotensin II-dependent arterial contractions. A-C, Representative time courses showing luminal diameters (as % passive diameter) of pressurized (60 mmHg) middle cerebral arterial segments exposed to Ang II (10 nmol/L) in the absence (A) or presence of the mitochondrial-targeted antioxidant mitoTEMPO (1 µmol/L) (B) or the non-targeted antioxidant TEMPOL (10 µmol/L) (C). The horizontal dashed grey lines represent approximate points of measurement for analysis. D, Plot of the mean±SEM induced contraction (% passive diameter) by Ang II in the absence or presence of mitoTEMPO or TEMPOL (n=5 arteries each). Bracketed values indicate effect size (r). * P<0.05

to mitoTEMPO, even at 10-fold higher concentration, TEMPOL did not reduce Ang II-dependent arterial constriction (**Figure 4.5C and D**; $P>0.05$; $r=-0.29$, n=5 arteries). From these data we conclude that mitochondrial-derived ROS contribute to Ang II-dependent constriction of pressurized intact arterial segments.

Reducing mitochondrial ROS production in vivo attenuates hypertensive arterial responses to endothelial dysfunction

To establish the importance of smooth muscle mitochondrial ROS production on arterial function *in vivo* we induced hypertension in rats by including the nitric oxide synthase inhibitor N^{ω}-nitro-L-arginine methyl ester (L-NAME; 0.75 mg/mL) in their drinking water (dose ≈50 mg/kg per day) (Bartunek et al., 2000; Lu et al., 2008; Takemoto et al., 1997). A key feature of L-NAME-induced hypertension is frank endothelial dysfunction and increased arterial constriction (Paulis et al., 2008). To examine the involvement of mitochondrial-derived ROS we infused L-NAME treated animals with mitoTEMPO at a rate of 150 µg/kg per day (Dikalova et al., 2010) via subcutaneous osmotic minipumps; rats implanted with saline minipumps served as control. Arterial blood pressure was monitored by telemetry.

L-NAME induced a time-dependent increase in mean arterial pressure (**Figure 4.6A**; $P<0.05$, $r=0.97$, n=3 rats). Similar to Ang II-induced hypertension (Dikalova et al., 2010), co-administration of mitoTEMPO blunted ($r=-0.76$) the hypertensive response to L-NAME (**Figure 4.6B**; $P<0.05$, $r=0.86$, n=3 rats). Thus, despite continued disruption of endothelial function, the blood pressure lowering capacity of mitoTEMPO remained intact. This observation suggests that mitoTEMPO could be working *in vivo*, at least in part, by reducing mitochondrial ROS generation and subsequent stimulation of arterial smooth muscle L-type Ca^{2+} channels.

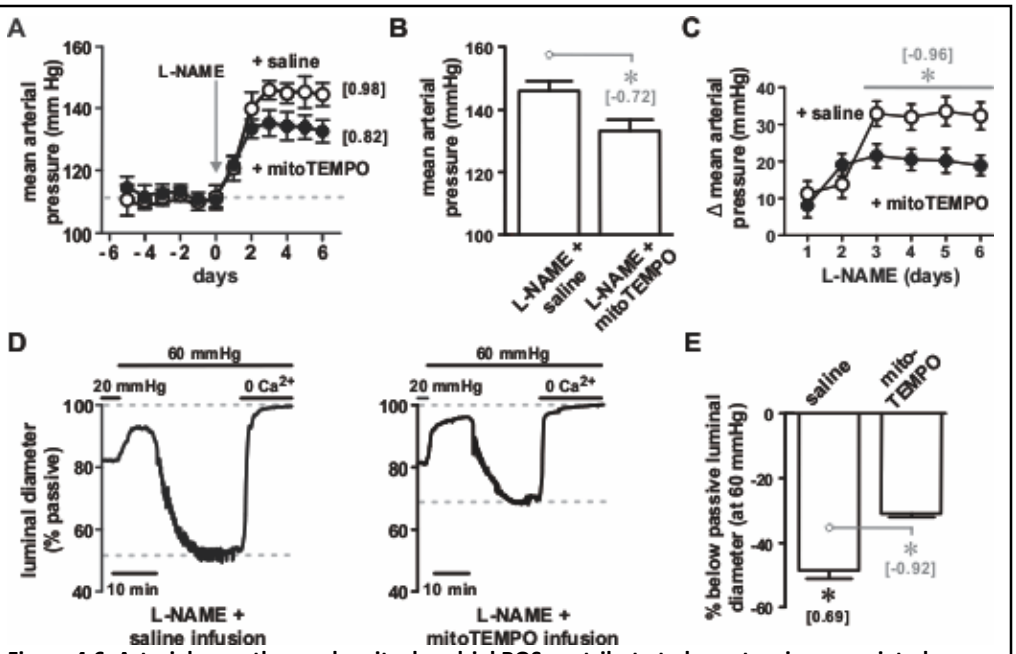

Figure 4.6. Arterial smooth muscle mitochondrial ROS contribute to hypertension-associated arterial dysfunction. A, Time courses of mean arterial pressures in rats treated with the nitric oxide synthase inhibitor L-NAME and infused with saline (open circles) or infused with the mitochondrial targeted antioxidant mitoTEMPO (closed circles). B, Bar plot of the change in mean arterial pressure for rats treated with L-NAME and infused with saline or infused with mitoTEMPO (n=3 rats each). C, Representative time courses showing luminal diameters (as % passive diameter) of pressurized middle cerebral arterial segments (as indicated) isolated from rats treated with L-NAME and infused with saline (left) or infused with mitoTEMPO (right). The horizontal dashed grey lines represent approximate points of measurement for analysis. D, Plot of the mean±SEM contraction induced by increasing the intraluminal pressure (20 to 60 mmHg) of middle cerebral arterial segments isolated from rats treated with L-NAME and infused with saline or infused with mitoTEMPO (n=5 arteries each). Bracketed values indicate effect size (r). * P<0.05

To investigate this we excised intact arterial segments from L-NAME and L-NAME plus mitoTEMPO treated animals and compared their myogenic set points (i.e., observed levels of myogenic tone). First we pressurized arteries to 20 mmHg and allowed them to equilibrate. Once a stable diameter was reached we increased the pressure to 60 mmHg and waited for an active myogenic contractile response to occur following passive dilation (**Figure 4.6C**). Experiments were terminated by superfusing the arteries with a nominally Ca^{2+}-free solution.

Arteries isolated from L-NAME treated animals infused with saline constricted robustly when the intraluminal pressure was increased from 20 to 60 mmHg (48.80±2.06% below passive diameter, n=5 arteries). Arteries from L-NAME treated animals infused with mitoTEMPO constricted substantially less following the same increase in pressure (30.43±1.46% below passive diameter, P<0.05, r=-0.92, n=5 arteries). Note that arteries isolated from normotensive rats pressurized to 60 mmHg constricted to

38.29±3.20% below their passive diameter (n=5 arteries) which was smaller than the constriction seen in arteries from L-NAME treated animals infused with saline (P<0.05) but not significantly different from the constriction seen in arteries from L-NAME treated animals infused with mitoTEMPO (P>0.05). From these data we conclude that systemic inhibition of mitochondrial ROS generation with mitoTEMPO reduces L-NAME-induced arterial dysfunction *in vivo* (lowers systemic arterial pressure) and *ex vivo* (lowers arterial myogenic tone).

To investigate the mechanisms underlying mitoTEMPO-dependent preservation of arterial function we examined baseline ROS and Ca^{2+} microdomain signaling activity in cells isolated from these animals. Using DCF fluorescence as an indicator of ROS generation with TIRF microscopy, we found that ROS puncta density (in the absence of acute stimulation) was elevated in smooth muscle cells from hypertensive L-NAME treated rats compared to non-L-NAME-treated controls (**Figure 4.7A and B**; P<0.05, r=0.70, n=5 cells). Importantly, ROS puncta densities in cells isolated from rats receiving L-NAME and mitoTEMPO were lower than those receiving L-NAME alone (P<0.05, r=-0.74, n=5 cells). The ROS puncta density in these cells was negligible and not different from unstimulated control cells (P>0.05, n=5 cells).

Paralleling our ROS puncta data and consistent with previous observations in Ang II-induced and genetic hypertension (Nieves-Cintrón et al., 2008), basal L-type Ca^{2+} channel function was enhanced in cells isolated from hypertensive L-NAME treated rats as evidenced by elevated Ca^{2+} sparklet site activities and densities (**Figure 4.7C and D**; P<0.05, nP_s r=0.75, density r=0.64, n=5 cells). Notably, as with ROS puncta, mitoTEMPO infusion abolished L-NAME enhancement of L-type Ca^{2+} channel activity (P<0.05, r=-0.51, n=5 cells) with levels not different from unstimulated cells from normotensive animals (P>0.05, n=5 cells). Taken altogether, we conclude that arterial smooth muscle mitochondrial-amplified

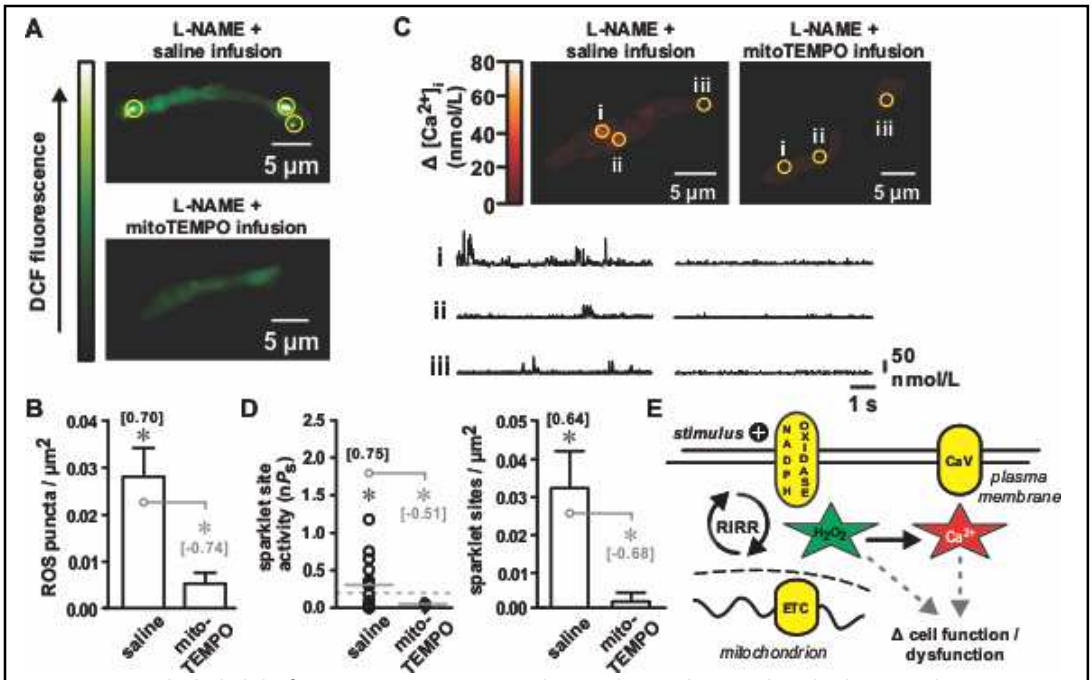

Figure 4.7. Endothelial dysfunction increases arterial smooth muscle mitochondrial ROS and Ca2+ microdomain signaling. A, Representative TIRF images showing subplasmalemmal DCF fluorescence in a cell isolated from rats treated with the nitric oxide synthase inhibitor L-NAME and infused with saline (top) or infused with the mitochondrial targeted antioxidant mitoTEMPO (bottom). Yellow circles indicate sites of ROS puncta formation. B, Plot of mean±SEM ROS puncta densities in cells isolated from rats treated with L- NAME and infused with saline or infused with mitoTEMPO (n=5 cells). C, Representative TIRF images showing Ca2+ influx in cells isolated from rats treated with L-NAME and infused with saline (left) or infused with mitoTEMPO (right). Traces show the time course of Ca2+ influx at the 3 circled sites. D, Plot of Ca2+ sparklet site activities (nPs) and plot of mean±SEM Ca2+ sparklet site densities (Ca2+ sparklet sites/µm2) in cells isolated from rats treated with L-NAME and infused with saline or infused with mitoTEMPO (n=5 cells). Black asterisks and effect sizes in panels B and D are in reference to non-L-NAME-

H_2O_2 microdomain signaling promotes Ca^{2+} influx through neighboring L-type Ca^{2+} channels and that this process contributes mechanistically to the contractile action of Ang II and the development of hypertension-associated arterial dysfunction.

4.5 Discussion

In this study we tested the hypothesis that mitochondrial amplification of H_2O_2 microdomain signaling stimulates L-type Ca^{2+} channels in arterial smooth muscle. The major findings supporting this hypothesis are: 1) Subplasmalemmal mitochondria associate with sites of elevated L-type Ca^{2+} channel activity; 2) mitochondrial-derived H_2O_2 stimulates Ca^{2+} influx through L-type channels; 3) inhibiting mitochondrial H_2O_2 production reduces Ang II-mediated arterial contraction; and 4) inhibiting

mitochondrial H_2O_2 production attenuates the development of hypertension-associated arterial smooth muscle dysfunction *ex vivo* and *in vivo*. From these data we conclude that mitochondrial amplification of H_2O_2 microdomain signaling is an important regulator of L-type Ca^{2+} channels in arterial smooth muscle and contributes to the development of hypertension-associated arterial dysfunction.

Our imaging of subplasmalemmal fluo-5F and MitoTracker fluorescence with TIRF microscopy provides compelling evidence that L-type Ca^{2+} channel activity is enriched at areas of the plasma membrane associated with mitochondria (**Figure 4.2**). Consistent with this observation, the small amount of plasma membrane associated with mitochondria (≈5%) is sufficient to influence the surface area necessary (≈4%) to accommodate the L-type Ca^{2+} channel sparklet activity observed. Our confocal imaging showed that mitochondria accounted for only ≈10% of the total arterial smooth muscle cell volume and only ≈10 % of this small volume was peripheral (≤0.5 μm from the plasma membrane). Therefore, the mitochondria ideally positioned to regulate L-type Ca^{2+} channels represented only ≈1% of the total cell volume. With TIRF microscopy we found that ≈5% of the plasma membrane was associated with mitochondria. Although direct comparison of these values is pointless, the small amount of plasma membrane associated with mitochondria (≈5%) and the small volume occupied by peripheral mitochondria (≈1%) are in relative accord with each other.

Arterial smooth muscle cells have an average surface area of ≈1000 μm (Navedo et al., 2005). Our observed L-type Ca^{2+} channel sparklet densities were ≈0.04/μm^2. As such we expect ≈40 active L-type Ca^{2+} channel sparklet sites per cell. Since the spatial spread of single L-type Ca^{2+} channel sparklets is ≈1 μm^2 (Amberg et al., 2007; Amberg and Navedo 2013; Navedo et al., 2005; Navedo and Amberg 2013), we estimate that ≈40 μm^2 (only ≈4%) of the plasma membrane is associated with active L-type Ca^{2+} channels. From this we conclude that the peripheral mitochondria visualized in our experiments, representing only ≈1% of the total cell volume and associated with only ≈5% of the plasma membrane, are sufficient to influence the surface area necessary (≈4%) to accommodate the L-type Ca^{2+} channel

sparklet activity observed. This logic supports the conclusion that subcellular localization is a key factor in determining the stimulatory influence of mitochondria on L-type Ca^{2+} channels.

Evidence suggests that mitochondrial buffering of proximate Ca^{2+} flux events is an important mechanism by which these organelles influence Ca^{2+} signaling (McCarron et al., 2012). With respect to L-type Ca^{2+} channels, localized Ca^{2+} buffering by mitochondria could reduce the amplitude of the Ca^{2+} microdomain formed near the pore when the channel is open (Demaurex et al., 2009). Lowering the effective Ca^{2+} concentration around the channel could alter Ca^{2+} signaling by reducing the Ca^{2+}-dependent inactivation characteristic of L-type Ca^{2+} channels (Ben-Johny and Yue, 2014). Prior work in smooth muscle suggests that mitochondrial Ca^{2+} buffering does not influence Ca^{2+} influx through L-type Ca^{2+} channels (McCarron and Miur, 1999; McCarron et al., 2012). However, our TIRF images demonstrate that L-type Ca^{2+} channel activity is associated with subplasmalemmal mitochondria (**Figure 4.2**). To reconcile these apparently contradictory observations we propose a mechanism of mitochondrial promotion of Ca^{2+} influx that does not rely on Ca^{2+} buffering *per se*. Rather, we propose that mitochondria promote Ca^{2+} influx by amplifying H_2O_2 microdomain signaling in the vicinity of L-type Ca^{2+} channels which leads to oxidant-dependent stimulation of Ca^{2+} influx (Amberg et al., 2010; **Chapters 2 and 3**).

Functionally compartmentalized submembranous accumulation of H_2O_2 is thought to bring about competent H_2O_2 signaling microdomains (Woo et al., 2010). We reported previously that H_2O_2 microdomains involving NADPH oxidase promote colocalized Ca^{2+} influx through L-type Ca^{2+} channels via oxidative activation of PKC (Amberg et al., 2010; **Chapters 2 and 3**). Experiments in this study provide evidence indicating that peripheral mitochondria also participate in H_2O_2 microdomain-dependent stimulation of L-type Ca^{2+} channels. Antimycin induced the formation of subplasmalemmal ROS puncta and induced L-type Ca^{2+} channel sparklet activity. Lastly, antimycin-dependent stimulation of L-type Ca^{2+} channels was abolished by enhanced decomposition of H_2O_2 with intracellular catalase.

To specifically reduce the influence of mitochondrial ROS on L-type Ca^{2+} channels we used the mitochondrial-targeted antioxidant mitoTEMPO at a concentration where cytosolic antioxidant effects are not apparent (Dikalov, 2011; Dikalov and Nazarewicz, 2012; Dikalova et al., 2010). MitoTEMPO prevented the induction of ROS puncta formation by Ang II and reduced the stimulatory effect on L-type Ca^{2+} channel sparklets. This suggests that mitochondrial ROS (visualized as ROS puncta) stimulate L-type Ca^{2+} channels. Intriguingly, unlike the effect on Ca^{2+} sparklet activity, mitoTEMPO did not reduce the effect of Ang II on L-type Ca^{2+} channel sparklet density (sites/μm^2). This is in contrast to the effects of NADPH oxidase inhibition and catalase on Ang II-dependent L-type Ca^{2+} channel sparklets where activity and density are reduced (Amberg et al., 2010; **Chapter 2**). While initially perplexing, we believe this subtle observation provides valuable mechanistic insight into the signaling events underlying oxidant-dependent regulation of L-type Ca^{2+} channels. Activation of Ang II type 1 receptors stimulates NADPH oxidase resulting in ROS formation (Griendling et al., 1994; Touyz and Schiffrin, 2000). Evidence suggests that ROS produced by NADPH oxidase can induce subsequent ROS generation from mitochondria through the process of ROS-induced ROS release (RIRR) (Dikalov. 2011; Diaklov and Ungvari, 2013; Dikalova et al., 2010). We suggest that a ROS-induced ROS release mechanism, initiated by NADPH oxidase and carried out by proximate mitochondria, is essential for Ang II-dependent stimulation of L-type Ca^{2+} channels in arterial smooth muscle.

This hypothesis is compatible with our data. Disrupting Ang II signaling by NADPH oxidase inhibition or enhancing H_2O_2 decomposition with catalase reduces the initial availability of signaling H_2O_2 and abolishes the stimulatory effect of Ang II on L-type Ca^{2+} channel sparklets (i.e., activity and density) (Amberg et al., 2010; **Chapter 2**). However, mitoTEMPO impairment of H_2O_2 generation occurs further along the signaling cascade by limiting ROS-induced ROS release by mitochondria. Thus, the initial production of signaling H_2O_2 by NADPH oxidase remains intact which could trigger limited stimulation of L-type Ca^{2+} channels leading to an increase in low-activity L-type Ca^{2+} channel sparklet sites. From this

we suggest that mitochondria, as a consequence of providing a means of ROS-induced ROS release, function as amplifiers of NADPH oxidase-initiated H_2O_2 microdomain signaling and that this mechanism is necessary for physiological stimulation of arterial smooth muscle cell L-type Ca^{2+} channels by Ang II (**Figure 4.7E**).

If mitochondrial ROS-induced ROS release is necessary for physiological stimulation of L-type Ca^{2+} channels by Ang II then disrupting this process with mitoTEMPO should reduce arterial contractile responses to Ang II. Consistent with this, mitoTEMPO reduced Ang II-dependent contraction of pressurized cerebral arteries by ≈70 %. In contrast, MitoTEMPO had no effect on the baseline myogenic tone of these arteries. Similarly, we noted previously that inhibition of NADPH oxidase (Amberg et al., 2010) and application of cell-permeable catalase (**Chapter 2**) reduced contractile responses to Ang II without altering arterial tone. These observations suggest that, at least in cerebral arteries from healthy rats, H_2O_2 microdomain stimulation of smooth muscle L-type Ca^{2+} channels contributes to the vasoconstrictor capacity of Ang II but does not influence baseline myogenic function.

In contrast to our observations, work by others has shown that mitochondrial and NADPH oxidase-derived ROS reduce arterial contractility by enhancing activation of hyperpolarizing large-conductance, Ca^{2+}-activated potassium (BK) channels (Cheranov and Jaggar, 2006; Xi et al., 2005). We contend that our H_2O_2 microdomain signaling hypothesis reconciles these seemingly diametrically opposed observations. In the case of our data, H_2O_2 microdomain signaling is coupled to the activation of L-type Ca^{2+} channels leading to contraction. For vasodilatory-associated ROS, we hypothesize that discrete ROS signaling events are selectively coupled to vasodilatory processes. In addition, we hypothesize that ROS microdomain signaling attains differential coupling specificity as a consequence of distinct subcellular distribution patterns inherent to the underlying ROS generating mechanisms.

Anomalous Ang II signaling is implicated in the development of arterial dysfunction and hypertension (Dikalov and Ungvari, 2013; Dikalova et al., 2010; Rajagopalan et al., 1996). We found that

mitoTEMPO attenuated the vasoconstrictive capacity of Ang II and, conversely, that stimulating mitochondrial ROS production with antimycin increased L-type Ca^{2+} channel activity. We therefore examined the efficacy of mitoTEMPO in mitigating arterial smooth muscle dysfunction in hypertension. Systemic administration of mitoTEMPO blunts the hypertensive response to Ang II infusion in mice, at least in part, by increasing the bioavailability of nitric oxide and preserving endothelial function (Dikalova et al., 2010). To investigate the effect of mitoTEMPO on arterial smooth muscle function we used a nitric oxide-deficient model of hypertension where endothelial dysfunction is an etiological hallmark (Paulis et al., 2008; Török, 2008). Similar to Ang II infusion (Dikalova et al., 2010), co-administration of mitoTEMPO reduced the hypertensive response to L-NAME. This observation suggests that the antihypertensive effect of mitoTEMPO reside, at least in part, at the level of arterial smooth muscle.

To examine the effect of systemically administered mitoTEMPO on arterial smooth muscle function we isolated and pressurized cerebral arteries obtained from L-NAME-treated rats. Arteries from these rats contracted to ≈50% below their passive diameter when pressurized to 60 mmHg. In contrast, arteries from L-NAME-treated rats infused with mitoTEMPO contracted to only ≈30% below their passive diameter. For perspective, the control arteries used in our Ang II/mitoTEMPO experiments contracted to ≈38% below their passive diameter, which was not significantly different from that seen with mitoTEMPO. Thus, systemically administered mitoTEMPO normalized the intrinsic myogenic set point of arteries isolated from L-NAME-treated rats.

To investigate the mechanisms by which mitoTEMPO normalized arterial function in L-NAME-treated rats we examined L-type Ca^{2+} channel and H_2O_2 microdomain signaling in isolated cells. Similar to Ang II-dependent and genetic hypertension (Nieves-Cintrón et al., 2008), basal L-type Ca^{2+} channel sparklet activity and ROS puncta density were elevated in cells from hypertensive L-NAME-treated rats. Strikingly, arterial smooth muscle cells isolated from rats infused with mitoTEMPO showed no increase

in either ROS puncta density or L-type Ca^{2+} channel sparklet activity. From these data we conclude that mitoTEMPO preserves arterial function and reduces arterial blood pressure, at least in part, by inhibiting mitochondrial amplified H_2O_2 microdomain dependent stimulation of arterial smooth muscle L-type Ca^{2+} channels.

The implications of our observations are broad. First, we suggest that mitochondrial amplification of H_2O_2 microdomain signaling in arterial smooth muscle is a potentially viable therapeutic target for reducing hypertension-associated arterial dysfunction. Second, as mitochondria and L-type Ca^{2+} channels are widely distributed we suggest that localized mitochondrial amplification of H_2O_2 microdomain signaling could be a general mechanism for promoting Ca^{2+} influx through L-type Ca^{2+} channels in many cell types including cardiac myocytes as demonstrated by others (Nickel et al., 2014; Viola et al., 2007; Zorov et al., 2000). Indeed, we recently described a mechanism responsible for localized L-type Ca^{2+} channel function in neuroendocrine pituitary gonadotrope cells which bears a striking resemblance to our observations in smooth muscle (Dang et al., 2014). Lastly, this mechanism could be an important factor contributing to the exaggerated ROS production and Ca^{2+} influx associated with the pathogenesis of numerous cardiovascular and non-cardiovascular diseases.

Chapter 5. Conclusion

This study provides strong evidence for a local signaling domain in which AT1R activation induces feed-forward ROS generation by NAD(P)H oxidase and mitochondria, resulting in persistent activation of LTCC's through PKC-mediated phosphorylation. AT1R activation by both paracrine/ autocrine Ang II signaling and mechaotransduction potentially provides a point of signal integration between these two pathways where activation of either mechanism potentiates the downstream effects of activation of the other. The downstream signaling molecules calcium and ROS also form distinct points of signal integration between these and other cellular signaling pathways such as endothelin and receptor tyrosine kinases. In this section, we will further discuss the major findings contained within this manuscript and possible future directions to build upon these observations.

Interplay between ROS and calcium signaling has been observed in various cell types. The voltage-dependent anion channel on the mitochondrial outer membrane, and the mitochondrial uniporter on the inner membrane provide a pathway through which cytosolic calcium can be rapdly sequestered within the mitochondrial matrix. Mitochondria have been demonstrated to modulate calcium release from external and intracellular sources and influence temporal aspects of global calcium transients. Mitochondrial calcium sequestration was shown to limit activation of calcium activated chloride channels in portal vein smooth muscle in response to membrane depolarization, therefore prolonging calcium influx through voltage-gated channels (Greenwood et al., 1997). Mitochondria influence global calcium transients in chromaffin cells (Babcock et al., 1997) by limiting the peak increase in global calcium, and contributing to rapid cytosolic calcium clearance. Mitochondrial calcium uptake has also been shown to prolong calcium influx through LTCC's in cardiomyocytes (Sánchez et al., 2001). ROS has been shown to additionally influence extracellular calcium influx indirectly through differential modification of potassium currents. In coronary circulation, vasodilation occurs through

H_2O_2- mediated activation of K_v1 family potassium channels (Rogers et al., 2007). Mitochondria are intimately coupled to mitochondria-associated-membrane complexes on the endoplasmic reticulum which are enriched with IP_3R's and in some cases RyR's. Uptake of calcium by mitochondria was shown to promote sustained calcium release by IP_3 receptors in colonic smooth presumably by preventing calcium-dependent inactivation of the channel, which occurs with high local [Ca^{2+}] (McCarron et al., 1999). Alternately, mitochondrial calcium uptake has been shown to limit IP_3R- mediated local calcium transients in astrocytes (Boitier et al., 1999). Mitochondrial ROS has been shown to increase RyR openings in vascular smooth muscle, leading to activation of BK_{ca} channels (XI et al., 2005). In contrast with this, we provide evidence that endogenous ROS is involved in vascular smooth muscle contraction in response to Ang II stimulation. To reconcile this discrepancy, emphasis should be placed on the spatial coordination of signaling machinery necessary for divergent signaling pathways observed even within a single cell type.

5.1 Localization and concerted activation of NAD(P)H oxidase and mitochondria are required for Ang II-derived high activity sparklets

Amberg et al., (2010) demonstrated the dependence of enhanced L-type calcium channel gating in this pathway on ROS derived locally from plasmalemmal NAD(P)H oxidase. The mean distance between NAD(P)H oxidase-associated plasmalemmal ROS puncta and high activity sparklets reported in this investigation was less than 1 μm. In **Chapter 4,** we demonstrated a similar close spatial relationship between high activity sparklets evoked by Ang II and subplasmalemmal mitochondria (mean<0.5 μm). Taken together with previous findings (Amberg et al., 2010; Navedo et al., 2008; Nieves-Cintrón et al., 2008), this suggests a closely coordinated signaling complex containing clusters of LTCC's, AKAP150, NAD(P)H oxidase, and mitochondria. Localization of ROS and calcium sources within a subcellular signaling domain allows compartmentalization of elevated $[Ca^{2+}]_i$ and ROS. This may be advantageous in

helping cells avoid the nontargeted and potentially toxic effects of global elevation of these species. An interesting line of inquiry to further develop this investigation centers on factors controlling the assembly of this ROS and calcium microdomain.

Caveolae serve as an attractive candidate for organizing this complex. These are cholesterol, sphingolipid, and phosphatidylinositide-enriched plasma membrane invaginations created by cholesterol binding and oligomerization of caveolin proteins. NAD(P)H oxidase has been isolated from caveolin-enriched membrane rafts in vascular smooth muscle (Hilenski et al., 2004). Additionally, PKCα, cSrc, EGFR, and other identified downstream targets of AT1R activation have been isolated from caveolar membrane fractions (reviewed in Ushio-Fukai and Alexander, 2006). In support of this theory, AT1R translocation to caveolae occurs rapidly following activation (Ishizaka et al., 1998), and AT1R activation likewise recruits Rac1 to caveolae (Zuo et al., 2004), although other data in the referenced study were found to be fraudulent, resulting in its retraction. Disorganization of caveolae by cholesterol depletion disrupts EGFR transactivation by Ang II, and Ang II-dependent vasoconstriction is blunted in arteries from caveolin-1 deficient mice (Drab et al., 2001). This signaling architecture may be upregulated in hypercholesteremia and hypertension, as caveolin-1 transcription is regulated by cholesterol (Bist et al., 1997), and Ang II treatment increases both caveolin-1 mRNA and protein synthesis (Ishizaka et al., 1998)

In addition to broadening our understanding of the sources of ROS involved in vascular smooth muscle Ang II signaling, **Chapter 4** of this study additionally demonstrates the necessity of both NAD(P)H oxidase-derived and mitochondrial ROS for persistent sparklet activity. In **Figure 4.4**, we demonstrate a reduction in Ang II- induced plasmalemmal ROS puncta in cells treated with the mitochondrial- specific superoxide dismutase mimetic mitoTEMPO. This result is similar to the reduction in puncta seen with treatment by apocynin (**Figure 2.5**) or the Nox1 specific inhibitor ML171 (1μM, **Figure 5.1A and B**), indicating both mitochondrial and NAD(P)H oxidase derived ROS are required for formation of

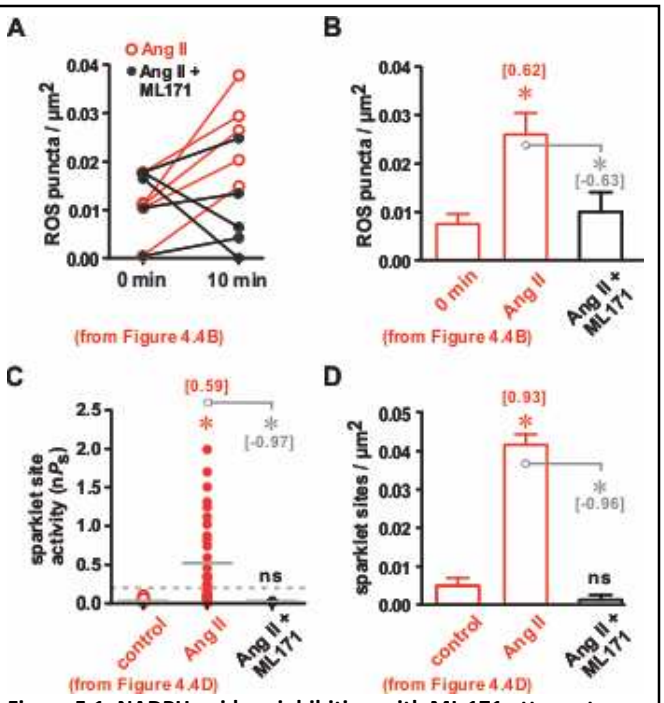

Figure 5.1. NADPH oxidase inhibition with ML 171 attenuates angiotensin II-dependent ROS and L-type Ca2+ channel microdomain signaling. A, Plot of individual ROS puncta densities in cells exposed to Ang II in the presence of ML171 at 0 min and at 10 min (n=5 cells) B, Plot of mean±SEM ROS puncta densities at 0 min (all values), at 10 min in Ang II, and 10 min in Ang II in the presence of ML171 (n=5 cells). C, Plot showing Ca2+ sparklet site activities (nPs) before after Ang II in control cells and in the presence of ML171 (n=5 cells). D, Plot of mean±SEM Ca2+ sparklet densities (Ca2+ sparklet sites/µm2) before after Ang II in control cells and in the presence of ML171 (n=5 cells). Bracketed values indicate effect size (r). * P<0.05

(detectable) ROS microdomains. Cells treated with mitoTEMPO (or rotenone) show increased sparklet density following exposure to Ang II, however the lack of persistent high activity sparklets suggest an attenuated increase in local and global calcium under these conditions. When compared with the absence of increased sparklet nP_s and density with inhibition of NAD(P)H oxidase by treatment with apocynin (Amberg et al., 2010) or ML171 (**Figure 5.1C and D**), this suggests NAD(P)H oxidase derived ROS precedes mitochondrial ROS, but is alone insufficient for sustained sparklet activity. Supplementary ROS provided by mitochondria in this situation may act to saturate local ROS buffering or inactivate relevant serine/threonine phosphatases within the signaling microdomain to provide sustained cofactor-independent PKC activity.

Oxidative inactivation of peroxyredoxin by H_2O_2 may be a relevant contributor to sparklet production in our studies. With regard to our experiments using exogenous H_2O_2 to stimulate sparklet activity, the concentration used (100µM) has been shown by others to induce hyperoxidative inactivation of peroxyredoxin (Charles et al., 2007). While DCF intensity is not a quantifiable indicator of ROS concentration, the increase in fluorescence intensity of ROS puncta upon Ang II exposure in **Figure 2.5** compared with the global fluorescence increase caused by external application of 100µM H_2O_2

(**Figure 2.3**) suggests the local concentration may be similar under these conditions. Further investigation into this mechanism is required to draw an adequate conclusion concerning whether this occurs physiologically.

5.2 H_2O_2 serves as an oxidant second messenger in Ang II-mediated LTCC sparklet signaling

While O_2^- is the primary oxidant produced by both NAD(P)H oxidase and mitochondria, enhanced cytosolic superoxide dismutation fails to diminish Ang II- mediated plasmalemmal ROS puncta formation (**Figure 2.8**) or sparklet activity (**Figure 2.7**) in isolated smooth muscle, and fails to attenuate Ang II-induced vasoconstriction in intact arteries (**Figure 4.5**). In contrast, enzymatic neutralization of H_2O_2 with catalase accomplishes each of these tasks (**Figures 2.8, 2.6, and 2.1**, respectively). Additionally, catalase prevents LTCC sparklet activity by mitochondrial ROS release induced by antimycin-a treatment (**Figure 4.3**). Torrecillas et al. (2001) similarly demonstrated that catalase prevents Ang II- induced elevation in $[Ca^{2+}]_i$ in cultured vascular smooth muscle. The functional necessity of H_2O_2 rather than O_2^- in this pathway is unsurprising, as an abundance of cytosolic and mitochondrial SOD outcompete other possible oxidative targets of O_2^- such as thiol groups in redox-sensitive proteins (Forman et al., 2010). Furthermore, NAD(P)H oxidase releases O_2^- to the extracellular compartment where it cannot readily re-enter the cell due to its charge. A similar condition occurs in the mitochondria, where the inner- and outer-mitochondrial membrane prevent O_2^- release from the matrix and intermembrane space respectively. H_2O_2 can more easily diffuse passively between compartments, however its polar nature slows its diffusion through membranes. Aquaporins have been suggested to play a role in facilitated diffusion of H_2O_2 across the plasma membrane (Winterbourne, 2013) and mitochondrial inner- and outer-membrane (Dröse et al., 2014).

We additionally demonstrated that exogenous H_2O_2 increases macroscopic L-type currents in isolated vascular smooth muscle cells (**Figure 2.2**). These data are fitting with other reports of H_2O_2- or

oxidant-mediated enhancement of L-type currents in various cell types (see **Table 5.1**). Interestingly, the type of oxidant used and level of exposure leads to differential regulation of channel activity. In general, low levels of oxidant exposure appear to favorably modify the activity of intracellular kinases (or their respective competing phosphatases), whereas stronger oxidative effects tend to have varying effects on channel activity by direct cysteine modification of exposed residues on the channel proper.

5.3 Oxidative activation of PKC mediates LTCC sparklet stimulation by Ang II

H_2O_2 was shown to increase macroscopic LTCC currents in this study (**Figure 2.2**). To provide greater detail regarding channel activity underlying this enhancement, TIRF microscopy revealed global exposure to H_2O_2 promotes heterogeneous activity of LTCC's (**Figure 2.4**), fitting with previous observations using other oxidant sources (Amberg et al., 2010). This argues strongly against direct interaction between the channel and H_2O_2 under these conditions, implicating an intermediary signaling molecule. Navedo et al. (2005) first recognized the requirement of local serine/threonine kinase activity for high activity sparklets in vascular smooth muscle. Amberg et al. (2010) demonstrated PKC activity was necessary for oxidative stimulation of high activity sparklets using xanthine/xanthine oxidase to generate exogenous ROS. All conventional PKC isoforms contain conserved, cysteine-rich regions (**C1**) within their autoinhibitory domains containing two functionally relevant zinc finger motifs. The Zn^{2+} ions in these structures are coordinated by three cysteine residues. Activation of PKC by DAG involves binding of the lipid second messenger to the C1 domain of PKC, causing a rearrangement of surface residues in the autoregulatory domain and the release of Zn^{2+}(Korichneva et al., 2002). In vitro studies using H_2O_2 and xanthine/ xanthine oxidase, and additionally isolated tissue from ischemic heart have demonstrated cofactor-independent activation of PKC and release of zinc (Gopalakrishna and Anderson, 1989; Knapp and Klann, 2000; Korichneva et al., 2002; Korichneva, 2005; Paulumbo et al., 1992). While excessive oxidation inactivates catalytic activity of the protein, the residues found in the C1 domain are

preferentially oxidized under lower levels of oxidant exposure (Knapp and Klann, 2000). By pretreating cells with safingol, which binds to the phorbol-binding site of PKC and prevents interaction with DAG, we demonstrated Ang II- and PKC-dependent LTCC sparklet activity occurs independent of DAG (**Figure 3.1**). This not only implicates oxidative mediation of LTCC phosphorylation status under AT1R stimulation, but also suggests initial activation of PKC by DAG is not necessary for NAD(P)H oxidase activation in this pathway. Investigating the role of tyrosine kinases and PI3K in NAD(P)H oxidase activation may provide clarity to this issue.

Another factor in determining the phosphorylation state of target proteins is the activity of protein phosphatases which directly oppose the activity of specific protein kinases. Navedo et al. (2006) demonstrated that inhibition of the calcium/ calmodulin dependent serine/threonine phosphatase calcineurin with cyclosporine- A, and additionally, inhibition of the calcium-independent protein phosphatase 2A (**PP2A**) with calyculin-A or okadaic acid increases sparklet activity similar to agonist-induced stimulation of PKC. Protein tyrosine phosphatases utilize a critical cysteine residue to form a phosphocysteine intermediate in dephosphorylation reactions. This low pK_a cysteine is a well characterized target for oxidative modification (reviewed in Klomsiri et al., 2011). Serine/threonine phosphatases utilize metal catalysts to dephosphorylate targets, however evidence of oxidative inactivation of PP2A during glutamate toxicity has been reported in cultured hippocampal neurons (Levinthal and DeFranco, 2005) and with exposure to low concentrations of exogenous H_2O_2 in Caco-2 cells (Rao and Clayton, 2002). Thus the precise effect on the endogenous balance of PKC/ PP2A activity in our system remains unclear.

5.4 Final Remarks

In this study, we demonstrate a localized signaling pathway by which spatially confined cellular ROS generation promotes calcium influx through LTCC's. Combining TIRF microscopy and patch-clamp electrophysiology allowed us to determine the spatial relationship between ROS and calcium signaling microdomains in vascular smooth muscle Ang II signaling as diagrammed in **Figure 5.2**. Relating these findings to isolated artery and *in-vivo* studies illustrates the importance of this model in physiological resistance artery regulation and the pathogenesis of hypertension. This study may aid not only in further understanding of the specific signaling pathway described here, but in various other systems including cardiac muscle and neurons, where calcium and ROS signaling are also interrelated.

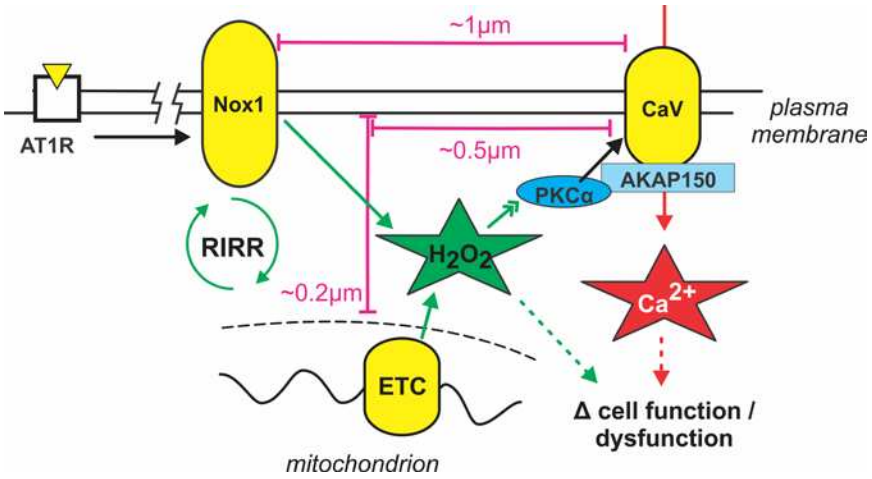

Figure 5.2. Revised model for Ang II-induced activation of LTCC sparklets. Activation of AT1R stimulates ROS release by plasmalemmal Nox1. Subsequent ROS production by mitochondria contributes sufficient H_2O_2 to allow ligand-independent activation of PKCα which in turn increases gating of LTCC's. The calcium and H_2O_2 signaling microdomain composed of Nox1, mitochondria, AKAP150-targeted PKC, and LTCC's is spatially localized to a distance of 1um or less from the target channel.

Table 1. Oxidant-dependent regulation of L-type calcium channels in the literature.

Cell (species)	Observation	Oxidant (source)	Proposed mechanism	Comment	Ref.
ventricular myocytes (rat)	↑ macroscopic current	**H_2O_2** (exogenous); **$\bullet O_2^-/H_2O_2$** (mitochondria*)	**indirect**, ↑ CaMKII signaling	$[H_2O_2]$ = 1 mM	Song et al., 2011
ventricular myocytes (guinea pig) & HEK expression (human Cav1.2)	↑ single channel open probability	**H_2O_2** (exogenous)	**direct**, glutathionylation	↑ glutathionylation in channels from ischemic human hearts	Tang et al., 2011
ventricular myocytes (guinea pig)	↑ macroscopic current	**H_2O_2** (exogenous); **$\bullet O_2^-/H_2O_2$** (mitochondria*)	**direct**, mitochondrial complex III generated $\bullet O_2^-$	$[H_2O_2]$ = 30 µM, persists following H_2O_2 removal	Viola et al., 2007; Viola and Hool, 2010
ventricular myocytes (guinea pig)	↑ single channel open probability	**H_2O_2** (exogenous)	**direct**, cysteine oxidation; **indirect**, ↑ CaMKII signaling	$[H_2O_2]$ = 1 mM	Yang et al., 2013
ventricular myocytes (guinea pig)	↔ macroscopic current	**H_2O_2** (exogenous, mitochondria*)	**direct** and/or **indirect** (via PKC and/or PKA)	↓ hypoxic inhibition, ↑ β adrenergic stimulation	Hool and Arthur, 2002
ventricular myocytes (guinea pig)	↓ macroscopic current	**H_2O_2** (exogenous)	-	$[H_2O_2]$ = 1 mM	Goldhaber and Liu, 1994
cerebral arterial myocytes (rat)	↑ Ca^{2+} sparklets and macroscopic current	**H_2O_2** (exogenous, NADPH oxidase*, mitochondria*)	**indirect**, ↑ PKC signaling	catalase but not SOD sensitive	Amberg et al., 2010, present study
aortic rings (rat)	↑ contraction (nifedipine sensitive)	**H_2O_2** (exogenous)	-	-	Sotníková,1998
coronary arterial myocytes (rat)	↑ $[Ca^{2+}]_i$ (nifedipine sensitive)	**H_2O_2** (exogenous)	-	-	Santiago et al., 2013
clonal A7r5 aortic myocytes (rat)	↑ $[Ca^{2+}]_i$ (lacidipine sensitive)	**H_2O_2** (exogenous)	**direct**, oxidative modification	$[H_2O_2]$ = 300 µM	Roveri et al., 1992
tracheal smooth muscle strips	↑ $[Ca^{2+}]_i$ (verapamil sensitive)	**H_2O_2** (exogenous)	-	$[H_2O_2]$ = 0.01 – 1 mM	Kojima et al., 2007

(guinea pig)					
clonal PC12 cells (rat)	↑ $[Ca^{2+}]_i$ (verapamil sensitive)	**H_2O_2** (exogenous)	**indirect**, depolarization; **direct**, thiol oxidation	$[H_2O_2]$ = 300 μM	Wang and Joseph, 2000
cultured dentate granule cells (rat)	↑ macroscopic current	**H_2O_2** (exogenous)	-	$[H_2O_2]$ = 1 and 10 mM, prevented by glutathione	Akaishi et al., 2004
HEK expression (human Cav1.2)	↑ macroscopic current	**H_2O_2** (exogenous)	-	$[H_2O_2]$ = 100 μM	Hudasek et al., 2004
cardiac myocytes (rat) & HEK expression (human Cav1.2)	↓ macroscopic current	**$\bullet O_2^-/H_2O_2$** (mitochondria*)	**direct**, C-terminal cysteine oxidation	CO-dependent ↑ in mitochondrial complex III ROS generation	Scragg et al., 2008
cultured mesenteric arterial myocytes (rat)	↑ $[Ca^{2+}]_i$ (verapamil sensitive)	**H_2O_2** (exogenous), **$\bullet O_2^-$** (via LY83583)	-	H_2O_2 effects ↑ and $\bullet O_2^-$ effects ↓ in hypertension	Tabet et al., 2004
cultured uterine myocytes (human)	↑ $[Ca^{2+}]_i$ (nifedipine sensitive)	**$\bullet O_2^-/H_2O_2$** (exogenous xanthine oxidase**)	-	-	Masumoto et al., 1990
HEK expression (human Cav1.2)	↑ macroscopic current	**$\bullet O_2^-/H_2O_2$** (exogenous xanthine oxidase**, mitochondria*)	**indirect**, ↑ channel trafficking/retention	$\bullet O_2^-$ effects retained in mitochondria-depleted cells	Brown et al., 2005

* mitochondria and NADPH oxidase produce $\bullet O_2^-$ proximally; H_2O_2 is formed subsequently via spontaneous and/or SOD catalyzed dismutation

** xanthine oxidase activity results in $\bullet O_2^-$ and H_2O_2 formation

References

Abe Ji, Takahashi M, Ishida M, Lee JD, Berk BC (1997) c-Src is required for oxidative stress-mediated activation of big mitogen-activated protein kinase 1. J Biol Chem. 272(33):20389-20394

Akaishi T, Nakazawa K, Sato K, Saito H, Ohno Y, Ito Y (2004) Hydrogen peroxide modulates whole cell Ca2+ currents through L-type channels in cultured rat dentate granule cells. Neurosci Lett. 356(1):25-28

Albarwani S, Nemetz LT, Madden JA, Tobin AA, England SK, Pratt PF, Rusch NJ (2003) Voltage-gated K+ channels in rat small cerebral arteries: molecular identity of the functional channels. J Physiol. 551(Pt 3):751-763

Alberti KGMM, Zimmet P, Shawb S (2005) The metabolic syndrome—a new worldwide definition. Lancet 366:1059-1062.

Amberg GC, Santana LF (2003) Downregulation of the BK channel beta1 subunit in genetic hypertension. Circ Res. 93(10):965-971

Amberg GC, Rossow CF, Navedo MF, Santana LF (2004) NFATc3 regulates Kv2.1 expression in arterial smooth muscle. J Biol Chem. 279(45):47326-47334

Amberg GC, Santana LF (2006) Kv2 channels oppose myogenic constriction of rat cerebral arteries. Am J Physiol Cell Physiol. 291(2): 348-356

Amberg GC, Navedo MF, Nieves-Cintrón M, Molkentin JD, Santana LF (2007) Calcium sparklets regulate local and global calcium in murine arterial smooth muscle. J Physiol. 579(Pt 1):187-201

Amberg GC, Earley S, Glapa SA (2010) Local regulation of arterial L-type calcium channels by reactive oxygen species. Circ Res. 107(8): 1002-1010

Babcock DF, Herrington J, Goodwin PC, Park YB, Hille B (1997) Mitochondrial participation in the intracellular Ca2+ network. J Cell Biol. 136(4):833-844

Bannister JP, Bulley S, Narayanan D, Thomas-Gatewood C, Luzny P, Pachuau J, Jaggar JH (2012) Transcriptional upregulation of α2δ-1 elevates arterial smooth muscle cell voltage-dependent Ca2+ channel surface expression and cerebrovascular constriction in genetic hypertension. Hypertension 60(4):1006-1015

Bannister JP, Leo MD, Narayanan D, Jangsangthong W, Nair A, Evanson KW, Pachuau J, Gabrick KS, Boop FA, Jaggar JH (2013) The voltage-dependent L-type Ca2+ (CaV1.2) channel C-terminus fragment is a bi-modal vasodilator. J Physiol. 591(Pt 12):2987-2998

Bae SW, Kim HS, Cha YN, Park YS, Jo SA, Jo I (2003) Rapid increase in endothelial nitric oxide production by bradykinin is mediated by protein kinase A signaling pathway. Biochem Biophys Res Commun. 306(4):981-7

Bartunek J, Weinberg EO, Tajima M, Rohrbach S, Katz SE, Douglas PS, Lorell BH (2000) Chronic *n*^{g}-nitro-l-arginine methyl ester-induced hypertension : Novel molecular adaptation to systolic load in absence of hypertrophy. Circulation. 101:423-429.

Ben-Johny M, Yue DT (2014) Calmodulin regulation (calmodulation) of voltage-gated calcium channels. J Gen Physiol. 143(6):679-692

Berridge MJ, Lipp P, Bootman MD (2000) The versatility and universality of calcium signalling. Nat Rev Mol Cell Biol. 2000 1(1):11-21

Bist A, Fielding PE, Fielding CJ (1997) Two sterol regulatory element-like sequences mediate up-regulation of caveolin gene transcription in response to low density lipoprotein free cholesterol. Proc Natl Acad Sci U S A. 94(20):10693-10698

Boitier E, Rea R, Duchen MR (1999) Mitochondria exert a negative feedback on the propagation of intracellular Ca2+ waves in rat cortical astrocytes. J Cell Biol. 145(4):795-808

Brayden JE, Nelson MT (1992) Regulation of arterial tone by activation of calcium-dependent potassium channels. Science. 256(5056):532-535

Briones AM, Tabet F, Callera GE, Montezano AC, Yogi A, He Y, Quinn MT, Salaices M, Touyz RM (2011) Differential regulation of Nox1, Nox2 and Nox4 in vascular smooth muscle cells from WKY and SHR. J Am Soc Hypertens. 5(3):137-153

Brown DI, Griendling KK (2009) Nox proteins in signal transduction. Free Radic Biol Med. 47(9):1239-1253

Brown ST, Scragg JL, Boyle JP, Hudasek K, Peers C, Fearon IM (2005) Hypoxic augmentation of Ca2+ channel currents requires a functional electron transport chain. The Journal of biological chemistry. 280:21706-1712.

Bulley S, Neeb ZP, Burris SK, Bannister JP, Thomas-Gatewood CM, Jangsangthong W, Jaggar JH. (2012) TMEM16A/ANO1 channels contribute to the myogenic response in cerebral arteries. Circ Res. 111(8):1027-1036

Catterall WA (2000) Structure and regulation of voltage-gated Ca2+ channels. Annu Rev Cell Dev Biol. 16:521-555

Catterall WA (2011) Voltage-gated calcium channels. Cold Spring Harb Perspect Biol. 3(8):a003947

Chan SH, Wu KL, Chang AY, Tai MH, Chan JY (2009) Oxidative impairment of mitochondrial electron transport chain complexes in rostral ventrolateral medulla contributes to neurogenic hypertension. Hypertension 53(2):217-227

Charles RL, Schröder E, May G, Free P, Gaffney PR, Wait R, Begum S, Heads RJ, Eaton P (2007) Protein sulfenation as a redox sensor: proteomics studies using a novel biotinylated dimedone analogue. Mol Cell Proteomics. 6(9):1473-1484

Cheranov SY, Jaggar JH (2006) TNF-alpha dilates cerebral arteries via NAD(P)H oxidase-dependent Ca2+ spark activation. Am J Physiol Cell Physiol. 290(4):C964-971

Chobanian AV, Bakris GL, Black HR, Cushman WC, Green LA, Izzo JL, Jones DW, Materson BJ, Oparil S, Wright JT, Roccella EJ, National High Blood Pressure Education Program Coordinating Committee (2003) Seventh report of the joint national committee on prevention, detection, evaluation, and treatment of high blood pressure. Hypertens. 42: 1206-1252

Clapham DE (2007) Calcium signaling. Cell 131(6):1047-1058.

Clempus RE, Griendling KK (2006) Reactive oxygen species signaling in vascular smooth muscle cells. Cardiovasc Res. 71(2):216-225

Cohen J (1988) Statistical power analysis for the behavioral sciences. Hillsdale, N.J.: L. Erlbaum Associates

Collier ML, Ji G, Wang Y, Kotlikoff MI (2000) Calcium-induced calcium release in smooth muscle: loose coupling between the action potential and calcium release. J Gen Physiol. 115(5):6536-62

Corson MA, James NL, Latta SE, Nerem RM, Berk BC, Harrison DG (1996) Phosphorylation of endothelial nitric oxide synthase in response to fluid shear stress. Circ Res. 79: 984 –991

Dananberg J, Sider RS, Grekin RJ (1993) Sustained hypertension induced by orally administered nitro-L-arginine. Hypertension. 21(3):359-363

Dang AK, Murtazina DA, Magee C, Navratil AM, Clay CM, Amberg GC (2014) GnRH evokes localized subplasmalemmal calcium signaling in gonadotropes. Mol Endocrinol. 28(12):2049-2059

Day BJ, Fridovich I, Crapo JD (1997) Manganic porphyrins possess catalase activity and protect endothelial cells against hydrogen peroxide-mediated injury. Arch Biochem Biophys. 347(2):256-262

Deanfield JE, Halcox JP, Rabelink TJ (2007) Endothelial function and dysfunction: testing and clinical relevance. Circulation. 115(10):1285-1295

Delli Gatti C, Osto E, Kouroedov A, Eto M, Shaw S, Volpe M, Lüscher TF, Cosentino F (2008) Pulsatile

stretch induces release of angiotensin II and oxidative stress in human endothelial cells: effects of ACE inhibition and AT1 receptor antagonism. Clin Exp Hypertens. 30(7):616-627

Demaurex N, Poburko D, Frieden M (2009) Regulation of plasma membrane calcium fluxes by mitochondria. Biochim Biophys Acta. 1787(11):1383-1394

Demuro A, Parker I (2004) Imaging the activity and localization of single voltage-gated Ca(2+) channels by total internal reflection fluorescence microscopy. Biophys J. 86(5):3250-3259

de Wit C, Roos F, Bolz SS, Pohl U (2003) Lack of vascular connexin 40 is associated with hypertension and irregular arteriolar vasomotion. Physiol Genomics 13(2): 169-177

Dikalov S (2011) Cross talk between mitochondria and NADPH oxidases. Free Radic Biol Med. 51(7):1289-1301

Dikalov SI, Ungvari Z (2013) Role of mitochondrial oxidative stress in hypertension. Am J Physiol Heart Circ Physiol. 305(10):H1417-1427

Dikalov SI, Nazarewicz RR (2013) Angiotensin II-induced production of mitochondrial reactive oxygen species: potential mechanisms and relevance for cardiovascular disease. Antioxid Redox Signal. 19(10):1085-1094

Dikalova AE, Bikineyeva AT, Budzyn K, Nazarewicz RR, McCann L, Lewis W, Harrison DG, Dikalov SI (2010) Therapeutic targeting of mitochondrial superoxide in hypertension. Circ Res107(1):106-116

Dittmer PJ, Dell'Acqua ML, Sather WA (2014) Ca2+/calcineurin-dependent inactivation of neuronal L-type Ca2+ channels requires priming by AKAP-anchored protein kinase A. Cell Rep. 7(5):1410-1416

Drab M, Verkade P, Elger M, Kasper M, Lohn M, Lauterbach B, Menne J, Lindschau C, Mende F, Luft FC, Schedl A, Haller H, Kurzchalia TV (2001) Loss of caveolae, vascular dysfunction, and pulmonary defects in caveolin-1 gene-disrupted mice. Science. 293(5539):2449-2452

Dröse S, Brandt U, Wittig I (2014) Mitochondrial respiratory chain complexes as sources and targets of

thiol-based redox-regulation. Biochim Biophys Acta. 1844(8):1344-1354

Duarte J, Jiménez R, O'Valle F, Galisteo M, Pérez-Palencia R, Vargas F, Pérez-Vizcaíno F, Zarzuelo A, Tamargo J (2002) Protective effects of the flavonoid quercetin in chronic nitric oxide deficient rats. J Hypertens. 20(9):1843-1854

Earley S, Waldron BJ, Brayden JE (2004) Critical role for transient receptor potential channel TRPM4 in myogenic constriction of cerebral arteries. Circ Res. 95(9):922-929

Eguchi S, Numaguchi K, Iwasaki H, Matsumoto T, Yamakawa T, Utsunomiya H, Motley ED, Kawakatsu H, Owada KM, Hirata Y, Marumo F, Inagami T (1998) Calcium-dependent epidermal growth factor receptor transactivation mediates the angiotensin II-induced mitogen-activated protein kinase activation in vascular smooth muscle cells. J Biol Chem. 273(15):8890-8896

Eguchi S, Iwasaki H, Inagami T, Numaguchi K, Yamakawa T, Motley ED, Owada KM, Marumo F, Hirata Y. (1999) Involvement of PYK2 in angiotensin II signaling of vascular smooth muscle cells. Hypertension. 33(1 Pt 2):201-206

Eguchi S, Dempsey PJ, Frank GD, Motley ED, Inagami T (2001) Activation of MAPKs by angiotensin II in vascular smooth muscle cells. Metalloprotease-dependent EGF receptor activation is required for activation of ERK and p38 MAPK but not for JNK. J Biol Chem. 276(11):7957-7962

Ermak G, Davies KJ (2002) Calcium and oxidative stress: from cell signaling to cell death. Mol Immunol. 38(10):713-721

Facundo HT, de Paula JG, Kowaltowski AJ (2007) Mitochondrial ATP-sensitive K+ channels are redox-sensitive pathways that control reactive oxygen species production. Free Radic Biol Med. 42(7):1039-48

Fan JL, Burgess KR, Thomas KN, Peebles KC, Lucas SJE, Lucas RAI, Cotter JD,. Ainslie PN (2011) Influence of indomethacin on the ventilatory and cerebrovascular responsiveness to hypoxia Euro J App Phys. 111 (4): pp 601-610

Feissner RF, Skalska J, Gaum WE, Sheu SS (2009) Crosstalk signaling between mitochondrial Ca2+ and ROS. Front Biosci (Landmark Ed.) 14:1197-1218

Ferron PM, Banner W Jr, Duckles SP (1984) Lack of specific (3H) prazosin binding sites in dog and rabbit cerebral arteries. Life Sci. 35(21): 2169-2176

Forman HJ, Maiorino M, Ursini F (2010) Signaling functions of reactive oxygen species. Biochemistry. 49(5):835-842

Fukai T, Ushio-Fukai M (2011) Superoxide dismutases: role in redox signaling, vascular function, and diseases. Antioxid Redox Signal. 15(6):1583-1606

Furchgott RF, Zawadzki JV (1980) The obligatory role of endothelial cells in the relaxation of arterial smooth muscle by acetylcholine. Nature; 288(5789): 373-376.

Fujiwara S, Itoh T, Suzuki H (1982) Membrane properties and excitatory neuromuscular transmission in the smooth muscle of dog cerebral arteries. Br J Pharmacol. 77(2): 197–208

Goldhaber JI, Liu E (1994. Excitation-contraction coupling in single guinea-pig ventricular myocytes exposed to hydrogen peroxide. J Physiol. 477 (Pt 1):135-147

Gonzales AL, Garcia ZI, Amberg GC, Earley S (2010a) Pharmacological inhibition of TRPM4 hyperpolarizes vascular smooth muscle. Am J Physiol Cell Physiol. 299(5): 1195-1202

Gonzales AL, Amberg GC, Earley S. (2010b) Ca2+ release from the sarcoplasmic reticulum is required for sustained TRPM4 activity in cerebral artery smooth muscle cells. Am J Physiol Cell Physiol. 299(2): 279-288

Gonzales AL, Yang Y, Sullivan MN, Sanders L, Dabertrand F, Hill-Eubanks DC, Nelson MT, Earley S (2014) A PLCγ1-dependent, force-sensitive signaling network in the myogenic constriction of cerebral arteries. Sci Signal. 7(327): ra49

Gonzalez-Lima F, Barksdale BR, Rojas JC (2014) Mitochondrial respiration as a target for neuroprotection and cognitive enhancement. Biochem Pharmacol. 88(4):584-593

Gopalakrishna R, Anderson WB (1989) Ca2+- and phospholipid-independent activation of protein kinase C by selective oxidative modification of the regulatory domain. Proc Natl Acad Sci U S A. 86(17):6758-6762

Graham D, Huynh NN, Hamilton CA, Beattie E, Smith RA, Cochemé HM, Murphy MP, Dominiczak AF (2009) Mitochondria-targeted antioxidant MitoQ10 improves endothelial function and attenuates cardiac hypertrophy. Hypertension 54(2):322-328.

Greenwood IA, Helliwell RM, Large WA (1997) Modulation of Ca(2+)-activated Cl- currents in rabbit portal vein smooth muscle by an inhibitor of mitochondrial Ca2+ uptake. J Physiol. 505 (Pt 1):53-64

Griendling KK, Minieri CA, Ollerenshaw JD, Alexander RW (1994) Angiotensin II stimulates NADH and NADPH oxidase activity in cultured vascular smooth muscle cells. Circ Res. 74(6):1141-1148

Guilluy C, Brégeon J, Toumaniantz G, Rolli-Derkinderen M, Retailleau K, Loufrani L, Henrion D, Scalbert E, Bril A, Torres RM, Offermanns S, Pacaud P, Loirand G (2010) The Rho exchange factor Arhgef1 mediates the effects of angiotensin II on vascular tone and blood pressure. Nat Med. 16(2):183-190

Guy HR and Seetharamulu P (1986) Molecular model of the action potential sodium channel. Proc Natl Acad Sci U S A. 83(2): 508–512

Hannun YA, Loomis CR, Merrill AH Jr, Bell RM (1986) Sphingosine inhibition of protein kinase C activity and of phorbol dibutyrate binding in vitro and in human platelets. J Biol Chem. 261(27):12604-12609

Harder DR (1984) Pressure-dependent membrane depolarization in cat middle cerebral artery. Circ Res.;55(2):197-202

Hayabuchi Y, Nakaya Y, Matsuoka S, Kuroda Y (1998) Hydrogen peroxide-induced vascular relaxation in porcine coronary arteries is mediated by Ca2+-activated K+ channels. Heart Vessels. 13(1):9-17

Hilenski LL, Clempus RE, Quinn MT, Lambeth JD, Griendling KK (2004) Distinct subcellular localizations of Nox1 and Nox4 in vascular smooth muscle cells. Arterioscler Thromb Vasc Biol. 24:677– 683.

Heumüller S, Wind S, Barbosa-Sicard E, Schmidt HH, Busse R, Schröder K, Brandes RP (2008) Apocynin is not an inhibitor of vascular NADPH oxidases but an antioxidant. Hypertension. 51(2):211-217

Hidalgo C, Donoso P (2008) Crosstalk between calcium and redox signaling: from molecular mechanisms to health implications. Antioxid Redox Signal10(7):1275-1312

Hofmann T, Obukhov AG, Schaefer M, Harteneck C, Gudermann T, Schultz G (1999) Direct activation of human TRPC6 and TRPC3 channels by diacylglycerol. Nature. 397(6716):259-263.

Hool LC, Arthur PG (2002) Decreasing cellular hydrogen peroxide with catalase mimics the effects of hypoxia on the sensitivity of the L-type Ca2+ channel to b-adrenergic receptor stimulation in cardiac myocytes. Circ Res91:601-609

Hool LC (2006) Reactive oxygen species in cardiac signalling: from mitochondria to plasma membrane ion channels. Clin Exp Pharmacol Physiol. 33(1-2):146-151

Hudasek K, Brown ST, Fearon IM (2004) H2O2 regulates recombinant Ca2+ channel alpha1C subunits but does not mediate their sensitivity to acute hypoxia. Biochem Biophys Res Commun318(1):135-141

Hulme JT, Yarov-Yarovoy V, Lin TW, Scheuer T, Catterall WA (2006) Autoinhibitory control of the CaV1.2 channel by its proteolytically processed distal C-terminal domain. J Physiol. 576(Pt 1):87-102

Iadecola C (2004) Neurovascular regulation in the normal brain and in Alzheimer's disease. Nat Rev Neurosci. 5: 347-360

Iida Y, Katusic ZS (2000) Mechanisms of cerebral arterial relaxations to hydrogen peroxide. Stroke. 31(9):2224-2230

Ishizaka N, Griendling KK, Lassègue B, Alexander RW (1998) Angiotensin II type 1 receptor: relationship with caveolae and caveolin after initial agonist stimulation. Hypertension. 32(3):459-466

Iwasaki Y, Saito Y, Nakano Y, Mochizuki K, Sakata O, Ito R, Saito K, Nakazawa H (2009) Chromatographic and mass spectrometric analysis of glutathione in biological samples. J Chromatogr B Analyt Technol Biomed Life Sci. 877(28):3309-3317

Izzard AS, Bund SJ, Heagerty AM (1996) Myogenic tone in mesenteric arteries from spontaneously hypertensive rats. Am J Physiol. 270(1 Pt 2):1-6

Kearney PM, Whelton M, Reynolds K, Muntner P, Whelton P, He J (2005) Global burden of hypertension: analysis of worldwide data. Lancet 365: 217- 223

Kelley EE, Khoo NK, Hundley NJ, Malik UZ, Freeman BA, Tarpey MM (2010) Hydrogen peroxide is the major oxidant product of xanthine oxidase. Free Radic Biol Med. 48(4):493-498

Kharade SV, Sonkusare SK, Srivastava AK, Thakali KM, Fletcher TW, Rhee SW, Rusch NJ (2013) The β3 subunit contributes to vascular calcium channel upregulation and hypertension in angiotensin II-infused C57BL/6 mice. Hypertension. 61(1):137-142

Kim J, Ghosh S, Nunziato DA, Pitt GS (2004) Identification of the components controlling inactivation of voltage-gated Ca2+ channels. Neuron. 41(5):745-754

Kimura S, Zhang GX, Nishiyama A, Shokoji T, Yao L, Fan YY, Rahman M, Suzuki T, Maeta H, Abe Y (2005) Role of NAD(P)H oxidase- and mitochondria-derived reactive oxygen species in cardioprotection of ischemic reperfusion injury by angiotensin II. Hypertension 45(5):860-866

Klomsiri C, Karplus PA, Poole LB (2011) Cysteine-based redox switches in enzymes. Antioxid Redox Signal. 14(6):1065-1077

Koller A, Sun D, and Kaley G (1993) Role of shear stress and endothelial prostaglandins in flow- and viscosity-induced dilation of arterioles in vitro. Circ. Res. 72(6): 1276–1284

Knapp LT, Klann E (2000) Superoxide-induced stimulation of protein kinase C via thiol modification and modulation of zinc content. J Biol Chem. 275(31):24136-24145

Knapp LT, Klann E (2002) Potentiation of hippocampal synaptic transmission by superoxide requires the

oxidative activation of protein kinase C. J Neurosci. 22(3):674-683

Kojima K, Kume H, Ito S, Oguma T, Shiraki A, Kondo M (2007) Direct effects of hydrogen peroxide on airway smooth muscle tone: roles of Ca2+ influx and Rho-kinase. Eur J Pharmacol. 556:151-156

Kontos HA, Raper AJ, Patterson JL (1977) Analysis of vasoactivity of local pH, PCO2 and bicarbonate on pial vessels. Stroke. 8(3):358-360.

Knot HJ, Nelson MT (1995) Regulation of membrane potential and diameter by voltage-dependent K+ channels in rabbit myogenic cerebral arteries. Am J Physiol. 269(1 Pt 2):348-355

Knot HJ, Nelson MT (1998) Regulation of arterial diameter and wall [Ca2+] in cerebral arteries of rat by membrane potential and intravascular pressure. J Physiol 508 (Pt 1):199-209

Korichneva I, Hoyos B, Chua R, Levi E, Hammerling U (2002) Zinc release from protein kinase C as the common event during activation by lipid second messenger or reactive oxygen. J Biol Chem. 277(46):44327-44331

Korichneva I (2005) Redox regulation of cardiac protein kinase C. Exp Clin Cardiol. 10(4):256-261

Krejcy K, Wolzt M, Kreuzer C, Breiteneder H, Schütz W, Eichler HG, Schmetterer L (1997) Characterization of angiotensin-II effects on cerebral and ocular circulation by noninvasive methods. Br J Clin Pharmacol. 43(5):501-508

Krishna MC, Samuni A, Taira J, Goldstein S, Mitchell JB, Russo A (1996) Stimulation by nitroxides of catalase-like activity of hemeproteins. Kinetics and mechanism. J Biol Chem. 271(42):26018-26025

Lassègue B, Sorescu D, Szöcs K, Yin Q, Akers M, Zhang Y, Grant SL, Lambeth JD, Griendling KK (2001) Novel gp91(phox) homologues in vascular smooth muscle cells : nox1 mediates angiotensin II-induced superoxide formation and redox-sensitive signaling pathways. Circ Res. 88(9):888-894

Lavrentyev EN, Estes AM, Malik KU. (2007) Mechanism of high glucose induced angiotensin II production in rat vascular smooth muscle cells. Circ Res. 101(5):455-464

LeBel CP, Ischiropoulos H, Bondy SC (1992) Evaluation of the probe 2',7'-dichlorofluorescin as an indicator of reactive oxygen species formation and oxidative stress. Chem Res Toxicol. 5(2):227-231

Lee, RM (1995) Morphology of cerebral arteries. Pharmacol Ther. 66(1): 149-173.

Lee MY, Griendling KK (2008) Redox signaling, vascular function, and hypertension. Antioxid Redox Signal. 10(6):1045-1059

Levinthal DJ, Defranco DB (2005) Reversible oxidation of ERK-directed protein phosphatases drives oxidative toxicity in neurons. J Biol Chem. 280(7):5875-5883

Li JM, Shah AM (2003) Mechanism of endothelial cell NADPH oxidase activation by angiotensin II. Role of the p47phox subunit. J Biol Chem. 278(14):12094-12100

Lincoln TM, Dey N, Sellak H. (2001) Invited review: cGMP-dependent protein kinase signaling mechanisms in smooth muscle: from the regulation of tone to gene expression. J Appl Physiol 91(3); 1421-1430

Liu Y, Bubolz AH, Mendoza S, Zhang DX, Gutterman DD (2011) H2O2 is the transferrable factor mediating flow-induced dilation in human coronary arterioles. Circ Res. 108(5):566-573

Lu Y, Zhang H, Gokina N, Mandala M, Sato O, Ikebe M, Osol G, Fisher SA (2008) Uterine artery myosin phosphatase isoform switching and increased sensitivity to snp in a rat l-name model of hypertension of pregnancy. American journal of physiology. Cell physiology 294:C564-571

Manea A (2010) NADPH oxidase-derived reactive oxygen species: involvement in vascular physiology and pathology. Cell Tissue Res. 342(3):325-339

Marañon RO, Juncos LA, Joo Turoni C, Karbiner S, Romero D, Peral de Bruno M (2014) Tempol blunts afferent arteriolar remodeling in chronic nitric oxide-deficient hypertension without normalizing blood pressure. Clin Exp Hypertens 36(3):132-139

Matoba T, Shimokawa H, Nakashima M, Hirakawa Y, Mukai Y, Hirano K, Kanaide H, Takeshita A (2000) Hydrogen peroxide is an endothelium-derived hyperpolarizing factor in mice. J Clin Invest. 106(12):1521-1530

Maravall M, Mainen ZF, Sabatini BL, Svoboda K (2000) Estimating intracellular calcium concentrations and buffering without wavelength ratioing Biophys J. 78:2655-2667.

Masumoto N, Tasaka K, Miyake A, Tanizawa O (1990) Superoxide anion increases intracellular free calcium in human myometrial cells. The Journal of biological chemistry. 265:22533-22536

McCarron JG, Muir TC (1999) Mitochondrial regulation of the cytosolic Ca2+ concentration and the InsP3-sensitive Ca2+ store in guinea-pig colonic smooth muscle. J Physiol. 516 (Pt 1):149-161

McCarron JG, Olson ML, Chalmers S (2012) Mitochondrial regulation of cytosolic Ca^{2+} signals in smooth muscle. Pflugers Arch. 464(1):51-62

Meehan J, Collister JP (2011) Lesion of the Subfornical Organ attenuates neuronal activation of the paraventricular nucleus in response to Angiotensin II in normal rats. Open J Neurosci. 23;1:1

Mehlhorn RJ, Swanson CE (1992) Nitroxide-stimulated H2O2 decomposition by peroxidases and pseudoperoxidases. Free Radic Res Commun. 17(3):157-175

Mishina NM, Tyurin-Kuzmin PA, Markvicheva KN, Vorotnikov AV, Tkachuk VA, Laketa V, Schultz C, Lukyanov S, Belousov VV (2011) Does cellular hydrogen peroxide diffuse or act locally? Antioxid Redox Signal. 14(1):1-7

Murga C, Laguinge L, Wetzker R, Cuadrado A, Gutkind JS (1998) Activation of Akt/protein kinase B by G protein-coupled receptors. A role for alpha and beta gamma subunits of heterotrimeric G proteins acting through phosphatidylinositol-3-OH kinase gamma. J Biol Chem. 273(30):19080-19085.

Murphy MP (2009) How mitochondria produce reactive oxygen species. Biochem J. 417(1):1-13

Navedo MF, Amberg GC, Votaw VS, Santana LF (2005) Constitutively active L-type Ca2+ channels. Proc

Natl Acad Sci U S A. 102(31):11112-11117

Navedo MF, Amberg GC, Nieves M, Molkentin JD, Santana LF (2006) Mechanisms underlying heterogeneous Ca2+ sparklet activity in arterial smooth muscle. J Gen Physiol. 127(6):611-622

Navedo MF, Amberg GC, Westenbroek RE, Sinnegger-Brauns MJ, Catterall WA, Striessnig J, Santana LF (2007) Ca(v)1.3 channels produce persistent calcium sparklets, but Ca(v)1.2 channels are responsible for sparklets in mouse arterial smooth muscle Am J Physiol Heart Circ Physiol. 293(3):1359-1370

Navedo MF, Nieves-Cintrón M, Amberg GC, Yuan C, Votaw VS, Lederer WJ, McKnight GS, Santana LF (2008) AKAP150 is required for stuttering persistent Ca2+ sparklets and angiotensin II-induced hypertension. Circ Res. 102(2):e1-e11

Navedo MF, Takeda Y, Nieves-Cintrón M, Molkentin JD, Santana LF (2010) Elevated Ca2+ sparklet activity during acute hyperglycemia and diabetes in cerebral arterial smooth muscle cells. Am J Physiol Cell Physiol. 298(2):C211-220

Navedo MF, Amberg GC (2013) Local regulation of L-type Ca^{2+} channel sparklets in arterial smooth muscle. Microcirculation. 20(4):290-298

Narayanan D, Xi Q, Pfeffer LM, Jaggar JH (2010) Mitochondria control functional CaV1.2 expression in smooth muscle cells of cerebral arteries. Circ Res. 107(5):631-641

Nelson MT, Cheng H, Rubart M, Santana LF, Bonev AD, Knot HJ, Lederer WJ. (1995) Relaxation of arterial smooth muscle by calcium sparks. Science. 270(5236):633-637

Nguyen Dinh Cat A, Touyz RM (2011) Cell signaling of angiotensin II on vascular tone: novel mechanisms. Curr Hypertens Rep. 13(2):122-128

Nickel A, Kohlhaas M, Maack C (2014) Mitochondrial reactive oxygen species production and elimination. J Mol Cell Cardiol. 73:26-33

Nickenig G, Harrison DG (2002) The AT(1)-type angiotensin receptor in oxidative stress and

atherogenesis: Part II: AT(1) receptor regulation Circulation. 105(4):530-536

Nieves-Cintrón M, Amberg GC, Nichols CB, Molkentin JD, Santana LF (2007) Activation of NFATc3 down-regulates the beta1 subunit of large conductance, calcium-activated K+ channels in arterial smooth muscle and contributes to hypertension. J Biol Chem. 282(5):3231-3240

Nieves-Cintrón M, Amberg GC, Navedo MF, Molkentin JD, Santana LF (2008) The control of Ca2+ influx and NFATc3 signaling in arterial smooth muscle during hypertension. Proc Natl Acad Sci U S A. 105(40):15623-15628

Nowicki PT, Flavahan S, Hassanain H, Mitra S, Holland S, Goldschmidt-Clermont PJ, Flavahan NA (2001) Redox signaling of the arteriolar myogenic response. Circ Res89(2):114-116

Oparil S (1986) The sympathetic nervous system in clinical and experimental hypertension. Kidney Int. 30(3):437-452

Ortego M, Bustos C, Hernández-Presa MA, Tuñón J, Díaz C, Hernández G, Egido J (1999) Atorvastatin reduces NF-kappaB activation and chemokine expression in vascular smooth muscle cells and mononuclear cells. Atherosclerosis. (2):253-261

Osol G, Laher I, Cipolla M (1991) Protein kinase C modulates basal myogenic tone in resistance arteries from the cerebral circulation. Circ Res. 68(2):359-367

Palmer RM, Ferrige AG, Moncada S (1987) Nitric oxide release accounts for the biological activity of endothelium- derived relaxing factor. Nature 327(6122): 524–526

Palumbo EJ, Sweatt JD, Chen SJ, Klann E (1992) Oxidation-induced persistent activation of protein kinase C in hippocampal homogenates. Biochem Biophys Res Commun. 187(3):1439-1445

Paul M, Poyan Mehr A, Kreutz R (2007) Physiology of local renin-angiotensin systems. Physiol Rev. 86(3):747-803.

Paulis L, Zicha J, Kunes J, Hojna S, Behuliak M, Celec P, Kojsova S, Pechanova O, Simko F (2008)

Regression of L-NAME-induced hypertension: the role of nitric oxide and endothelium-derived constricting factor. Hypertens Res. 31(4):793-803

Peinado JR, Diaz-Ruiz A, Frühbeck G, Malagon MM (2014) Mitochondria in metabolic disease: getting clues from proteomic studies. Proteomics. 14(4-5):452-466

Phillips MI (1987) Functions of angiotensin in the central nervous system. Annu Rev Physiol. 49: 413-435

Pueyo ME, Arnal JF, Rami J, Michel JB (1998) Angiotensin II stimulates the production of NO and peroxynitrite in endothelial cells. Am. J. Phys. - Cell Phys. 274 (1): 214-220

Quayle JM, McCarron JG, Brayden JE, Nelson MT (1993a) Inward rectifier K+ currents in smooth muscle cells from rat resistance-sized cerebral arteries. Am J Physiol. 265(5 Pt 1):C1363-1370

Quayle JM, McCarron JG, Asbury JR, Nelson MT (1993b) Single calcium channels in resistance-sized cerebral arteries from rats. Am J Physiol. 264(2 Pt 2):470-478.

Rajagopalan S, Kurz S, Münzel T, Tarpey M, Freeman BA, Griendling KK, Harrison DG (1996) Angiotensin II-mediated hypertension in the rat increases vascular superoxide production via membrane NADH/NADPH oxidase activation. Contribution to alterations of vasomotor tone. J Clin Invest. 97(8):1916-1923.

Rao RK, Clayton LW (2002) Regulation of protein phosphatase 2A by hydrogen peroxide and glutathionylation. Biochem Biophys Res Commun. 293(1):610-616

Rhee SG, Chang TS, Jeong W, Kang D (2010) Methods for detection and measurement of hydrogen peroxide inside and outside of cells. Mol Cells. 29(6):539-549

Rhee SG, Woo HA, Kil IS, Bae SH (2011) Peroxiredoxin functions as a peroxidase and a regulator and sensor of local peroxides. J Biol Chem. 287(7):4403-4410

Ricciotti E, FitzGerald GA (2011) Prostaglandins and inflammation. Arterioscler Thromb Vasc Biol. 31(5):986-1000

Rizzoni D, Castellano M, Porteri E, Bettoni G, Muiesan ML, Agabiti-Rosei E (1994) Vascular structural and

functional alterations before and after the development of hypertension in SHR. Am J Hypertens. 7(2):193-200

Rizzoni D, De Ciuceis C, Porteri E, Paiardi S, Boari GE, Mortini P, Cornali C, Cenzato M, Rodella LF, Borsani E, Rizzardi N, Platto C, Rezzani R, Rosei EA (2009) Altered structure of small cerebral arteries in patients with essential hypertension. J Hypertens. 27(4):838-845

Robertson BE, Nelson MT (1994) Aminopyridine inhibition and voltage dependence of K+ currents in smooth muscle cells from cerebral arteries Am J Physiol. 267(6 Pt 1):1589-1597

Rogers PA, Chilian WM, Bratz IN, Bryan RM Jr, Dick GM (2007) H2O2 activates redox- and 4-aminopyridine-sensitive Kv channels in coronary vascular smooth muscle. Am J Physiol Heart Circ Physiol. 292(3):H1404-1411

Rosenthal R, Cooper H, Hedges L (1994) Parametric measures of effect size. The handbook of research synthesis. 231-244

Rosenthal R, Rubin DB (2003) r equivalent: A simple effect size indicator. Psychol Methods. 8(4):492-496

Rosnow RL, Rosenthal R, Rubin DB (2000) Contrasts and correlations in effect-size estimation. Psychol Sci. 11(6):446-453

Roveri A, Coassin M, Maiorino M, Zamburlini A, van Amsterdam FT, Ratti E (1992) Effect of hydrogen peroxide on calcium homeostasis in smooth muscle cells. Arch Biochem Biophys. 297:265-270.

Rubart M, Patlak JB, Nelson MT (1996) Ca2+ currents in cerebral artery smooth muscle cells of rat at physiological Ca2+ concentrations. J Gen Physiol 107(4):459-472.

Sánchez JA, García MC, Sharma VK, Young KC, Matlib MA, Sheu SS (2001) Mitochondria regulate inactivation of L-type Ca2+ channels in rat heart. J Physiol 536(Pt 2):387-396

Santiago E, Contreras C, García-Sacristán A, Sánchez A, Rivera L, Climent B (2013) Signaling pathways involved in the H2O2-induced vasoconstriction of rat coronary arteries. Free Radic Biol Med. 60:136-46.

Saward L, Zahradka P (1997) Angiotensin II activates phosphatidylinositol 3-kinase in vascular smooth muscle cells. Circ Res. 81(2):249-57

Schiffrin EL, Thomé FS, Genest J (1984) Vascular angiotensin II receptors in SHR. Hypertension 6(5):682-688

Schleifenbaum J, Kassmann M, Szijártó IA, Hercule HC, Tano JY, Weinert S, Heidenreich M, Pathan AR, Anistan YM, Alenina N, Rusch NJ, Bader M, Jentsch TJ, Gollasch M (2014) Stretch-activation of angiotensin II type 1a receptors contributes to the myogenic response of mouse mesenteric and renal arteries. Circ Res 115(2):263-72

Schröder E, Eaton P (2008) Hydrogen peroxide as an endogenous mediator and exogenous tool in cardiovascular research: issues and considerations. Curr Opin Pharmacol. 8(2):153-159

Scragg JL, Dallas ML, Wilkinson JA, Varadi G, Peers C (2008. Carbon monoxide inhibits L-type Ca2+ channels via redox modulation of key cysteine residues by mitochondrial reactive oxygen species. The Journal of biological chemistry. 283:24412-24419

Serpillon S, Floyd BC, Gupte RS, George S, Kozicky M, Neito V, Recchia F, Stanley W, Wolin MS, Gupte SA (2009) Superoxide production by NAD(P)H oxidase and mitochondria is increased in genetically obese and hyperglycemic rat heart and aorta before the development of cardiac dysfunction. The role of glucose-6-phosphate dehydrogenase-derived NADPH. Am J Physiol Heart Circ Physiol. 297(1):H153-162

Slish DF, Welsh DG, Brayden JE (2002) Diacylglycerol and protein kinase C activate cation channels involved in myogenic tone. Am J Physiol Heart Circ Physiol. 283(6):2196-2201.

Simon G, Illyes G, Csiky B (1998) Structural vascular changes in hypertension: role of angiotensin II, dietary sodium supplementation, blood pressure, and time. Hypertension. 32(4):654-660

Somlyo AP (1985) Excitation-contraction coupling and the ultrastructure of smooth muscle. Circ Res. 57(4):497-507

Song YH, Choi E, Park SH, Lee SH, Cho H, Ho WK (2011) Sustained CaMKII activity mediates transient oxidative stress-induced long-term facilitation of L-type Ca2+ current in cardiomyocytes. Free Radic Biol Med. 51:1708-1716

Sotníková R (1998) Investigation of the mechanisms underlying H2O2-evoked contraction in the isolated rat aorta. Gen Pharmacol. 31:115-119

Stone JR, Yang S (2006) Hydrogen peroxide: a signaling messenger. Antioxid Redox Signal. 8(3-4):243-270

Sun C, Sellers KW, Sumners C, Raizada MK (2005) NAD(P)H oxidase inhibition attenuates neuronal chronotropic actions of angiotensin II. Circ Res. 96(6):659-666

Tabet F, Savoia C, Schiffrin EL, Touyz RM (2004) Differential calcium regulation by hydrogen peroxide and superoxide in vascular smooth muscle cells from spontaneously hypertensive rats. J Cardiovasc Pharmacol. 44(2):200-208

Taguchi H, Heistad DD, Kitazono T, Faraci FM (1994) ATP-sensitive K+ channels mediate dilatation of cerebral arterioles during hypoxia. Circ Res. 74(5):1005-1008

Takemoto M, Egashira K, Usui M, Numaguchi K, Tomita H, Tsutsui H, Shimokawa H, Sueishi K, Takeshita A (1997) Important role of tissue angiotensin-converting enzyme activity in the pathogenesis of coronary vascular and myocardial structural changes induced by long-term blockade of nitric oxide synthesis in rats. J Clin Invest. 99(2):278-287

Tang H, Viola HM, Filipovska A, Hool LC (2011) Cav1.2 calcium channel is glutathionylated during oxidative stress in guinea pig and ischemic human heart. Free Radic Biol Med. 51:1501-1511.

Terada LS (2006) Specificity in reactive oxidant signaling: think globally, act locally. J Cell Biol. 174(5):615-623

Toda N (1990) Mechanism underlying responses to histamine of isolated monkey and human cerebral arteries. Am J Physiol. 258(2 Pt 2): 311-317.

Török J (2008) Participation of nitric oxide in different models of experimental hypertension. Physiol Res. 57(6):813-825

Torrecillas G, Boyano-Adánez MC, Medina J, Parra T, Griera M, López-Ongil S, Arilla E, Rodríguez-Puyol M, Rodríguez-Puyol D (2001) The role of hydrogen peroxide in the contractile response to angiotensin II. Mol Pharmacol. 59(1):104-112

Touyz RM (2000) Oxidative stress and vascular damage in hypertension. Curr Hypertens Rep. 2(1):98-105

Touyz RM, Schiffrin EL (2000) Signal transduction mechanisms mediating the physiological and pathophysiological actions of angiotensin II in vascular smooth muscle cells. Pharmacol Rev. 52(4):639-672

Touyz RM, Wu XH, He G, Park JB, Chen X, Vacher J, Rajapurohitam V, Schiffrin EL (2001) Role of c-Src in the regulation of vascular contraction and Ca2+ signaling by angiotensin II in human vascular smooth muscle cells. J Hypertens.19(3):441-449

Touyz RM, Chen X, Tabet F, Yao G, He G, Quinn MT, Pagano PJ, Schiffrin EL (2002). Expression of a functionally active gp91phox-containing neutrophil-type NAD(P)H oxidase in smooth muscle cells from human resistance arteries: regulation by angiotensin II. Circ Res. 90(11):1205-1213

Touyz RM (2005) Reactive oxygen species as mediators of calcium signaling by angiotensin II: implications in vascular physiology and pathophysiology. Antioxid Redox Signal. 7(9-10):1302-1314

Tran CH, Taylor MS, Plane F, Nagaraja S, Tsoukias NM, Solodushko V, Vigmond EJ, Furstenhaupt T, Brigdan M, Welsh DG (2012) Endothelial Ca2+ wavelets and the induction of myoendothelial feedback. Am J Physiol Cell Physiol 302(8): 1226-1242

Trebak M, Ginnan R, Singer HA, Jourd'heuil D (2010) Interplay between calcium and reactive

oxygen/nitrogen species: an essential paradigm for vascular smooth muscle signaling. Antioxid Redox Signal. 12(5):657- 674

Veal E, Day A (2011) Hydrogen peroxide as a signaling molecule. Antioxid Redox Signal. 15(1):147-151

Venkatachalam K, Zheng F, Gill D. (2003) Regulation of canonical transient receptor potential (TRPC) channel function by diacylglycerol and protein kinase C. J Biol Chem 278: 29031–29040

Vieira AA, Nahey DB, Collister JP (2010) Role of the organum vasculosum of the lamina terminalis for the chronic cardiovascular effects produced by endogenous and exogenous ANG II in conscious rats. Am J Physiol Regul Integr Comp Physiol. 299(6): 1564-1571

Viola HM, Arthur PG, Hool LC (2007) Transient exposure to hydrogen peroxide causes an increase in mitochondria-derived superoxide as a result of sustained alteration in L-type Ca2+ channel function in the absence of apoptosis in ventricular myocytes. Circ Res. 100(7):1036-1044

Viola HM, Hool LC (2010) Qo site of mitochondrial complex III is the source of increased superoxide after transient exposure to hydrogen peroxide. J Mol Cell Cardiol 49:875-885

Wackenfors A, Vikman P, Nilsson E, Edvinsson L, Malmsjö M (2006) Angiotensin II-induced vasodilatation in cerebral arteries is mediated by endothelium-derived hyperpolarising factor. Eur J Pharmacol. 531(1-3):259-263

Wang G, Anrather J, Huang J, Speth RC, Pickel VM, Iadecola C (2004) NADPH oxidase contributes to angiotensin II signaling in the nucleus tractus solitarius. J Neurosci. 24(24):5516-5524

Wang H, Joseph JA (2000) Mechanisms of hydrogen peroxide-induced calcium dysregulation in PC12 cells. Free Radic Biol Med. 28:1222-1231

Wang SQ, Song LS, Lakatta EG, Cheng H (2001) Ca2+ signalling between single L-type Ca2+ channels and ryanodine receptors in heart cells. Nature. 410(6828):592-596

Wellman GC, Cartin L, Eckman DM, Stevenson AS, Saundry CM, Lederer W, Nelson MT (2001) Membrane

depolarization, elevated Ca(2+) entry, and gene expression in cerebral arteries of hypertensive rats. Am J Physiol Heart Circ Physiol. 281(6):2559-2567

Wilcox CS, Pearlman A (2008) Chemistry and antihypertensive effects of tempol and other nitroxides. Pharmacol Rev. 60(4):418-469

Winterbourn CC (2008) Reconciling the chemistry and biology of reactive oxygen species. Nat Chem Biol. 4(5):278-286

Winterbourn CC (2013) The biological chemistry of hydrogen peroxide. Methods Enzymol. 528:3-25

Woo HA, Yim SH, Shin DH, Kang D, Yu DY, Rhee SG (2010) Inactivation of peroxiredoxin I by phosphorylation allows localized H(2)O(2) accumulation for cell signaling. Cell. 140(4):517-528

Xi Q, Cheranov SY, Jaggar JH (2005) Mitochondria-derived reactive oxygen species dilate cerebral arteries by activating Ca2+ sparks. Circ Res. 97(4):354-362

Xie Z, Pimental DR, Lohan S, Vasertriger A, Pligavko C, Colucci WS, Singh K (2001) Regulation of angiotensin II-stimulated osteopontin expression in cardiac microvascular endothelial cells: role of p42/44 mitogen-activated protein kinase and reactive oxygen species. J Cell Physiol. 188(1):132-138

Yang L, Xu J, Minobe E, Yu L, Feng R, Kameyama A (2013) Mechanisms underlying the modulation of L-type Ca2+ channel by hydrogen peroxide in guinea pig ventricular myocytes. The journal of physiological sciences : JPS. 63:419-426.

Zhou XB, Wulfsen I, Utku E, Sausbier U, Sausbier M, Wieland T, Ruth P, Korth M (2010) Dual role of protein kinase C on BK channel regulation. Proc Natl Acad Sci U S A. 107(17):8005-8010.

Zhu H, Bannenberg GL, Moldéus P, Shertzer HG (1994) Oxidation pathways for the intracellular probe 2',7'-dichlorofluorescein. Arch Toxicol. 68(9):582-587

Zoccali C, Mallamaci F, Finocchiaro P (2002) Atherosclerotic renal artery stenosis: epidemiology, cardiovascular outcomes, and clinical prediction rules. J Am Soc Nephrol. 13(S3): 179-183

Zorov DB, Filburn CR, Klotz LO, Zweier JL, Sollott SJ (2000) Reactive oxygen species (ROS)-induced ROS release: a new phenomenon accompanying induction of the mitochondrial permeability transition in cardiac myocytes. J Exp Med. 192(7):1001-1014

Zorov DB, Juhaszova M, Sollott SJ (2014) Mitochondrial reactive oxygen species (ROS) and ROS-induced ROS release. Physiol Rev. 94(3):909-950

Zuo L, Ushio-Fukai M, Hilenski LL, Alexander RW (2004) Microtubulesregulate angiotensin II type 1 receptor and Rac1 localization in caveolae/lipid rafts: role in redox signaling. Arterioscler Thromb Vasc Biol. 24:1223–1228

Appendix: Permissions to Reproduce Copyright Protected Works

Chapter 2: American Physiological Society (AJP Cell)

Rights of Authors of APS Articles:

"For educational purposes only, authors may make copies of their own articles or republish parts of these articles (e.g., figures, tables), without charge and without requesting permission, provided that full acknowledgement of the source is given in the new work. Authors may not post a PDF of their published article on any website; instead, links may be posted to the article on the APS journal website.

Posting of articles or parts of articles is restricted and subject to the conditions below:

Theses and dissertations. APS permits whole published articles to be reproduced without charge in dissertations and posted to thesis repositories. Full citation is required."

http://www.the-aps.org/mm/Publications/Info-For-Authors/Copyright

Chapter 3: Taylor and Francis (Channels, Austin)

Copyright at Taylor & Francis

"When publishing in a Taylor & Francis subscription journal, we ask you to assign copyright to us. Alternatively, any author publishing with us can also opt to retain their own copyright and sign a license to publish (Sample license to publish).

Share your work

Make printed copies of your article to use for lecture or classroom purposes.

Include your article in a thesis or dissertation.

Present your article at a meeting or conference and distribute printed copies of the article.

Republish the article (making sure you cite the original article).

Adapt and expand your published journal article to make it suitable for your thesis or dissertation."

http://authorservices.taylorandfrancis.com/copyright-and-you/

Chapter 4: American Heart Association (Circ.Res.):

"Authors may use parts of the Work (eg, tables, figures) in subsequent works without asking the AHA's permission."- Copyright Transfer Agreement

"If your institution has a policy requiring your manuscript to be deposited in an institutional repository, the AHA CTA grants you those rights. The manuscript should be available in the institutional repository but made publicly accessible no earlier than 6 months after publication."

http://www.ahajournals.org/site/rights/